Weak Interference Direction of Arrival Estimation in the GPS Frequency Band

by

Zili Xu

Thesis submitted for the degree of

Doctor of Philosophy

School of Electrical and Electronic Engineering

Faculty of Engineering, Computer and Mathematical Science

The University of Adelaide

Adelaide, South Australia

December, 2016

Contents

Abstract

The GPS signal is vulnerable to both intentional and unintentional interferences due to its low received power. The need to localise GPS interference sources is becoming more pressing as more systems rely on GPS, while GPS jammers are becoming more widely available. This thesis discusses techniques to estimate the direction of arrival (DOA) of weak interferences in the GPS frequency band using antenna arrays.

The main issues which affect weak GPS interference DOA estimation accuracy are the antenna array errors, interference from other GPS signals, the number of snapshots required for DOA estimation and system coloured noise.

In order to estimate antenna array errors, a modelled eigenstructure based antenna array calibration algorithm is presented. This algorithm describes the antenna array errors using a physical model and uses the GPS signals with known DOAs as disjoint calibration sources to reduce the number of unknown calibration parameters and to enable a larger number of possible calibration sources to be used.

GPS calibration sources often have multipath components. These multipath components will contaminate the mutual coupling estimation result due to a similar directional behaviour. In order to solve this issue, a new calibration algorithm is developed to estimate the mutual coupling matrix in the presence of multipath signals. This algorithm first uses the decomposed signal subspace to construct its calibration cost function and then estimates the calibration parameters using alternating projection based methods iteratively.

The GPS signals typically have a SNR range from -15dB to -30dB. If the INR of the weak GPS interference is close or lower than this range, GPS signals need to be mitigated as they act like strong interferences. A Multiple

Subspace Projection (MSP) algorithm is proposed to cancel GPS signals. This algorithm projects the received signal onto the orthogonal subspace of GPS signals to cancel them completely even if the signals are band-limited, have multipath components, or have fractional delays.

The number of snapshots in the received data significantly influences the DOA estimation variance. The Cramer-Rao Lower Bound (CRLB) is derived and analysed for the antenna array DOA estimation. By using the CRLB, the number of snapshots is required to be larger than 1×10^6 to have the DOA estimation standard deviation to be smaller than 0.25º for a signal with a SNR of -20dB.

Finally, after cancelling GPS signals using the MSP algorithm, whitening the coloured noise in the system by using noise only data and calibrating the antenna array, the experimental results using an eight-element GPS antenna array showed that the DOA of a weak GPS interference with a SNR of -22dB could be accurately estimated.

Declaration

I certify that this work contains no material which has been accepted for the award of any other degree or diploma in my name, in any university or other tertiary institution and, to the best of my knowledge and belief, contains no material previously published or written by another person, except where due reference has been made in the text. In addition, I certify that no part of this work will, in the future, be used in a submission in my name, for any other degree or diploma in any university or other tertiary institution without the prior approval of the University of Adelaide and where applicable, any partner institution responsible for the joint-award of this degree.

I give consent to this copy of my thesis when deposited in the University Library, being made available for loan and photocopying, subject to the provisions of the Copyright Act 1968.

I also give permission for the digital version of my thesis to be made available on the web, via the University's digital research repository, the Library Search and also through web search engines, unless permission has been granted by the University to restrict access for a period of time.

Signature:

Date: 27 December, 2016

Acknowledgements

I would like to thank Professor Douglas Gray, my principal supervisor, for supervising and supporting this thesis. He introduced me to the field of array processing and gave me freedom to explore new ideas.

I wish to thank my supervisor Mr. Matthew Trinkle for his patience, guidance and assistance during my Ph.D. study, and providing me with extremely useful analysis, discussions and suggestions on my research.

I also would like to thank my friends and colleagues at the University of Adelaide Radar Research Centre and Sensor and Signal Processing Group at the University of Adelaide, in particular Ruiting Yang, Chow Yii Pui, Federica Salvetti, Tishampati Dhar, Rowen Fry, Joy Li, Mr. Marian Viola and Dr. Danny Gibbins.

Finally, thanks to my parents and my daughter, for all the love and strength they give me. And thanks to my wife Xiuran Zhu, without her support and encouragement, I would never have had the energy to see this thesis through to completion.

List of Figures

List of Tables

Abbreviations

ADC:	Analog-to-Digital Converter
AGC:	Automatic Gain Control
AP:	Alternating Projections
BF:	Beamformer
BPSK:	Binary Phase Shift Keying
C/A:	Coarse/Acquisition Code
CBF:	Conventional Beamformer
C/No:	Carrier-to-Noise ratio
CRLB:	Cramer-Rao Lower Bound
CW:	Continuous Wave
DOA:	Direction of Arrival
DS-SS:	Direct Sequence-Spread Spectrum
ESPRIT:	Estimation of Signal Parameter via Rotational Invariance Techniques
FIM:	Fisher Information Matrix
FIR:	Finite Impulse Response
GNSS:	Global Navigation Satellite System
GPS:	Global Positioning System
INR:	Interference-to-Noise Ratio
LF:	Likelihood Function
LPF:	Low Pass Filter
LS:	Least Squares
L1:	L1 Frequency Band, 1575.42MHz

L2: L2 Frequency Band, 227.6MHz

MaxSINR: Maximum Signal-to-Interference and Noise Ratio

ML: Maximum Likelihood

MMSE: Minimum Mean Square Error

MUSIC: Multiple Signal Classification

MVDR: Minimum Variance Distortionless Response

NCO: Numerically Controlled Oscillator

PRN: Pseudo Random Noise

RF: Radio Frequency

RFI: Radio Frequency Interference

RHCP: Right Hand Side Circularly Polarisation

RMSE: Root Mean Squared Error

SINR: Signal-to-Interference and Noise Ratio

SNR: Signal-to-Noise Ratio

STD: Standard Deviation

SV: Space Vehicle

UCA: Uniform Circular Array

ULA: Uniform Linear Array

Publications

The list of publications related to this thesis are:

- Z. Xu, M. Trinkle, and D. A. Gray, "A modelled eigenstructure based antenna array calibration algorithm for GPS," in *Proceedings of the 23rd International Technical Meeting of The Satellite Division of the Institute of Navigation (ION GNSS 2010)*, Portland, OR, 2010, pp. 3220-3228.

- Z. Xu, M. Trinkle, and D. A. Gray, "A Maximum-likelihood based mutual coupling calibration algorithm in the presence of multipath for GPS antenna array," in *Proceedings of the 24th International Technical Meeting of The Satellite Division of the Institute of Navigation (ION GNSS 2011)*, Portland, OR, 2011, pp. 1111-1119.

- Z. Xu and M. Trinkle, "Interference angle of arrival estimation within the GNSS Environmental Monitoring System (GEMS) using antenna arrays," in *International Symposium on GPS/GNSS (IGNSS 2011)*, Sydney, Australia, 2011.

- Z. Xu, M. Trinkle, and D. A. Gray, "A gain/phase and mutual coupling calibration algorithm for GPS antenna array in the presence of multipath," in *International Symposium on GPS/GNSS (IGNSS 2011)*, Sydney, Australia, 2011.

- Z. Xu and M. Trinkle, "Weak GPS interference direction of arrival estimation using GPS signal cancellation," in *Proceedings of the 25th International Technical Meeting of The Satellite Division of the Institute of Navigation (ION GNSS 2012)*, Nashville, TN, 2012, pp. 2940-2945.

- Z. Xu, M. Trinkle, and D. A. Gray, "Weak interference direction of arrival estimation in the GPS L1 frequency band," in *IEEE International Conference on Acoustics, Speech, and Signal Processing (ICASSP 2015)*, Brisbane, Australia, 2015, pp. 2649-2653.

Chapter 1: Introduction

1.1 Problem Description

This section introduces the background of the Global Positioning System (GPS) first. The types of the GPS interferences and their damage to GPS receivers are presented later. Finally, the need for localising weak GPS interferences using antenna arrays is discussed.

1.1.1 Global Positioning System (GPS)

The Global Positioning System (GPS) is a satellite navigation system used in localisation, navigation, tracking, mapping, and timing [1]. It uses a constellation of between 24 and 32 medium earth orbit (MEO) satellites which are at a height of approximately 20,000 km and with an orbital period of about 12 hours. At least four GPS satellites are necessary to compute accurate positions in three dimensions and the time offset of the receiver clock. GPS was originally designed for the U.S. military in the 1970s, but is now also extensively used for a number of civilian applications. GPS was fully operational on 27 April, 1995. Because of its high precision, general acceptance and ease of use, GPS has gradually become the main means of global navigation.

The GPS signal is a Direct Sequence-Spread Spectrum (DS-SS) signal modulated with a Pseudo Random Noise (PRN) binary code. With PRN codes, GPS is able to use the Code Division Multiple Access (CDMA) concept. By using DS-SS, GPS satellites can transmit low power signals that still have adequate Carrier to Noise Power ratio (C/No) after correlation in the

receiver [2]. However, the low power received GPS signal, typically 15-30 dB below the receiver's thermal noise level, is susceptible to interferences from either intentional or unintentional sources. As a result, the performance of GPS and the code synchronization process degrades dramatically.

The characteristics of the GPS signal structure determine the GPS receiver algorithms and applications. As shown in figure 1.1.1, there are three main components in a civilian GPS signal: the navigation message, the PRN code and the L1 RF carrier frequency.

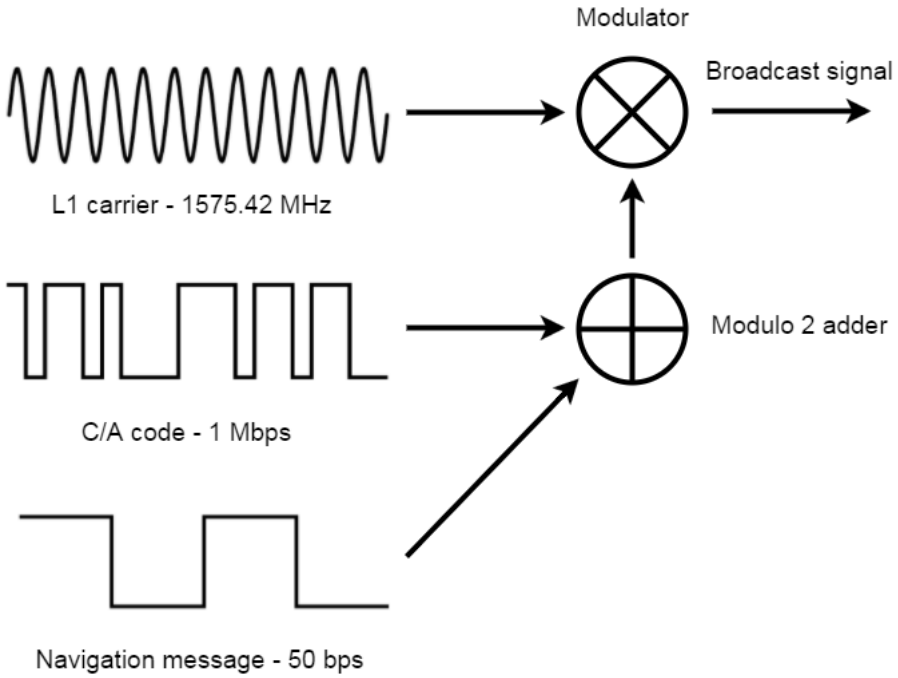

Figure 1.1.1: GPS L1 signal structure.

The GPS navigation (NAV) message contains the ephemeris and the almanac data with +1 and -1 binary values, by which the satellite orbit and time can be obtained. The navigation data rate is 50 bps. In figure 1.1.1, the 50 bps navigation message is modulated onto the 1 Mbps C/A code by Modulo-2 operation. The signal is then modulated onto 1575.42 MHz by the L1 carrier using a Binary Phase Shift Keying (BPSK) scheme.

There are two types of PRN codes in GPS, Coarse/Acquisition (C/A) code with a length of 1023 chips and a transmission rate of 1.023 Mchips/s and Precision (P/Y) code with a length of 6.1871×10^{12} chips and a transmission rate of 10.23 Mchips/s. The Coarse/Acquisition (C/A) signal which is for civilian use is the identification of each satellite and is modulated on the L1 carrier frequency 1575.42 MHz. The encrypted Precision (P/Y) signal which is for military use is modulated on the L2 carrier frequency 1227.6 MHz and the L1 carrier frequency 1575.42MHz with a one week long encryption key. The encrypted P/Y signal is an anti-spoofing mode and only military receivers can acquire it. Although there are techniques which can use the P/Y signal without knowledge of the encrypted code [3], only the civilian C/A signal in the L1 frequency band is considered in this thesis. However, all the algorithms in this thesis can be adapted to the L2 frequency band with small modifications.

The PRN code is the key component in GPS. It is a Direct Sequence-Spread Spectrum (DS-SS) signal, which is also known as Direct Sequence Code Division Multiple Access (DS-CDMA). DS-SS enables signal transmissions with very low power spectral densities, and the received GPS signals are below the thermal noise level. For an antenna with 0 dB isotropic gain and Right-Hand Circular Polarization (RHCP) near the Earth's surface, the minimum specified received signal power of a L1 C/A signal viewed at 5 degrees above local horizon is -160 dBW. Assuming that the thermal noise has a power density of No = -205 dBW/Hz, the C/A codes spread the GPS signal power over a 1 MHz bandwidth, hence the resulting noise power over 1 MHz is -205 dBW + 60 dB = -145 dBW/Hz [4]. The GPS signal power is thus 15 dB below the noise power. In practice the SNR is lower than the predicted value due to receiver losses, so GPS signals are typically 15-30 dB below the receiver's thermal noise level.

1.1.2 Interference in the GPS Frequency Band

It is illegal to transmit RF signals in the GPS frequency band, so any RF signals, either intentional or unintentional, in or close to the GPS frequency band which are not GPS signals are interferences. As discussed in Section 1.1.1, due to the weak power of incident GPS signals (15-30 dB below thermal noise level), they are vulnerable to even weak interferences, and as a result it is relatively easy to jam most commercial GPS receivers [5]. Reference [6] reported that the typical jamming threshold Jammer to Signal level (J/S) is 40-50 dB which will prevent the GPS receivers from obtaining a position fix. In [7], it is reported that a 1W jammer can make a GPS receiver in a radius of 10km fail to track the satellites, and fail to acquire the satellites in a radius of up to 85km.

Class	Type	Potential Sources
Wideband	Band-limited Gaussian	Intentional matched bandwidth noise jammers
	Phase/frequency modulation	Television transmitters' harmonics or near-band microwave link transmitters overcoming the front end filter of a GPS receiver
	Matched spectrum	Intentional matched-spectrum jammers, spoofers, or nearby pseudolites
	Pulse	Any type of burst transmitters such as radar or ultra-wideband (UWB)
Narrowband	Phase/frequency modulation	Intentional chirp jammers or harmonics from an amplitude modulation (AM) radio station, citizens band (CB) radio, or amateur radio transmitter
	Swept continuous wave	Intentional swept CW jammers or frequency modulation (FM) stations transmitter' harmonics
	Continuous wave	Intentional CW jammers or near-band unmodulated transmitter's carriers

Table 1.1.1: Types and potential sources of RF interferences.

Jammers can be categorised in to two basic groups based on the bandwidth they occupy relative to the GPS bandwidth: Continuous wave (CW) / Narrowband jammers and wideband jammers. Table 1.1.1 shows the types and potential sources of RF interferences as summarized in [2] and [8]. Radio Frequency Interference (RFI) can impact a GPS receiver in many ways. It can affect the operation of the Automatic Gain Control (AGC) [2], the Low Noise Amplifier (LNA) in the RF front-end [9] and the carrier and code tracking loops [10, 11]. Reference [4] showed that Continuous Wave (CW) interference has severe effects on the GPS C/A code signal. The detailed effects of different types of interferences, such as continuous-wave (CW) and wideband signals, as well as pulsed and continuous signals were studied in [12].

1.1.3 The Need for GPS Interference Localisation

As discussed in Sections 1.1.1 and 1.1.2, the GPS signal is vulnerable to both intentional and unintentional interference due to its low incident power. A number of GPS interference events have been reported. Reference [13] reported that the third order harmonic of a TV transmitter tower in Sydney, Australia, was in the GPS L1 frequency band and prevented a software receiver from tracking the satellite. Reference [14] reported a preamplifier in an active TV antenna unintentionally jammed an area with a radius of up to 3km. Reference [15] reported one of the Ground Based Augmentation System (GBAS) GNSS receivers at the Newark Liberty International Airport was jammed periodically due to a low-power jamming device located in a truck on the nearby highway. The need to localise GPS interference sources is becoming more pressing as more systems begin to rely on GPS, while GPS jammers are becoming more widely available. GPS jamming source localization is important especially for safety critical applications such as airports or machine guidance [16].

A lot of research has been done to suppress and mitigate GPS interferences. Research topics include:

Temporal processing [17-20]. These techniques assume clear jammer time-frequency (TF) signatures and rely on the distinct differences in the temporal structure of the jammer and the spread-spectrum signals and use a time domain filter, typically an adaptive prediction filter, to suppress the interferences;

Spectral-based processing [21-23]. These techniques transform the signal to the frequency domain with an FFT, where the signal is filtered by using an appropriate weighting to mitigate the interference, such as removing peaks in the spectrum, and then transform the signal back to the time domain.

Subspace projection [24-26]. These techniques use the fact that the jammer IF (Instantaneous Frequency) defines the temporal signature of the interference within a one-dimensional signal sub-space per interference source to construct a subspace orthogonal to the jammer. The resulting projection matrix is used to excise the jammer power in the incoming signal prior to correlation with the receiver pseudo random noise (PRN) sequence.

Spatial signal processing [27-32]. These techniques use multiple antenna elements combined with an optimum beamforming algorithm to adjust the radiation pattern of the antenna array. The gain in each direction depends on the choice of the array weights thus implementing a spatial filter. Several optimality criteria have been studied aimed at enhancing the SNR of GPS signals in the receivers and mitigating interferences. Examples include Null steering, Maximum SINR and MVDR. Combinations of these techniques, such as time-frequency processing [33] and space-time processing [34-38] have also been considered and provide better results compared to single antenna and/or single domain processing.

However in order to disable the GPS interference source it must first be localised. While there has been a lot of research on GPS interference

suppression and mitigation, not as much research has been done in the GPS interference localisation area. Three main methods have been used to localise GPS interferences: the first method uses the C/No values on a network of GPS receivers to estimate the ranges to the interference position and thus estimate the position [39-42]; the second method attempts to locate the interference using widely separated antennas using the Time Difference of Arrival (TDOA) of the interference signal between antennas [43-45]; the third method estimates the Direction of Arrival (DOA) of the interference source by using adaptive antenna array processing techniques [46, 47].

So far publications in the GPS interference localisation area have not considered the minimum interference power for which DOA estimation algorithms will be effective. However, for GPS systems, interference sources transmitting several milliwatts can affect other nearby GPS receivers due to the very low received signal level of the GPS signals of -160 dBW at the surface of the earth. As a result, it is important to have a highly sensitive interference DOA estimation system that is able to accurately estimate DOAs of weak interference sources at a reasonable distance of several kilometres. It is thus important to research algorithms which enable the DOA of weak GPS interferences to be estimated reliably and accurately using an adaptive antenna array. In order to achieve this, the main issues that are addressed in this thesis are:

1. The adaptive antenna array DOA estimation algorithms assume no errors in antenna arrays, so uncertainties such as gain/phase errors in each channel and mutual coupling between antennas existing in the antenna array will degrade the performance of DOA estimation techniques, especially for high resolution, subspace based DOA estimation algorithms such as Multiple Signal Classification algorithm (MUSIC).

2. If the interferences power is lower than the GPS signal power level, which is typically 15 dB to 30 dB below the thermal noise, estimation of the interference DOA will be severely compromised or fail

completely due to the large number of relatively strong and directional GPS signals.

3. Because of the intended low power level of the interference and its potentially unknown waveform, a large number of non-coherent integrations are required to reduce the variance of the DOA estimation to an acceptable level. So, in order to achieve a certain performance, the number of the snapshots used in the spatial non-coherent integration and the performances of weak interference DOA estimations need to be statistical analysed.

4. In practice there may be other imperfections in the system such as coloured receiver noise and other interfering sources in the GPS L1 frequency band.

1.2 Thesis Outline and Contributions

Chapter 2

Background information on adaptive antenna array processing techniques including DOA estimation algorithms is introduced. The applications of these array processing techniques in the GPS area are also presented along with a review of current GPS interference localisation methods.

Chapter 3

An eigenstructure GPS antenna array calibration algorithm based on a physical model of the array errors is proposed to estimate array orientation, gain/phase errors and antenna mutual coupling effects by using GPS signals as disjoint calibration sources.

Contributions

1. GPS antenna array errors are described by matrices based on physical models of the errors, which reduces the number of unknown parameters in the cost function, thus reducing the number of sources required for calibration and giving an understanding of the underlying causes of the array manifold errors.
2. GPS signals are used as disjoint GPS antenna array calibration sources, which largely simplifies the computations required to estimate directions of arrival of calibration sources and also enables the number of calibration sources used to be larger than the number of GPS antenna array elements.
3. The unknown parameters are estimated iteratively by minimising the highly sensitive eigenstructure based cost function.

Chapter 4

A Maximum Likelihood (ML) based GPS antenna array calibration algorithm is proposed to estimate antenna mutual coupling effect and array orientation in the presence of multipath signals of calibration sources.

Contributions

1. The multipath signals of the calibration sources and the mutual coupling effect which have a similar behaviour are both modelled in the GPS array calibration cost function.
2. Antenna mutual coupling effect, array orientation error and the multipath signals of the calibration sources are estimated iteratively by minimising the eigenstructure based cost function.
3. The DOAs of the multipath signals are estimated by minimising the cost function using a low computational maximum likelihood algorithm – Alternating Projection (AP).

Chapter 5

The effect of the GPS signals on the DOA estimation of weak GPS interferences is presented. The Multiple Subspace Projection (MSP) algorithm is proposed to cancel GPS signals.

Contributions

1. The effect of GPS signals on the DOA estimation of weak interferences is analysed.
2. GPS signals are cancelled by the proposed Multiple Subspace Projection (MSP) algorithm. This algorithm extends the current single dimensional subspace based GPS cancellation algorithms [48, 49] to multi-dimensional subspace structure and thus achieves better cancellation of the received GPS signals.

Chapter 6

The requirement of the number for snapshots of antenna array processing and the technique to whiten the coloured noise in the system are discussed first. An eight-element GPS antenna array and data-recording system are described later. The experimental results of weak GPS interference DOA estimation are presented in the end.

Contributions

1. The Cramer-Rao Lower Bound (CRLB) is derived and analysed for a circular array with one element in the centre.
2. The number of snapshots used to estimate the covariance matrix for weak GPS interference DOA estimation is determined by CRLB analysis.
3. Coloured noise in the system is whitened by pre-whitening technique using noise-only data.

4. Experimental results demonstrate an accurate DOA estimation at an input SNR of -22dB after cancelling the GPS signals, pre-whitening the system coloured noise and calibrating the antenna array.

Chapter 7

The conclusion of the thesis and suggestions for future work are presented.

Throughout this thesis, although other DOA estimation algorthims can be used, attention is restricted to use of the MUSIC algorithm as it provides a good balance between sensitivity to system errors and accurate DOA estimation.

Chapter 2: Background of GPS Antenna Array Processing

2.1 Introduction

This chapter first introduces the general background of the application of antenna array techniques in the GPS area in Section 2.2. Then, Section 2.3 discusses direction of arrival (DOA) estimation algorithms by subspace methods. Antenna array calibration techniques are reviewed in Section 2.4, while previous work in GPS interference DOA estimation and localisation is discussed in Section 2.5.

2.2 Antenna Array Beamforming in the GPS Area

An antenna array is a set of antenna elements deployed in space whose outputs are combined to achieve an overall radiation pattern that can be different from the radiation pattern of the individual elements [50]. Antenna arrays can thus be used to electronically steer a beam in a desired direction without requiring mechanical steering. The beam can be steered using either conventional or adaptive techniques. The main difference between optimum beamforming and conventional beamforming is the method used to adjust the "weights" of each antenna: conventional Beamforming has fixed "weights" for a given beam direction which means its beampattern is fixed, while optimum beamforming chooses the weights for each beam direction according to a predefined optimality criterion. It is thus able to minimise the effects of interfering signals by adapting the weights to track changes in the interference parameters such as direction of arrival (DOA). Conventional beamforming achieves the maximum SNR in spatially uncorrelated noise and

in the absence of interference, but its performance drops compared with optimum beamforming when there are one or more interferences. This is because optimum beamforming takes both received signals and noise into account through the covariance matrix of the receiver outputs and can then be made adaptive by adjusting its weights in response to changes in the interference environment. Most of these beamforming algorithms are used to enhance the SNR of the received GPS signal and to mitigate against interference. However, some can also be used for direction finding. The main optimum antenna array processing algorithms (null-steering, MaxSINR and MVDR) will be discussed in the following paragraphs.

Null steering steers deep nulls to the directions of the interferences and attempts to keep a uniform beampattern in all the other directions. The optimization algorithm minimises the mean square error between a chosen reference antenna (the choice varies depending on the antenna array geometry) and a linear combination of the remaining antenna outputs. The advantage of this approach is that a-priori knowledge of the DOA of the GPS signals relative to the array is not required. This simplifies the implementation of the algorithm, which can be completely separate from the GPS receiver. As a result, null steering is widely used in GPS applications. References [27, 31, 51, 52] discuss and test the performance of this technique when applied to GPS. However, this technique is only useful for canceling interferences and does not improve the SNR of the GPS signals over a single antenna and indeed in some case can lead to a loss in C/No for some satellites.

MaxSINR maximises the signal-to-interference plus noise ratio. To implement this technique, the GPS signal covariance matrix must be separated from the overall signal covariance matrix. As a result, MaxSINR is usually applied after correlation so that the GPS signal components can be separated. In [53], a subspace technique was used to estimate interference DOAs and was combined with the MaxSINR technique to remove these interferences from the received data. A similar technique was used in [8]. A technique that combines the capability of rejecting narrowband interferences and multipath components when using the MaxSINR criteria was applied in

[54]. It gives the best improvement and achieves the theoretical limit that adaptive algorithms such as MaxSINR and MMSE can achieve. In [55], an adaptive algorithm with improved convergence speed was introduced. This approach acquires GPS signals first to either get a reference signal or to be able to separate covariance matrices.

Minimum Variance Distortionless Response (MVDR) is also known as optimal beamformer, Capon beamformer and Linearly Constrained Minimum Variance Beamformer (LCMV). It aims to minimise the output power subject to a unity gain constraint in the direction of the desired signal. MVDR makes the best use of the available degrees of freedom to shape the spatial nulls and has a greater probability of preserving the GPS signals. Compared with null steering, MVDR will give a narrower null if the interference is close to a GPS signal because it seeks to maintain the array gain in the direction of the GPS signals [32]. In [47, 56], the performance of MVDR for estimating the DOA of interferences was tested by scanning optimum beam over a range of angles and finding local maxima. The result shows that although MVDR requires a well calibrated array, it gave a surprisingly good performance when separating two interferences with an array that was not well calibrated. This indicates that errors in the GPS array were small enough to allow the MVDR technique to be used relatively robustly for direction finding. The MVDR technique is thus a good technique against which high resolution subspace based DOA estimation techniques that are more sensitive to phase errors can be compared.

2.3 Subspace Based DOA Estimation Algorithms

Subspace or eigenstructure and high resolution methods estimate the directions of signals by using the eigenstructure of the covariance matrix and the fact that the signal subspace and the array manifold intersect at locations corresponding to the directions of the signals [57]. Eigenvalues and eigenvectors are important in many physical systems as generally an

eigenvector corresponds to a natural mode of oscillation of the system and its corresponding eigenvalue gives the intensity of that oscillation [58]. There are two main subspace methods commonly used to estimate the DOA: MUltiple SIgnal Classification (MUSIC) and Estimation of Signal Parameters via Rotational Invariance Techniques (ESPRIT).

The MUltiple SIgnal Classification (MUSIC) algorithm [59-61] uses the property that the array manifold is orthogonal to the noise subspace at the signal directions of arrival to estimate the direction of signals with the assumptions that the signals are uncorrelated and the noise is also spatially uncorrelated. If the signals are correlated, the noise subspace will not be orthogonal to the array manifold and hence the MUSIC algorithm will provide incorrect signal directions, as MUSIC cannot handle coherent sources without spatial smoothing. When the number of the snapshots and signal to noise ratio are large and the sources are uncorrelated and the noise is spatially uncorrelated, MUSIC performs similarly to the Maximum Likelihood method which is derived from the DOA likelihood function based on the observation data probability density function and is thus the optimal method for direction finding [62]. When the number of the snapshots and the signal to noise ratios are small or the signals are correlated, MUSIC will not be able to resolve closely spaced sources even in the absence of modeling errors [63]. To overcome the problems caused by correlated signals, in [64, 65], spatial smoothing techniques have been proposed.

In [66], the sensitivity of the MUSIC algorithm is quantified by a first–order analysis. The analysis shows that even small modeling errors can lead to significant degradation in the performance of the MUSIC algorithm.

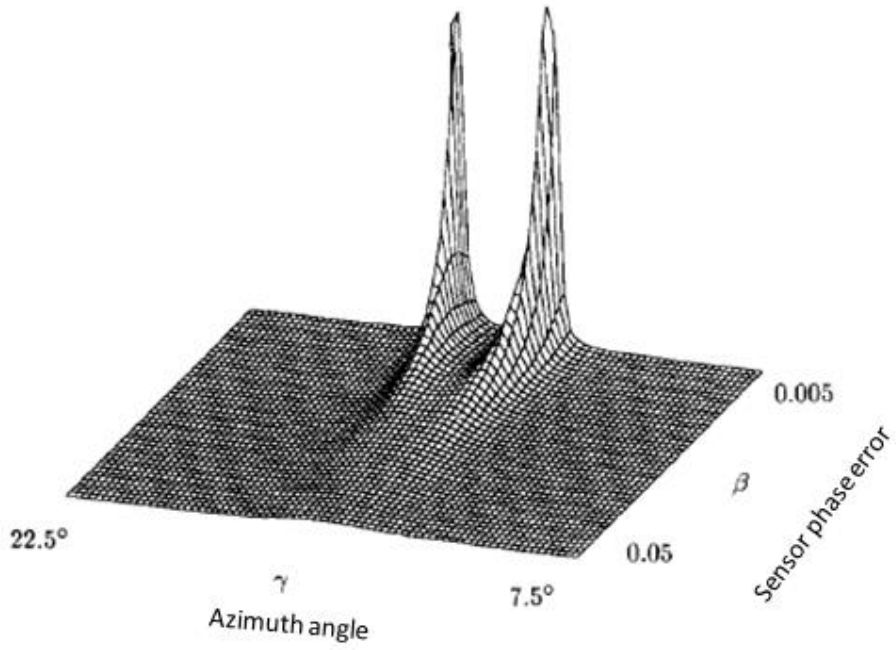

Figure 2.3.1: The MUSIC “spectrum” in the presence of phase errors, the sensor phase error β is between 0.005º<β<0.05º [66].

Figure 2.3.1 shows that the MUSIC “spectrum” gradual degrades from two sharp peaks to a flat single peak as the modeling phase errors increase for a circular array of four uniformly spaced sensors, half a wavelength apart. The two sources are at directions 13.5º and 16.5º. Due to the small phase errors, the peak locations are no longer at the true directions of the signals. The high sensitivity of the MUSIC algorithm to modeling errors is a serious problem that needs to be solved if MUSIC is to be practically used [66].

The weighted MUSIC algorithm is a modification of the MUSIC algorithm. It adds a weighting matrix to weight the relative contributions of the eigenvectors. When the weighting matrix is identity matrix, the weighted algorithm simplifies to the MUSIC algorithm. The weighted MUSIC performs better than MUSIC when the number of snapshots is small and the signal sources are correlated [67].

The root MUSIC algorithm estimates the directions of the signals by computing the roots of polynomial equations. When there is only a limited number of snapshots available, root MUSIC is better than MUSIC [68]. A

technique for extending root MUSIC from a ULA array to 2D non-ULA arbitrary array was given in [69] and demonstrated good performance.

Estimation of Signal Parameters via Rotational Invariance Techniques (ESPRIT) estimates signal arrival direction by exploiting the rotational invariance of the signal subspaces of subsets of the array receivers [58]. This means that the signal subspace of particular subsets of receivers can be obtained from a different subset with the same number of receivers by a simple vector rotation. ESPRIT is more efficient than MUSIC because it avoids searching the array manifold. The major limitation of this method is in the use of estimated covariances and the subtraction of the estimated noise power which is critical [70]. In the absence of modeling errors, MUSIC is always more accurate than ESPRIT [71]. In the presence of modeling errors the situation becomes more complicated. However, it is possible to prove that if the errors in the response of the different sensors are complex Gaussian random variables which are mutually independent but have equal variance, then MUSIC is always more accurate than ESPRIT [72].

2.4 Antenna Array Calibration

Antenna array processing techniques assume no array errors, and their performance degrades or fails completely when the array manifold is poorly described. As discussed in the previous sub-section, direction finding algorithms by subspace methods are quite sensitive to modeling errors such as array manifold errors, so array calibration is important for high resolution direction finding methods to work well.

There are two basic array calibration methods based on the type of sources. Active array calibration methods use special sources with known parameters for array calibration and the source DOAs are usually known, while passive array calibration methods use sources in the received data and the source DOAs are usually unknown. When the sources are far from the arrays, the

transmitted waves can be assumed to be planar. In [73] and [74], the Cramer-Rao lower bound for active array calibration was analysed. The analyses showed that the bearing of the calibration sources must be uniformly distributed in angle to minimise the Cramer-Rao lower bound for uncorrelated sources and the minimum value of the Cramer-Rao lower bound is inversely proportional to the number of sources and the number of data points. The papers also suggested that active array calibration is expected to provide better accuracy than passive array calibration. Two methods – iterative Newton-type algorithms for ML estimation and eigenstructure–based algorithms - are proposed to estimate the array sensor positions using non-disjoint sources with known DOAs.

In [75], a ML method was developed for estimating sensor positions. The method is a two-step approach using disjoint sources. Disjoint sources can be separated independently of array processing, which is possible if they are separated in the time, frequency or code domains. In the first step, the DOAs of the sources are estimated using the nominal sensor positions and searching for local maxima over a range of steering directions. In the second step, the sensor positions are estimated using the DOAs estimated in the first step. This process is iterated and the cost function converges to a minimum depending on the accuracy of the nominal sensor positions and the initial DOA estimates.

An eigenstructure based method for estimating unknown sensor parameters (gain, phase, position) is proposed in [76] and [77]. The method is based on the assumption that the eigenstructure based calibration parameter estimation cost function will be a minimum when the signal steering vector is almost orthogonal to the estimated noise subspace. The values at which the cost function reaches a minimum are taken as the estimated values of the respective parameters. The process iterates between two steps: Step1: The sources' directions are estimated by MUSIC using the estimated array parameters in the last round. Step2: A closed form solution that is related to the Gauss-Newton technique is used to estimate the sensor positions using the last estimated source DOAs or the gain/phase can be estimated from a

quadratic minimization problem. In [78], the array is calibrated for mutual coupling errors as well as sensor gain and phase errors where a three step process is used based on the same method as in [76, 77]. The conditions for uniqueness are also derived. The ML method [75] which is an optimal method is expected to be more computationally intense than the eigenstructure method. This eigenstructure based self-calibration method is of particular interest because of its simplicity in implementation and its relative robustness. However, the papers represent only the first few steps in the development of self-calibration techniques. A considerable amount of work remains to be done before these techniques are fully developed and validated [57], especially in the context of GPS.

The performance of self-calibration algorithms is analysed in [57], which showed that imbalances of the sensor gains has very little effect on the accuracy of direction of arrival estimation and most of the loss in performance is due to phase errors. Increasing the number of sensors improves estimation accuracy and reduces the loss of performance due to the need to estimate relatively fewer unknown parameters. The analysis also seems to indicate that attempting to estimate all of these parameters using only four sensors leads to a very ill-conditioned problem. Finally, it is very desirable to have the sources used for self-calibration well separated in angle.

The calibration algorithms considered so far assume that the DOA of the calibration signal is unknown and needs to be estimated as part of the calibration process. [79] uses the similar eigenstructure method to [76], but the key difference is that it uses sources with known DOAs, making the algorithm a one step process rather than an iterative process. This is an interesting modification because the GPS signal directions are usually known. To improve the standard self-calibration method based on MUSIC, [80] adds a regularization term to the MUSIC cost function so that it takes on the form of a Maximum a posteriori (MAP) estimator. This can make the self-calibration methods more robust and enables them to handle direction-dependent errors for which the usual self-calibration algorithms will fail.

Reference [81] takes the novel approach of formulating the problem of direction finding using an uncalibrated array in an H∞ framework. Based on a state-space equivalent for the conventional array signal model, results from linear estimation in Krein space can be used to easily derive an H∞ filter that removes the “uncertainties” of the array signal model that are otherwise manifest in the received signal. The H∞ approach results in a minimisation of the worst-case scenario. The algorithm iterates between two steps. The algorithm is initialised with nominal values of the DOAs supplied by an algorithm such as MUSIC. Based on the nominal DOAs, the H∞ filter is constructed, and the received signal is fed as the filter input. The filter output is then fed back into MUSIC to update the DOA estimates, and the process repeats itself. This algorithm is computationally intensive.

The calibration performance between the approaches outlined in [80] and [81] is compared in [82]. The results show that the algorithm in [80] outperforms the algorithm in [81] for high SNR and also has the advantage of outputting array calibration updates in addition to DOA estimates. The algorithm proposed in [81] does offer a performance advantage in a low SNR environment, as anticipated from its H∞ design criterion. For practical applications in which an array is initially calibrated and self-calibration is employed for calibration updates, high SNR signals of opportunity would most likely be used. The algorithm [80] would thus be a better match to this application. For this project, GPS signals will be used as the calibration sources. Although GPS signals are 20-30 dB below the noise, long integration times can be used to increase the effective SNR. The achievable SNR and hence the optimal calibration algorithms for the GPS scenario are the subject of this research.

2.5 Previous Work in GPS Interference DOA Estimation and Localisation Area

This section summarises the previous GPS interference DOA estimation and localisation work. Three main types of methods have been proposed to localise GPS interferences:

1. C/No value based range estimation
2. TDOA based location estimation
3. Antenna array based DOA estimation

References [39-42] use the C/No values on a network of GPS receivers to estimate the ranges to the interference position and thus estimate the position of the interference. This method typically uses GPS modules to set up a network of GPS receivers at determined locations, so the localisation system can be easily setup with relatively low cost. As described in [39], the experimental interference source localisation accuracy is within a few of tens of meters with both 5 receivers and the interference within 500 metres. The performance of this method degrades quickly when interference source is close to the receivers because AGC may saturate or far away from the receivers because AGC voltage relation to distance may be insufficient.

References [40, 43-45] attempt to localise the interference by using widely separated antennas using the Time Difference of Arrival (TDOA) of the interference signal between antennas. This method requires highly accurate clock synchronisation among the receiver stations. As described in [45], the experimental interference source localisation accuracy is about a few metres with 3 receivers located within 81 metres of each other when the interference is about100 metres away from the furthest receiver. A major disadvantage is that the performance of TDOA degrades quickly if the interference source is a narrow band signal. Performance of the technique also depends on the geometry of the antenna positions and the relative orientation of the

interference. Increasing the number of antennas leads to performance improvements.

References [46, 47, 83] estimate the Direction of Arrival (DOA) of the interference source by using adaptive antenna array processing techniques. The experimental results in [47] shows the standard deviation error of DOA estimation using an 8 element circular array is about 4 degrees with four far-field GPS jammers a few kilometres away from the antenna array. The estimation error can be improved with better antenna array calibration and longer integration time.

Chapter 3: GPS Antenna Array Calibration I: Modelled Eigenstructure based GPS Antenna Array Calibration

3.1 Introduction

Most antenna array DOA estimation algorithms assume the steering vector lies on the true array manifold determined by the array geometry. However, uncertainties, such as gain/phase errors in each channel and mutual coupling between antennas exist in practical antenna arrays and will degrade the performance of DOA estimation algorithms. Subspace based high sensitivity DOA estimation algorithms, such as Multiple Signal Classification algorithm (MUSIC), are especially vulnerable to such errors as they exploit the assumed orthogonality between the signal and noise subspaces.

The MUSIC algorithm will be used in Chapter 6 of this thesis to estimate the DOAs of a weak interference in the GPS frequency band because of its high estimation sensitivity for weak targets. References [66], [57] and [84] quantified the sensitivity of the MUSIC algorithm to system errors using a first-order analysis by assuming that the exact covariance matrix of the array element outputs is known. The results showed that even small modelling errors can lead to significant degradation in the DOA estimation performance of the MUSIC algorithm. As a result, in order to estimate the DOAs of weak GPS interferences reliably and accurately, antenna array calibration is necessary.

In the GPS area, several different types of calibration techniques have been proposed. In references [85] and [86], the phase errors of each channel were measured experimentally. The results showed that the phase deviations were

significant for patch antenna elements. Reference [87] proposed a least squares based calibration algorithm which used GPS signals as the calibrating reference sources to estimate and record the array steering vector errors as a function of azimuth and elevation angles. The results showed good calibration performance and the structure of the algorithm is simple, but this method did not assume any physical model of the system errors, so it is only able to accurately calibrate the array gain/phase errors in the directions of the GPS ephemeris. The errors are expected to increase as the signal DOA moves away from the GPS ephemeris directions at which the array was calibrated. Reference [87] also pointed out that their algorithm was not practical for dynamic operation at present due to the loss of accuracy in the orientation estimation of the array. Reference [88] used a mixed LMS/H^{∞} optimal approach to estimate the array uncertainties. The simulation results showed the improved capabilities for anti-jamming, interference rejection and minimising the effect of system uncertainties. But the algorithm did not appear to have been tested on real data. Similar to [87], reference [88] also needed a large number of calibration sources as the algorithm did not make use of any additional information about how the array errors were related to each other. Reference [89], similar to [87] and [88], used a Minimum Mean Square Error (MMSE) criteria to solve the equations relating the received signal and the calibration parameters. Reference [90] calibrated the gain/phase mismatch between the antenna array channels by measuring the received gain/phase differences of the receiving channels from a single GPS signal.

Friedlander proposed an eigenstructure based method for estimating unknown sensor parameters in [77], [78], [76] and [57]. This method is based on the assumption that the array is calibrated when the signal steering vector is almost orthogonal to the estimated noise subspace. The cost function is thus the projection of the signal steering vector onto the noise subspace. The values at which the cost function reaches the minimum are taken as the estimated values of the respective parameters. This eigenstructure based self-calibration method is simple to implement and

relatively robust, so it has been investigated and applied widely in areas such as Over-The-Horizon radar [91-93] and wireless communications [94].

A model based approach to GPS array calibration that makes use of the array geometry to determine an underlying model of how the array errors are interrelated is proposed in this chapter. This model based approach reduces the number of calibration sources that are required and gives an understanding of the underlying causes of the array manifold errors. Unlike previous array calibration methods, which assume there is no prior knowledge of the error models in the calibration process, the method proposed here is a modelled eigenstructure based self-calibration algorithm for estimating the array orientation, gain/phase errors and mutual coupling effects in the antenna array by using GPS satellite signals as the disjoint calibration sources. The gain/phase errors and mutual coupling effects are described by the matrices based on a physical model which forms the basis of the algorithm error minimization process and hence reduces the number of calibration sources required to calibrate the array. GPS signals are used as the calibration sources and thus there is no need to estimate the direction of the calibration sources. However, the orientation of the antenna array relative to the satellites may not be known precisely and needs to be estimated. Thus in the GPS context, there is no need to estimate the DOA of all calibration sources as was the case in [91], but only the array orientation. Due to the orthogonality of the GPS PRN codes, the covariance matrices of GPS signals are able to be extracted disjointly, so GPS signals are used as disjoint calibration sources in this algorithm, which enables the number of the GPS signals used in the calibration process to be equal or larger than the number of the array elements.

The remainder of this chapter is structured as follows: The assumed calibration signal model is described in Section 3.2. In Section 3.3, the proposed calibration algorithm is outlined and the simulation results are given in Section 3.4. In Section 3.5, experimental results based on a 4 element equally spaced linear array are presented. Finally, conclusions are given in Section 3.6.

3.2 Signal Model

3.2.1 Ideal Array Model

Consider an array of *M* elements in the absence of gain/phase errors and mutual coupling. The output of the m^{th} sensor at the time *t* in the presence of a far field narrowband signal *s(t)* is

$$x_m(t) = e^{-j\omega\tau_m} s(t) + n_m(t) \tag{3.2.1}$$

where ω is the radian frequency of the narrowband signal (for GPS L1 carrier frequency, it is $2\pi \times 1.575 \times 10^9$ radians/s) and $n_m(t)$ is additive receiver noise which is assumed to be White Gaussian Noise. Because the signal *s(t)* is assumed to be in the far field, the signal wavefront is effectively planar over the array. Thus, $\tau_m = (x_m \cos\theta + y_m \sin\theta) sin\varphi / v$ represents the time delay of the signal received at the m^{th} sensor with respect to the reference origin, x_m and y_m are the position coordinates of the m^{th} sensor for a two dimensional array, θ and φ are the azimuth and elevation directions of arrival of the signal respectively.

For simplicity in the remainder of this chapter, all the signals are assumed to lie in the same plane as the array, i.e. the elevation angle φ = 90°.

The vector form of the *M* sensors outputs is

$$\underline{x}(t) = \underline{v}\, s(t) + \underline{n}(t) \tag{3.2.2}$$

where $\underline{x}(t) = [x_1(t), x_2(t), \cdots, x_M(t)]^T$, $\underline{v} = [e^{j\omega\tau_1}, e^{j\omega\tau_2}, \ldots, e^{j\omega\tau_M}]^T$ ($\underline{v}(\theta)$ is the steering vector) and $\underline{n}(t) = [n_1(t), n_2(t), \ldots, n_M(t)]^T$.

3.2.2 Array Error Model

The calibration algorithm seeks to calibrate for the gain/phase errors in each individual channel, mutual coupling effects between the antennas and the array orientation error based on the models described below.

Gain/phase error model

The gain/phase error model describes the gain/phase mismatch in the individual antenna channels which can be directly modelled by a diagonal *M* by *M* matrix

$$\mathbf{\Gamma} = diag\{1, \alpha_2 e^{-j\phi_2}, \cdots, \alpha_m e^{-j\phi_m}, ..., \alpha_M e^{-j\phi_M}\} \tag{3.2.3}$$

where α_m and $\emptyset_m$ are the gain and phase error of channel *m*. All the gain/phase errors are referenced to channel 1.

Mutual Coupling model

The mutual coupling model tries to describe the behavior of the coupling between the antennas according to the shape of the antenna array using a matrix model. The physical behavior of antenna mutual coupling and its mathematical expressions are discussed in [95] and [96]. In [57] and [78], appropriate matrix models for the case of equally spaced linear and circular arrays are given based on two assumptions below, other array geometries are considered in reference [97].

(a) The mutual coupling coefficients are inversely proportional to the distance between the antennas.
(b) The coupling between any two equally spaced antennas is the same.

If the array is an equally spaced linear array, the mutual coupling matrix becomes a symmetric Toeplitz matrix with value 1 at the diagonal positions. The *M* by *M* symmetric Toeplitz matrix **C** is given by

$$\mathbf{C} = \begin{bmatrix} 1 & c_1 & c_2 & \cdots & c_{M-2} & c_{M-1} \\ c_1 & 1 & c_1 & \cdots & c_{M-3} & c_{M-2} \\ c_2 & c_1 & 1 & \cdots & c_{M-4} & c_{M-3} \\ \vdots & \vdots & \vdots & \ddots & \vdots & \vdots \\ c_{M-2} & c_{M-3} & c_{M-4} & \cdots & 1 & c_1 \\ c_{M-1} & c_{M-2} & c_{M-3} & \cdots & c_1 & 1 \end{bmatrix} \qquad (3.2.4)$$

where c_n is the complex mutual coupling coefficient for the two antennas, for which the antenna number difference is n.

For an equally spaced circular array, a symmetric circulant matrix provides an excellent model. The M by M symmetric circulant matrix **C** is given by

$$\mathbf{C} = \begin{bmatrix} 1 & c_1 & c_2 & \cdots & c_{M/2-1} & c_{M/2} & c_{M/2-1} & \cdots & c_2 & c_1 \\ c_1 & 1 & c_1 & c_2 & \cdots & c_{M/2-1} & c_{M/2} & c_{M/2-1} & \cdots & c_2 \\ \vdots & \vdots & \vdots & \ddots & \ddots & \ddots & \vdots & \vdots & \vdots & \vdots \\ \cdots & c_2 & c_1 & 1 & c_1 & c_2 & \cdots & c_{M/2-1} & c_{M/2} & c_{M/2-1} \\ c_{M/2-1} & \cdots & c_2 & c_1 & 1 & c_1 & c_2 & \cdots & c_{M/2-1} & c_{M/2} \\ c_{M/2} & c_{M/2-1} & \cdots & c_2 & c_1 & 1 & c_1 & c_2 & \cdots & c_{M/2-1} \\ \vdots & \vdots & \vdots & \ddots & \ddots & \ddots & \vdots & \vdots & \vdots & \vdots \\ c_2 & \cdots & c_{M/2-1} & c_{M/2} & c_{M/2-1} & \cdots & c_2 & c_1 & 1 & c_1 \\ c_1 & c_2 & \cdots & c_{M/2-1} & c_{M/2} & c_{M/2-1} & \cdots & c_2 & c_1 & 1 \end{bmatrix} \qquad (3.2.5)$$

if the number of antennas M is even, or

$$\mathbf{C} = \begin{bmatrix} 1 & c_1 & c_2 & \cdots & c_{(M-1)/2} & c_{(M+1)/2} & \cdots & c_2 & c_1 \\ c_1 & 1 & c_1 & c_2 & \cdots & c_{(M-1)/2} & c_{(M+1)/2} & \cdots & c_2 \\ \vdots & \vdots & \vdots & \ddots & \ddots & \ddots & \vdots & \vdots & \vdots \\ \cdots & c_2 & c_1 & 1 & c_1 & c_2 & \cdots & c_{(M-1)/2} & c_{(M+1)/2} \\ c_{(M+1)/2} & \cdots & c_2 & c_1 & 1 & c_1 & c_2 & \cdots & c_{(M-1)/2} \\ \vdots & \vdots & \vdots & \ddots & \ddots & \ddots & \vdots & \vdots & \vdots \\ c_2 & \cdots & c_{(M-1)/2} & c_{(M+1)/2} & \cdots & c_2 & c_1 & 1 & c_1 \\ c_1 & c_2 & \cdots & c_{(M-1)/2} & c_{(M+1)/2} & \cdots & c_2 & c_1 & 1 \end{bmatrix} \qquad (3.2.6)$$

if the number of antennas is odd and where c_n is the mutual coupling effect for the two antennas, of which the antenna number difference is *n*.

Array orientation error

As the GPS signals are to be used as the calibration sources, the directions of the calibration sources can be obtained accurately from the satellite constellation and estimated user position. However, any error in the estimation of the array orientation will affect the DOA of the calibration sources relative to the array. To model this error, an orientation error angle θ_e will be added to the DOAs of all the calibration sources.

$$\underline{\theta}_{DOA} = [\theta_1 + \theta_e, \theta_2 + \theta_e, \cdots, \theta_n + \theta_e, ..., \theta_N + \theta_e]^T \qquad (3.2.7)$$

where $\underline{\theta}_{DOA}$ are the true azimuth directions of the signals and $[\theta_1, \theta_2, \cdots, \theta_N]$ are the azimuth directions of the signals referenced to the chosen array reference direction.

The final steering vector for source *n* can be written as

$$\underline{v} = [e^{j\frac{2\pi}{\lambda}k^T\underline{u}_1}, e^{j\frac{2\pi}{\lambda}k^T\underline{u}_2}, \ldots, e^{j\frac{2\pi}{\lambda}k^T\underline{u}_m}, \ldots, e^{j\frac{2\pi}{\lambda}k^T\underline{u}_M}]^T \qquad (3.2.8)$$

where, $k^T = [\cos(\theta_n + \theta_e), sin(\theta_n + \theta_e)]$ and $\underline{u}_m = [x_m, y_m]^T$ is the m^{th} sensor position.

3.2.3 Array Model with the Errors

The vector form of the antenna array outputs at the time *t* for a single far field narrowband signal *s(t)* in the presence of a gain/phase error matrix $\mathbf{\Gamma}$, mutual coupling matrix **C**, and array orientation error θ_e is given by

$$\underline{x}(t) = \mathbf{C\Gamma} \cdot \underline{v}(\theta + \theta_e)s(t) + \underline{n}(t)\,. \qquad (3.2.9)$$

The covariance matrix of this received signal is

$$\mathbf{R} = E\{\underline{x}(t)\underline{x}^H(t)\} = \mathbf{C\Gamma}\underline{v} \cdot {\sigma_s}^2 \cdot \underline{v}^{\mathrm{H}}\mathbf{\Gamma}^{\mathrm{H}}\mathbf{C}^{\mathrm{H}} + {\sigma_n}^2 \cdot \mathbf{I} \qquad (3.2.10)$$

where ${\sigma_s}^2$ is the signal power, ${\sigma_n}^2$ is the noise power and **I** is order M identity matrix.

Once the estimated covariance matrices $\widehat{\mathbf{R}}$ are obtained, the gain/phase errors and mutual coupling effects together with the array orientation error will be estimated by minimising a formulated cost function with respect to these error models.

3.2.4 Solution Existence Condition

The GPS signals can be considered disjoint sources due to their orthogonal spreading codes. Calibration sources are said to be disjoint if the estimated receiver covariance matrices of the signals can be estimated separately from each other. For an *M* sensor uniform linear array with N disjoint sources there are *2(M-1)* gain/phase errors, 2(*M-1)* mutual coupling parameters and 1 array orientation error in the *M* sensor array. N disjoint sources give *2N(M-1)* least squares equations.

A solution exists if $2(M-1)+2(M-1)+1 \leq 2N(M-1)$, that is $N \geq 2 + \frac{1}{2(M-1)}$. For GPS antenna array with any number of antennas ($M > 1$), the requirement is $N \geq 3$. The number of available GPS signals is typically larger than 4, so the solution existence condition requirement is not difficult to achieve when calibrating GPS antenna arrays.

If the calibration signals are joint, i.e., the sources are not clearly separable by other means, then the individual signal covariance matrices cannot be separately estimated and only a single joint covariance matrix can be used. Thus there will be only *2N(M-N)* least squares equations, resulting in the

maximum number of calibration sources being limited by the number of the antennas in the array.

3.3 Calibration Algorithm

The array manifold is the locus of steering vectors in a multidimensional space. The array manifold is orthogonal to the noise subspace at the signal bearings under the assumptions that the signals are uncorrelated and the noise is also spatially uncorrelated. This orthogonality condition is used by this calibration algorithm to formulate the cost function. The array errors are estimated by minimising the cost function.

As shown in figure 3.3.1, the proposed algorithm iterates between three steps: Step 1, the array orientation angle is estimated using the estimated array parameters in the last round. Step 2, the gain/phase error diagonal matrix is estimated using the array orientation angle obtained from step 1 and the mutual coupling matrix from the last round. Step 3, the mutual coupling matrix is estimated using the array orientation angle obtained from step 1 and gain/phase error diagonal matrix from step 2. The process will complete when the cost function converges. The final array orientation, gain/phase error diagonal matrix and the mutual coupling matrix are the estimated results.

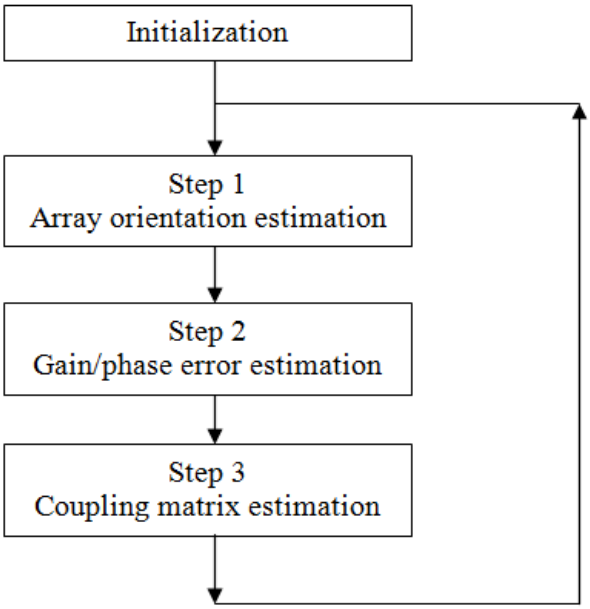

Figure 3.3.1: Calibration algorithm flow chart.

Whilst this approach following that of Friedlander will give a local optimum solution, it is not necessarily guaranteed to give a global optimum solution.

3.3.1 Cost function

The covariance matrix of each GPS signal across the antenna array can be extracted separately by cross-correlating with the CA code for that particular GPS signal and integrating. Because the GPS signals can be separated in this way, the post-correlation covariance matrices for each GPS satellite can be treated as coming from disjoint sources.

Consider *N* disjoint GPS calibration sources, the estimated post-correlation covariance matrix for the n^{th} disjoint source is

$$\widehat{\mathbf{R}}_{\boldsymbol{n}} = \frac{1}{T}\sum_{t=1}^{T} \underline{x}_n(t)\, \underline{x}_n{}^{H}(t) \qquad (3.3.1)$$

where $\underline{x}_n(t)$ is the vector of the M post-correlation sensor outputs for the n^{th} GPS calibration source at time t and T is the total number of contiguous post correlation outputs needed to estimate the covariance matrix and perfect correlation is assumed.

The eigen-decomposition of the n^{th} estimated covariance matrix $\widehat{\mathbf{R}}_{\boldsymbol{n}}$ gives the *M×1* signal eigenvector $\underline{\hat{\lambda}}_n$ which correspond to the largest eigenvector and *M×M-1* noise eigenvectors $\hat{\mathbf{U}}_n$ which corresponds to the column wise stored *M-1* smallest eigenvectors. Hence the formulated cost function is

$$Q = \sum_{n=1}^{N} \left\| \widehat{\mathbf{U}}_{\boldsymbol{n}}^{H} \mathbf{C}\boldsymbol{\Gamma} \cdot \underline{v}(\theta_n + \theta_e) \right\|^2 \qquad (3.3.2)$$

where **C** is the mutual coupling matrix, $\boldsymbol{\Gamma}$ is the gain/phase error matrix, $\underline{v}$ is the steering vector, θ_n is the DOA of the *n*th GPS calibration source, θ_e is the array orientation error and $\mathbf{C}\boldsymbol{\Gamma} \cdot \underline{v}$ is the array manifold, *N* is the number of GPS calibration sources.

The array is perfectly calibrated if the signal steering vector is orthogonal to the noise subspace, hence the cost function is minimised.

3.3.2 Initialization

The initial values of the gain/phase error $\boldsymbol{\Gamma}$ and mutual coupling matrix **C** can be selected based on prior knowledge gained through electromagnetic modelling. If no such prior knowledge is available, the gain/phase error and mutual coupling matrices can be initialised by the identity matrix $\mathbf{I}_M$.

The nominal DOAs of the calibration sources are calculated from the constellation of the satellites and the location of the antenna array. If the array orientation angle can be estimated initially, this angle will be included to calculate the nominal DOAs.

3.3.3 Orientation Error Estimation

The values of the gain/phase error $\mathbf{\Gamma}$ and mutual coupling matrix **C** from the last round are used as the current values and fixed in the cost function. If this is the first round, the initial values of $\mathbf{\Gamma}$ and **C** are used.

The minimisation of the cost function in equation 3.3.2 with respect to the orientation angle θ_e is given by

$$\hat{\theta}_e = arg \min_{\theta_e} \sum_{n=1}^{N} \left\| \hat{\mathbf{U}}_{\boldsymbol{n}}^{H} \mathbf{C\Gamma} \cdot \underline{v}(\theta_n + \theta_e) \right\|^2 \tag{3.3.3}$$

The minimisation defined by equation 3.3.3 is performed by a grid (0.01° step size) search over the space of θ_e. The corresponding angle at which the minimum occurs is the estimated orientation error.

Note that whilst each of the steps in the iterative process may require a smaller number of calibration sources, the question of whether the same or different sources are required for each of the separate steps needs to be resolved. A complete study of this is beyond the scope of this work and the bound derived, although it may not be the lowest bound, suffices the practical perspective.

3.3.4 Gain/phase Error Estimation

In this step, the gain/phase errors are estimated by minimising the cost function with respect to the gain/phase errors. The values of the orientation error θ_e from the orientation error estimation step and the mutual coupling matrix $\mathbf{C}$ from the last round are used as the current values and are fixed in the cost function in equation 3.3.2 which can be conveniently rewritten as

$$Q = \sum_{n=1}^{N} \underline{v}(\theta_n + \theta_e)^H \mathbf{\Gamma}^H \mathbf{C}^H \widehat{\mathbf{U}}_n \widehat{\mathbf{U}}_n{}^H \mathbf{C} \mathbf{\Gamma} \underline{v}(\theta_n + \theta_e) \tag{3.3.4}$$

Using Lemma 1 in Appendix A to swap the positions of the vector $\underline{v}(\theta_n + \theta_e)$ and the matrix $\mathbf{\Gamma}$

$$Q = \underline{\eta}^H \left\{ \sum_{n=1}^{N} \mathbf{A_1}{}^H(n) \mathbf{C}^H \widehat{\mathbf{U}}_n \widehat{\mathbf{U}}_n{}^H \mathbf{C}\, \mathbf{A_1}(n) \right\} \underline{\eta} \tag{3.3.5}$$

where $\underline{\eta} = [\mathbf{\Gamma}_{11}, \mathbf{\Gamma}_{22}, \dots, \mathbf{\Gamma}_{MM}]^T$, $\mathbf{A_1}(n) = diag\{\underline{v}(\theta_n + \theta_e)\}$.

The minimisation problem becomes a quadratic minimisation problem under the linear constraint $\underline{\eta}^H \underline{w} = 1$, where $\underline{w} = [1,0,0,\dots,0]^T$. The result is given by

$$\underline{\hat{\eta}} = \frac{\mathbf{Z}^{-1} \underline{w}}{\underline{w}^T \mathbf{Z}^{-1} \underline{w}} \tag{3.3.6}$$

where $\mathbf{Z} = \sum_{n=1}^{N} \mathbf{A_1}{}^H(n) \mathbf{C}^H \widehat{\mathbf{U}}_n \widehat{\mathbf{U}}_n{}^H \mathbf{C}\, \mathbf{A_1}(n)$.

Finally, the gain/phase error matrix $\mathbf{\Gamma}$ can be recovered from $\underline{\hat{\eta}}$ using the equation $\mathbf{\Gamma} = diag(\underline{\hat{\eta}})$.

3.3.5 Mutual Coupling Matrix Estimation

In this step, the values of the orientation error θ_e from the orientation error estimation and the gain/phase error matrix $\mathbf{\Gamma}$ from the gain/phase errors estimation step are used as the current values and fixed in the cost function. The mutual coupling matrix is estimated by minimising the cost function with respect to the mutual coupling matrix.

Assuming that the antenna array is a circular array (the mutual coupling matrix is symmetric circulant matrix) and using Lemma 2 of Appendix A gives the following cost function

$$Q = \underline{c}^H \left\{ \sum_{n=1}^{N} \mathbf{A_2}^H(n) \widehat{\mathbf{U}}_n \widehat{\mathbf{U}}_n{}^H \mathbf{A_2}(n) \right\} \underline{c} \tag{3.3.7}$$

where $\underline{c} = \mathbf{C}_{1i}$, $i = 1,2,..,L$, $L = M/2 + 1$ when M is even and $L = M/2 + ½$ when M is odd, and the $M \times L$ matrix $\mathbf{A_2}(n)$ is the sum of the four $M \times L$ following matrices

$$\begin{aligned}
[\mathbf{W}_1]_{pq} &= \begin{cases} \mathbf{X}_{p+q-1}, & p+q \le M+1 \\ 0, & otherwise \end{cases} \\
[\mathbf{W}_2]_{pq} &= \begin{cases} \mathbf{X}_{p-q+1}, & p \ge q \ge 2 \\ 0, & otherwise \end{cases} \\
[\mathbf{W}_3]_{pq} &= \begin{cases} \mathbf{X}_{M+1+p-q}, & p < q \le l \\ 0, & otherwise \end{cases} \\
[\mathbf{W}_4]_{pq} &= \begin{cases} \mathbf{X}_{P+q-M-1}, & 2 \le q \le l, p+q \ge M+2 \\ 0, & otherwise \end{cases}
\end{aligned} \tag{3.3.8}$$

where $l = M/2$ for even M and $l = (M+1)/2$ for odd M, and $\mathbf{X} = \mathbf{\Gamma} \cdot \underline{v}(\theta_n + \theta_e)$.

If the antenna array is a linear array, the mutual coupling matrix will be a Toeplitz matrix. In this case, Lemma 3 of Appendix A needs to be used to swap the positions of the matrix **C** and the vector $\mathbf{\Gamma}\underline{v}(\theta_n + \theta_e)$.

Again, the minimisation problem becomes quadratic minimisation problem under the linear constraint $\underline{c}^H \underline{w} = 1$, where $\underline{w} = [1,0,0,\ldots,0]^T$. The result is given by

$$\underline{\hat{c}} = \frac{\mathbf{G}^{-1}\underline{w}}{\underline{w}^T \mathbf{G}^{-1} \underline{w}} \tag{3.3.9}$$

where $\mathbf{G} = \sum_{n=1}^{N} \mathbf{A_2}^H(n) \widehat{\mathbf{U}}_n \widehat{\mathbf{U}}_n{}^H \mathbf{A_2}(n)$.

The symmetric circulant mutual coupling matrix **C** can be recovered from $\underline{\hat{c}}$ using the relationship $\mathbf{C}_{1i} = \underline{c}$, $i = 1,2,..,L$, $L = M/2 + 1$ when M is even and $L = M/2 + ½$ when M is odd.

3.3.6 Convergence Check

The cost function Q^k is calculated at the end of the k^{th} iteration using the estimated array orientation error, gain/phase errors and mutual coupling matrix. If the difference in the previous and current cost function is larger than a preset threshold, ε, ie.

$$Q^{k-1} - Q^k > \varepsilon \tag{3.3.10}$$

then another iteration of the algorithm is performed, otherwise the calibration algorithm will stop and the current array orientation error, gain/phase errors and mutual coupling matrix are taken to be the estimated results.

3.4 Simulation Results

The performance of the proposed algorithm was verified by simulations. In the simulations no prior knowledge of the array error parameters was assumed, so the gain/phase error matrix and mutual coupling matrix were initially all set to be the identity matrix.

The simulations assumed a uniform circular array with 8 omni-directional antennas spaced by half a wavelength of the calibration signals, which is 9.5 cm. The 6 calibration sources were in the far field of the array and are assumed to be narrow-band signals with a carrier frequency of 1.575 GHz and the SNR was 10 dB after GPS signal coherent post-correlation for one CA code period. The azimuth DOAs of the 6 sources were 56°, 98°, 146°, 250°, 290° and 325° with elevation DOAs at 45° for all sources. The sources, similarly to real GPS signals, were assumed to be disjoint and uncorrelated with each other. The noise in the system was uncorrelated additive white Gaussian noise (AWGN) with zero mean. The number of snapshots was 1,000 for a recording length of 1 second (1000 CA code periods in 1 second), and as a result, the estimated noise covariance matrix $\hat{\mathbf{R}}_n$ was assumed to

be equal to the exact noise covariance matrix $\mathbf{R}_n$. The gain and phase errors were assumed to be stationary in the data and thus fixed for each realisation. The antenna array errors were simulated as

1. Array orientation error relative to GPS north: 10º.
2. Gain/phase errors in each channel (Gain is linear and not in dB):

Channel	1	2	3	4	5	6	7	8
Gain (in amplitude)	1	1	1.2	0.8	0.85	0.9	1.2	1.22
Phase	0	-25º	-15º	50º	20º	-15º	65º	45º

Table 3.4.1: The mutual coupling parameters used in the simulations.

3. Mutual coupling coefficients: *c* = [1 0.22 0.11 0.06 0.03].

The above values were chosen to be similar to those measured experimentally in anechoic chamber. The calibration convergence threshold was 1×10^{-9}. The calibration process converged after 11 iterations.

3.4.1 Beampattern

Figures 3.4.1 and 3.4.2 show the ideal beampattern and the beampattern of a conventional beamformer before and after the proposed calibration scheme is applied respectively.

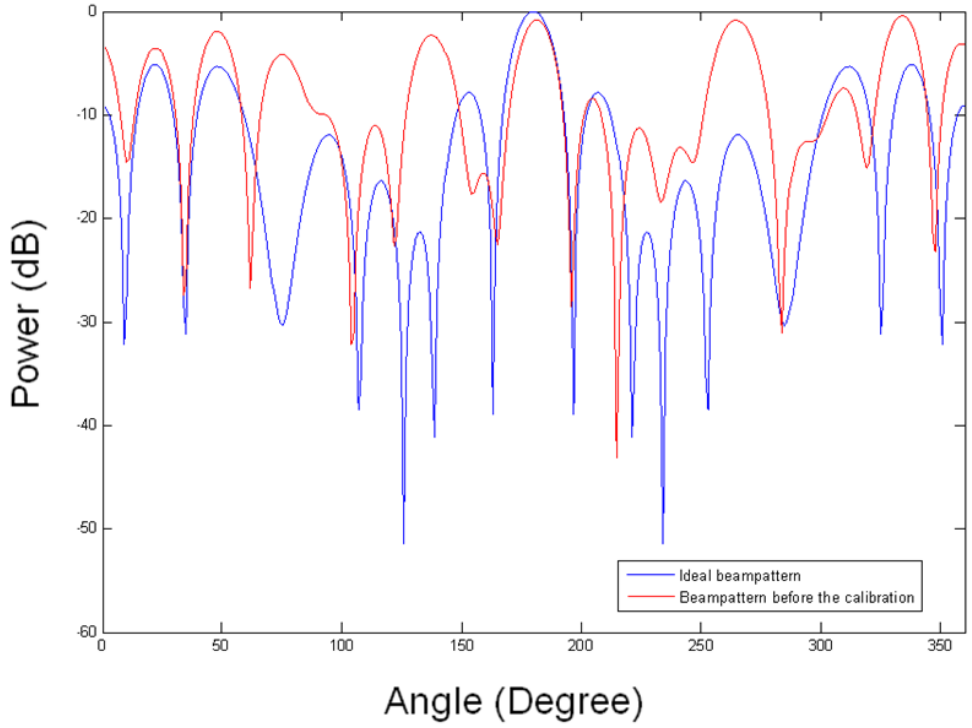

Figure 3.4.1: Ideal beampattern and original beampattern (no calibration), beam steering direction: 180°.

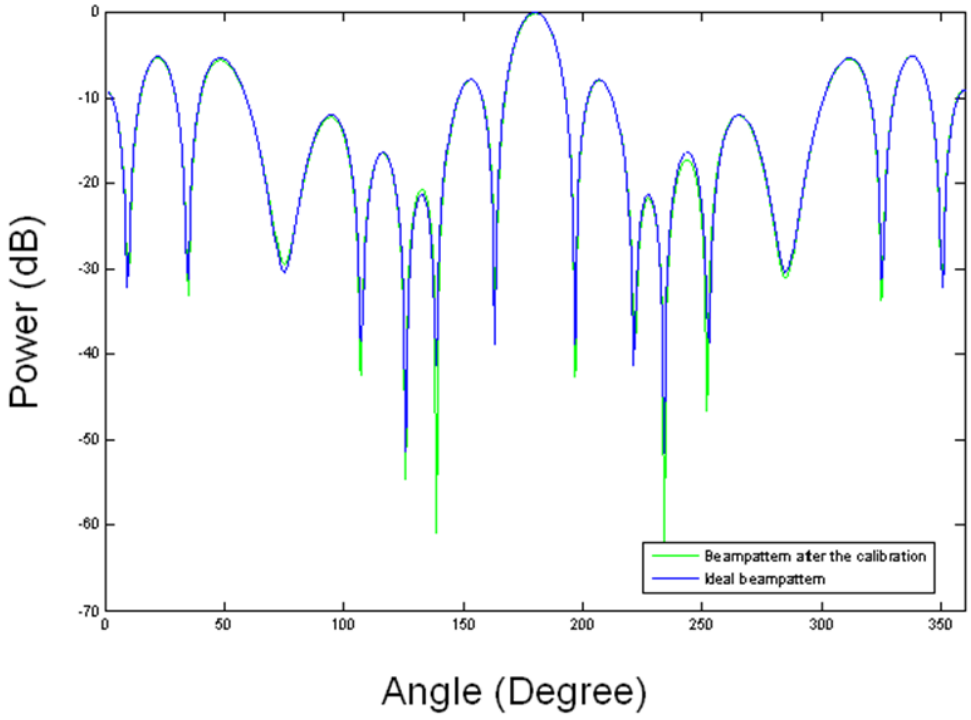

Figure 3.4.2: Ideal and calibrated beampattern, beam steering direction:180º.

Before calibration, the main beam of the beampattern is shifted and attenuated slightly and the sidelobe levels increase significantly. After the calibration, the beam pattern is very close to the ideal beampattern. Although there are still some very small differences in the sidelobe structure, the main beam is nearly the same as the ideal main beam and can be easily distinguished from the sidelobes.

3.4.2 Calibration Error Analysis

The calibration error is defined as the absolute value of the difference between the estimated value and the real value of a parameter. Figure 3.4.3 shows the averaged channel gain of 7 channels was quite accurately estimated with an averaged calibration error of 0.00146 after convergence which was significantly reduced from the initial value - 0.153.

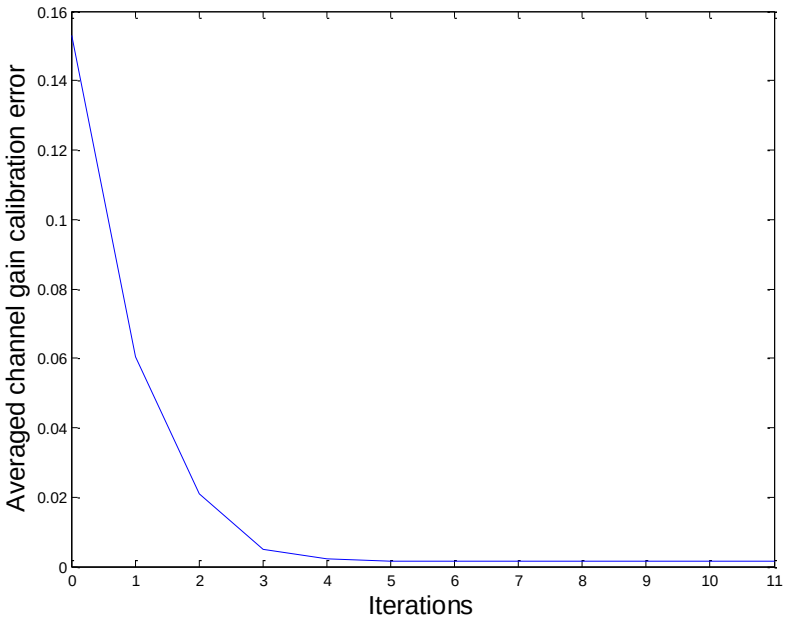

Figure 3.4.3: Averaged channel gain calibration error versus iteration number.

Figure 3.4.4 shows the calibration errors of the channel with the largest initial gain error – channel 8, the channel with the lowest initial gain error – channel

6 and the channel with no initial error – channel 1. Although these three channels had very different initial values, they have about the same convergence rate.

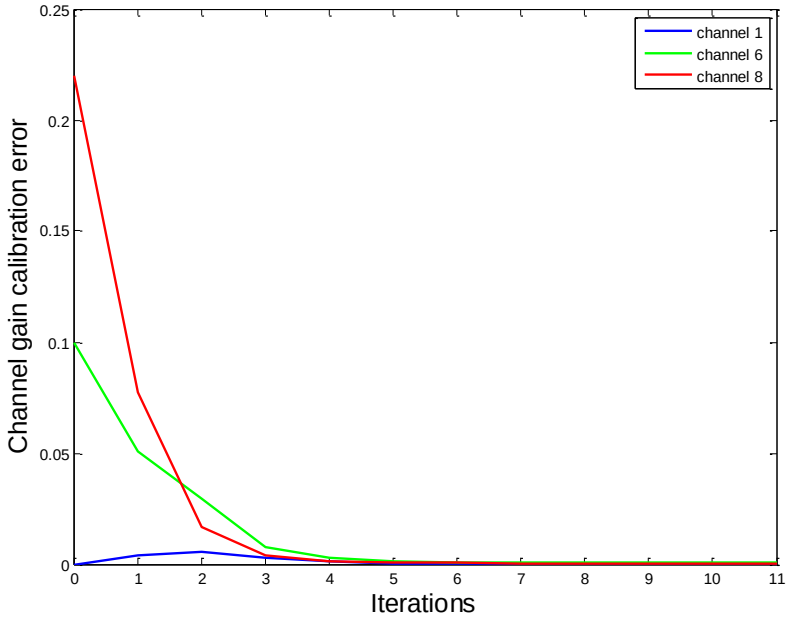

Figure 3.4.4: Gain calibration error of channel 1, 6 and 8.

Figure 3.4.5 shows the averaged mutual coupling calibration error was 0.003 after convergence which was not as good as the gain/phase error estimation, but it was still a large improvement from the initial averaged mutual coupling error of 0.116.

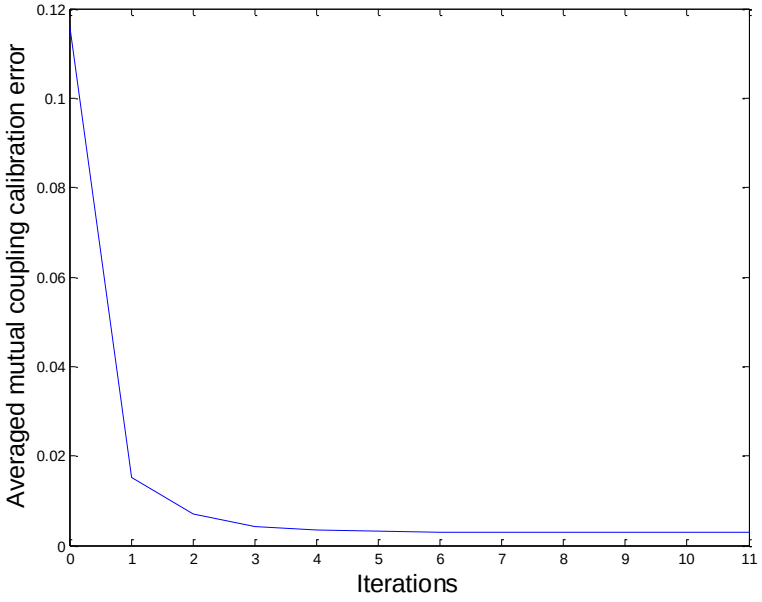

Figure 3.4.5: Averaged mutual coupling calibration error versus iteration number.

As shown in figure 3.4.6, the array orientation estimation converged after one iteration. The orientation was accurately estimated to be 10.01º, where 0.01º was the array orientation searching step.

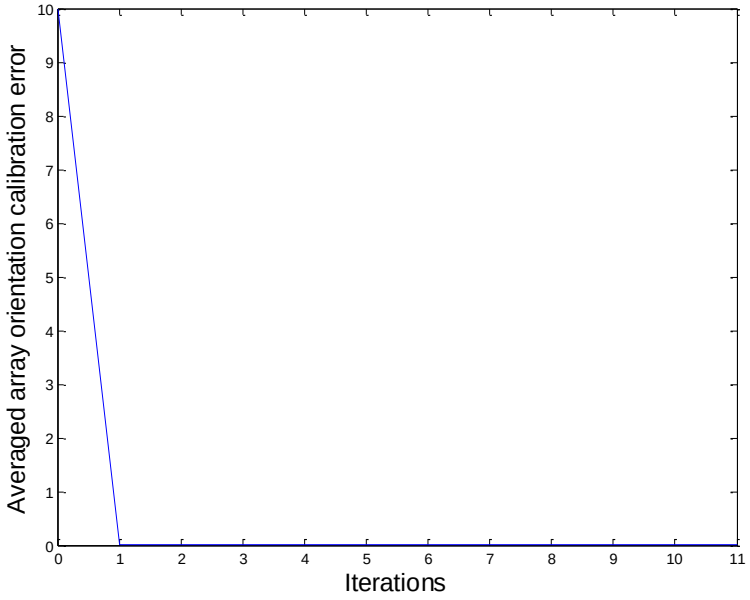

Figure 3.4.6: Orientation estimation error in degrees versus iteration number.

3.4.3 Effect of the Number of Calibration Sources and DOAs

Monte Carlo analysis was conducted to test the algorithm's performance for the number of calibration sources and their DOAs. The azimuth and elevation DOAs of the calibration sources were randomly and uniformly generated from 0° to 360° and from 0° to 90° respectively. 200 simulations were conducted for each test. Figure 3.4.7 shows the mean and standard deviation (STD) of the estimated array orientations. The algorithm performed well in all the test cases except for 2 calibration sources, which is expected as discussed in Section 3.2.4.

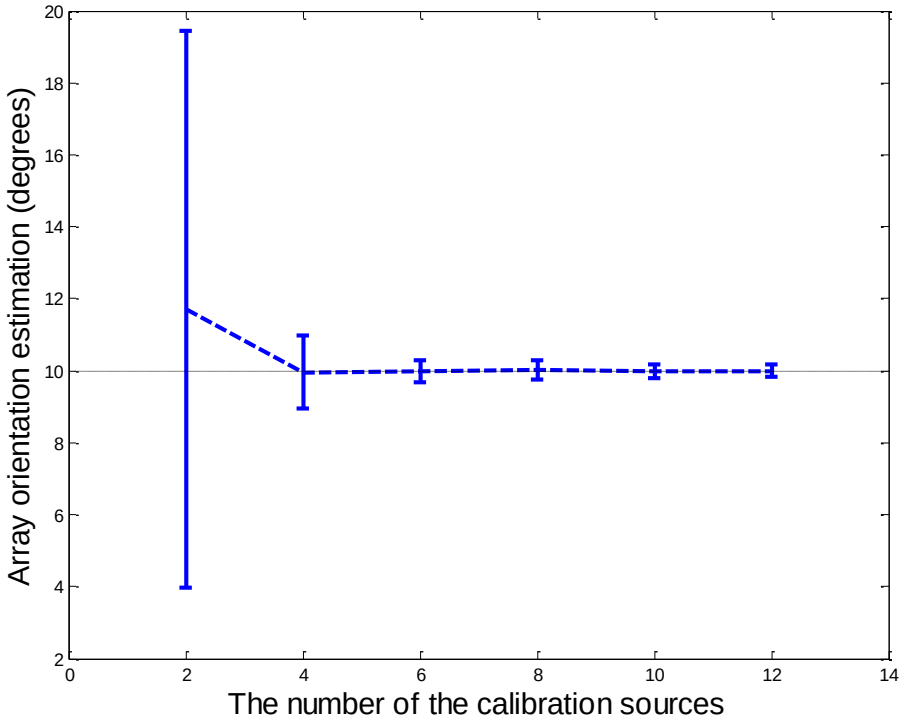

Figure 3.4.7: Statistical performance (mean and STD) of array orientation estimation.

The details of an example of the effect of a different number of calibration sources are discussed below. The results are analysed using 6, 4 and 2 calibration sources. The elevation angle was 45° for all sources.

1. The azimuth DOAs for the 6 calibration sources were 56°, 98°, 146°, 250°, 290° and 325°.
2. The azimuth DOAs for the 4 calibration sources were 56^0, 98^0, 250^0 and 290^0.
3. The azimuth DOAs for the 2 calibration sources were 56^0 and 250^0.

As shown in figure 3.4.8, the calibration cost function value of 2 calibration sources is very small after convergence but its convergence rate is much slower than 4 and 6 calibration sources. 6 calibration sources have the fastest convergence rate. However, 2 and 4 calibration sources have a lower calibration cost function value at convergence than 6 calibration sources. This can be due to the lesser number of least squares equations for 2 and 4 calibration sources. Although 2 and 4 calibration sources have a lower cost function value at convergence, figure 3.4.9 shows 6 calibration sources have better mutual coupling estimation accuracy than 2 and 4 sources. This suggests more calibration sources provide better calibration accuracy but not lower cost function convergence value.

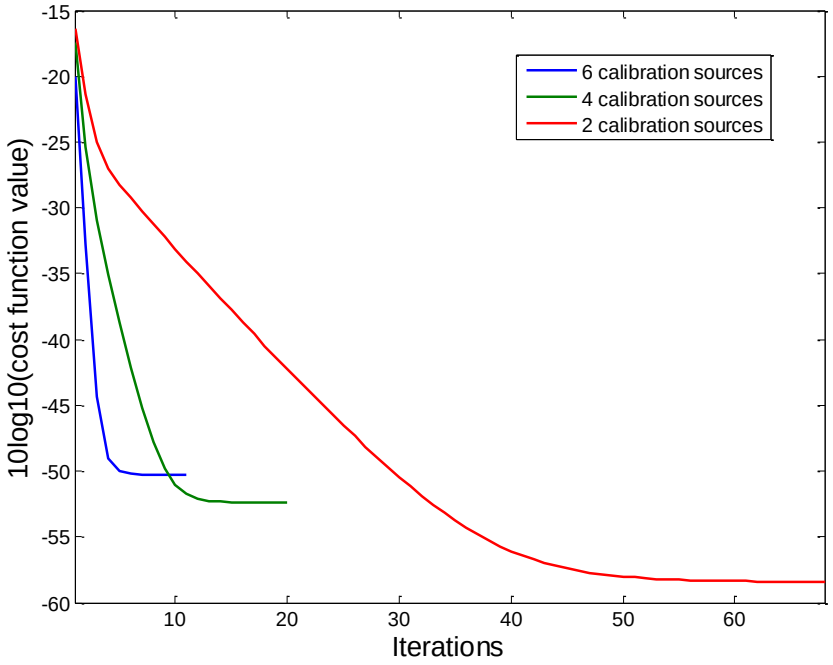

Figure 3.4.8: Cost function value with different number of calibration sources versus iteration number.

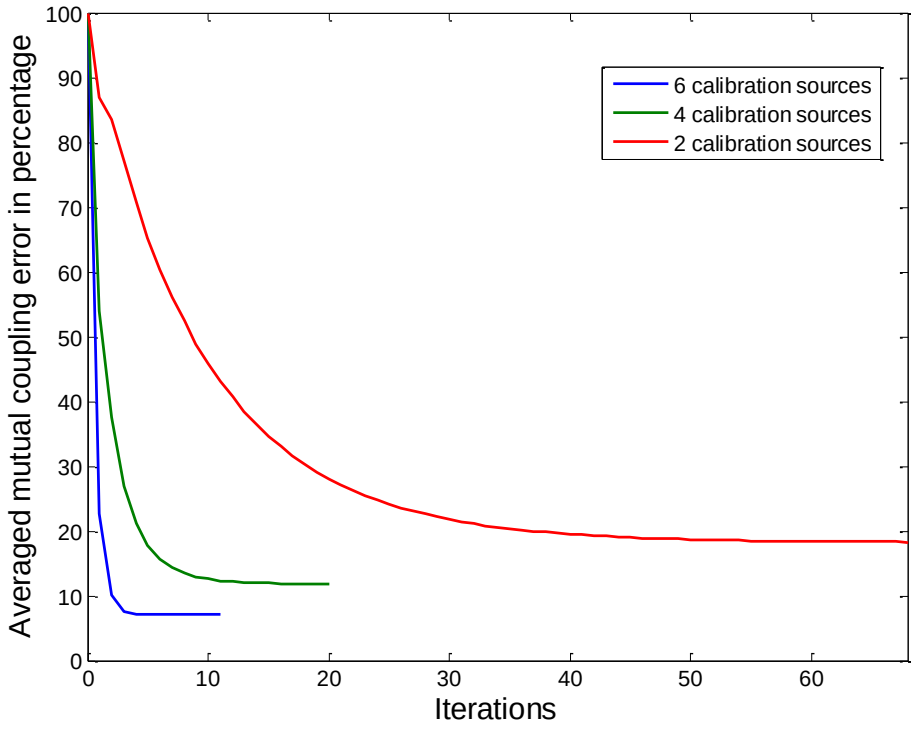

Figure 3.4.9: Averaged mutual coupling relative error with different number of calibration sources versus iteration number. The percentage is calculated by the formula error_in_percentage = estimation_error/initial_error*100%.

Figure 3.4.10 shows the mean and 95% confidence interval of the array orientation estimation performance with different number of the sources versus source SNR. 100 simulations were conducted for each test with different noise realisations. The result shows 6 calibration sources have the best estimation accuracy and variation. As the calibration source SNR increases to 20dB, the estimation mean value 10.006º of 6 source calibration converges to the true array orientation error 10º, while the estimation mean values of 4 and 2 calibration sources have a bias of 0.150º and 1.553º respectively.

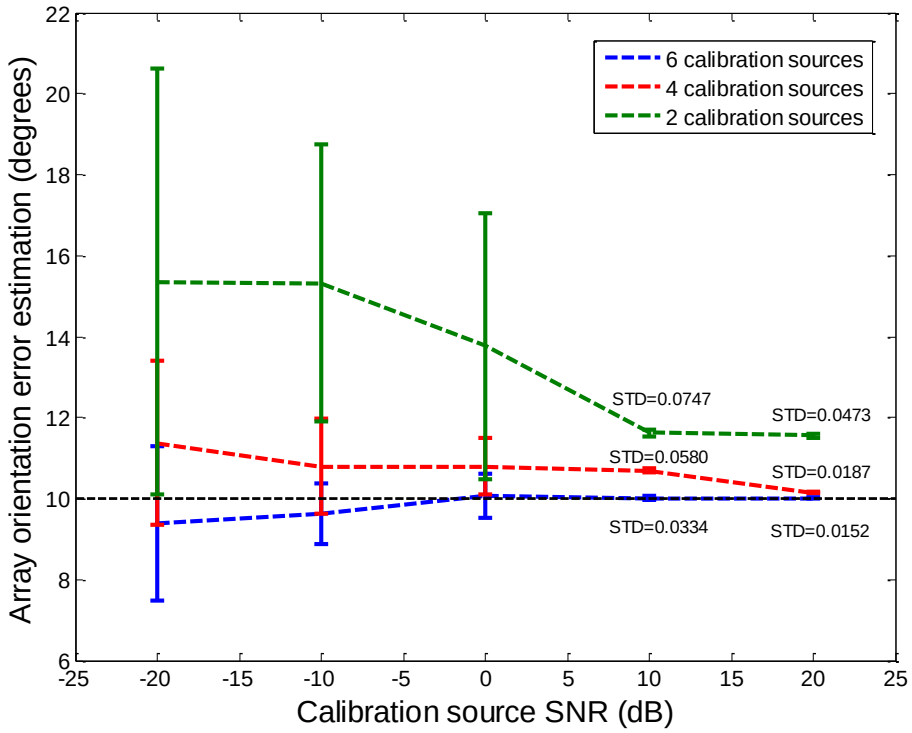

Figure 3.4.10: Array orientation error estimation mean and 95% confidence interval with different number of calibration sources versus the calibration source SNR.

3.4.4 Comparison between Orientation Error Estimation and Source DOA Estimation

One important feature of the proposed calibration algorithm is estimating the antenna array orientation instead of the DOAs of the calibration sources. The performance of the two methods was analysed by Monte-Carlo simulations and are presented below. Each result was simulated by 100 independent experiments.

The channel 2 gain estimation mean values of the two methods are shown in figure 3.4.11. The true value of channel 2 gain is 1. The calibration with array orientation estimation has better estimation accuracy than the calibration with

source DOA estimation unless the calibration sources have SNRs larger than about 10dB or smaller than about -20dB. In these cases, the two methods have similar performance.

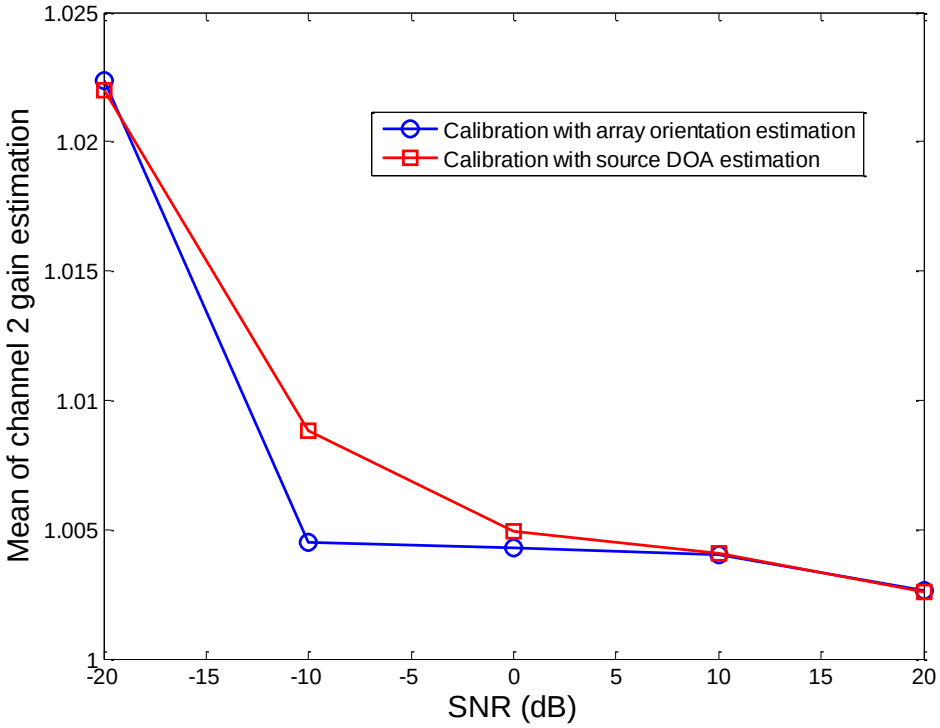

Figure 3.4.11: Channel 2 gain estimation mean values versus SNR using array orientation estimation (blue) and source DOA estimation (red).

As shown in figure 3.4.12, the array orientation estimation has a lower estimation standard deviation than the source DOA estimation for all source SNRs. The comparisons above show the array orientation estimation has better performance than the source DOA estimation in terms of smaller estimation errors and less variance.

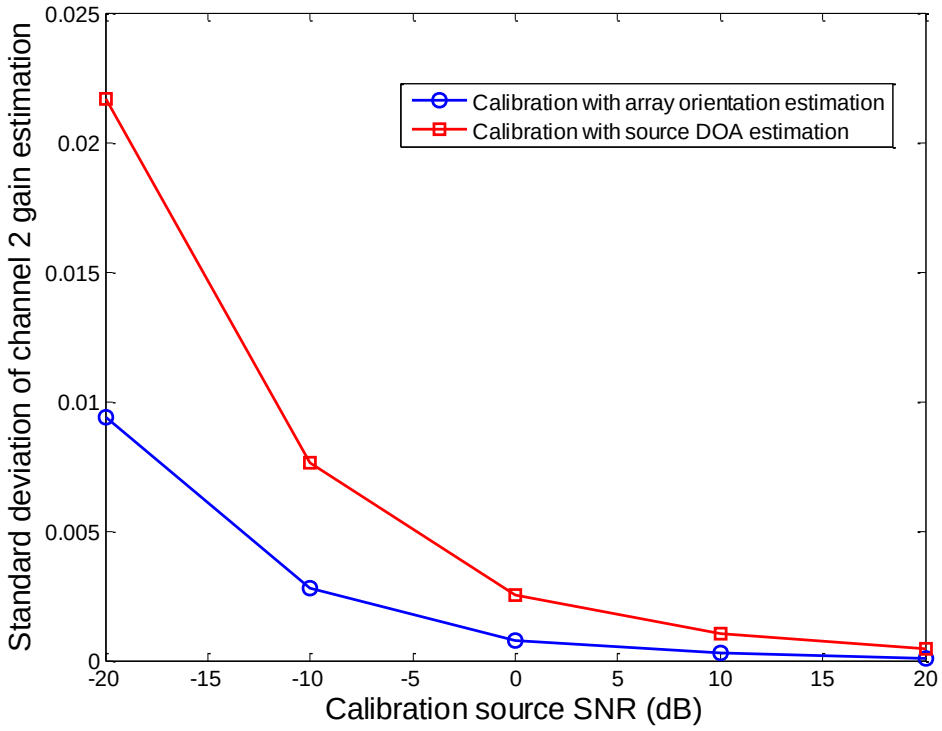

Figure 3.4.12: Channel 2 gain estimation standard deviation versus SNR using array orientation estimation (blue) and source DOA estimation (red)

3.5 Experimental Results

An experiment was carried out using real GPS signals with a uniform linear array of 4 dipole antennas spaced by 9 cm. The number of data points per channel that were used in the cross-correlation to extract the GPS signal was 800,000; this corresponds to a total time length of 50 ms at the sampling frequency of 16 MHz. The array was rotated to the southeast direction, which is 145º from north (The exact direction was unknown). After cross-correlation processing, 6 satellites 4, 7, 11, 13, 16, 23 were obtained. By referring to the GPS almanac, the azimuth and elevation angles of the satellites are given in table 3.5.1.

	SV 4	SV 7	SV 11	SV 13	SV 16	SV 23
Azimuth	222º	321º	328º	259º	68º	231º
Elevation	11º	8º	24º	31º	29º	55º

Table 3.5.1: GPS satellite DOAs referring to the GPS almanac.

By using the nominal array orientation value 145º, the DOAs of the GPS satellites, which are the projections of the azimuth and elevation angles onto the orientated plane of the array, are calculated in the table 3.5.2.

	SV 4	SV 7	SV 11	SV 13	SV 16	SV 23
DOA	77º	171º	156º	110º	79º	88º

Table 3.5.2: GPS satellite DOAs referring to the GPS antenna array with the nominal array orientation value.

The formula used for the above calculations is shown in equation 3.5.1.

$$DOA = \operatorname{acos}(\cos(azimuth - orientation) * \sin(90^0 - elevation)) \quad (3.5.1)$$

Satellites 4, 7, 13, 16 are used as the disjoint calibration sources while the directions of the satellites 11 and 23 are estimated by the calibrated array to verify the performance of the algorithm. (Please note the current number of calibration sources is 4. If joint sources are used to calibrate the array, the maximum number of the calibration sources will be limited by M-1 which is 3 for the current case, where M is the number of the antennas in the array).

After calibration, the algorithm gave the estimated parameters in table 3.5.3.

	CH1	CH2	CH3	CH4
Array orientation	134 º			
Channel gain	1	0.74	0.49	0.58
Channel phase error	0	-3º	6º	33º
Mutual coupling gain	1	0.15	0.073	0.067
Mutual coupling phase	0	10º	-159º	27º

Table 3.5.3: Estimated antenna array parameters.

	SV 4	SV 7	SV 11	SV 13	SV 16	SV 23
DOA	88 º	169 º	153 º	119 º	69 º	94 º

Table 3.5.4: GPS Satellite DOAs relative to the GPS antenna array after correcting the array orientation.

The estimated array orientation of 134º is in a southeasterly direction (145º) as expected. The array orientation was not measured accurately, but only with reference to a nearby road, hence cannot be compared directly to ground truth. However the DOA of the GPS signals given in table 3.5.1 are accurate and will be used to evaluate the accuracy of the calibration along with the general shape of the multiple signal classification algorithm (MUSIC) spectrum. MUSIC is a high resolution direction of arrival estimation algorithm and it is sensitive to the array errors, so the MUSIC spectra before and after calibration indicate the performance of the calibration algorithm.

Figure 3.5.1 and figure 3.5.2 show the MUSIC spectra before and after calibration for satellites 11 and 23. Both of the figures show an improvement in the height of the peaks and better DOA accuracy after calibration. The estimated DOAs of satellites 11 and 23 are 157º and 93.3º respectively which correspond reasonably well with the true GPS satellite DOAs given in

table 3.5.4. Thus the array manifold is closer to the true array manifold after calibration.

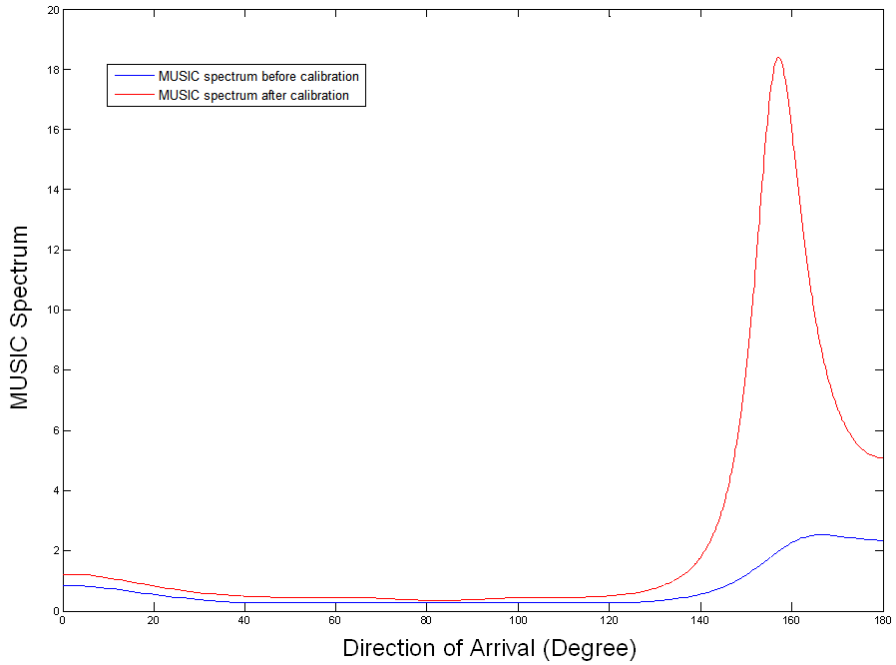

Figure 3.5.1: MUSIC spectrums before (blue) with peak value at 167.3º and after (red) the calibration with peak value at 157 º for satellite 11.

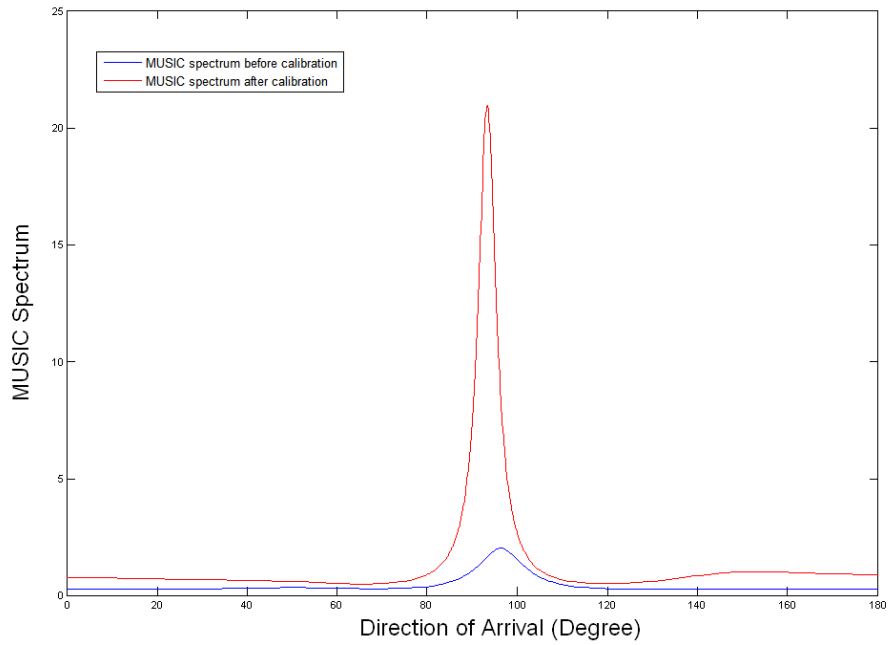

Figure 3.5.2: MUSIC spectrums before (blue) with peak value at 96.4º and after (red) the calibration with peak value at 93.3 º for satellite 23.

The calibration performance is further tested by splitting the 6 GPS data sets into the 4 calibration data sets and 2 test data sets differently. With 6 GPS data sets, the number of possible validation subsets is $C_6^2 = 15$, so the total number of DOAs to be tested is 30. The results of the DOA estimation errors are shown in figure 3.5.3. The small averaged estimation error (0.68°) suggests the calibration algorithm perform well for the experimental data sets.

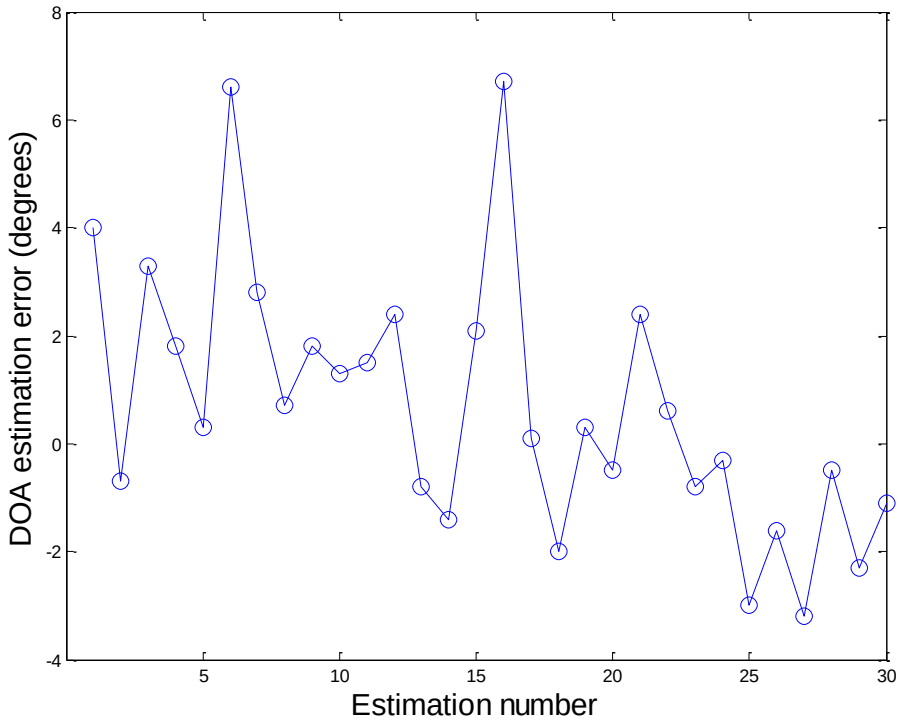

Figure 3.5.3: DOA estimation errors after calibration by cross validating the experimental data sets. Mean = 0.68°, STD = 2.44°.

3.6 Conclusion

In this chapter, an eigenstructure antenna array calibration algorithm based on a physical model of the array errors is presented. This algorithm uses GPS signals as the disjoint calibration sources to estimate the array orientation error, gain/phase errors and mutual coupling coefficients in the

antenna array with the assumption that if the estimation of these errors are correct, the model should be able to provide the true array manifold by making the signal subspace orthogonal to the noise subspace.

The simulations demonstrate an improvement in the beampattern after the calibration and give an accurate estimation of array error parameters. The simulations also indicate that the algorithm is computational efficient as an accurate estimation of the error parameters were achieved after only the first few iterations. Experimental results show improved DOA estimation accuracy and resolution. Results not presented here show that changing the order of the steps in the iterative process did not affect the final estimation result which was most sensitive to initial conditions.

So far the model has not included multipath components of the calibration sources which could occur due to ground reflections or nearby objects. This adds errors to the nominal DOAs of the calibration sources and couples with the mutual coupling effects degrading the calibration accuracy. In the next chapter, multipath signals will be included in the signal model and the additional parameters estimated by an alternating projection based calibration process.

Chapter 4: GPS Antenna Array Calibration II: Mutual Coupling Calibration in the Presence of Multipath Signals

4.1 Introduction

Chapter 3 discussed an eigen-structure based calibration method using direct path line of sight (LOS) GPS signals as the disjoint calibration sources. However, GPS signals suffer from reflections from various objects such as the ground, hills and buildings, which is commonly known as the GPS multipath problem. The GPS multipath signals are typically highly correlated or fully coherent with the LOS signals due to their limited bandwidth. High resolution subspace based direction of arrival (DOA) estimation methods, such as the MUltiple Signal Classification algorithm (MUSIC) in Chapter 3, assume the received signals are uncorrelated. As a result the performance of these algorithms will be degraded or even fail completely in a multipath environment. Various algorithms have been developed to solve the multipath problem in both antenna array and GPS signal processing.

In the antenna array processing area, there are two main categories of algorithms that are able to estimate the DOAs of correlated signals: Maximum Likelihood (ML) based algorithms and spectrum based low computational algorithms.

The Maximum Likelihood (ML) methods for DOA estimation [60, 98-102] estimate the DOAs of signals by using a multi-dimensional grid based search to maximise the likelihood function (LF). The ML estimators are not easy to implement in practice due to the high computational complexity [103]. Some ML algorithms with reduced complexity have been developed, such as the

Alternating Projection (AP) algorithm [104], Expectation Maximisation (EM) algorithm [105, 106], Data Supported Optimisation algorithm (DSO) [103] and Space-Alternating Generalised EM (SAGE) algorithm [107]. The Alternating Projection algorithm is particularly interesting due to its low computational burden, straight forward structure and fast convergence rate.

The classic spectrum based algorithms are quadratic based Minimum Variance Distortionless Response (MVDR) or Capon algorithm [108], subspace based MUtiple Signal Classification (MUSIC) algorithm [59, 60] and Estimation of Signal Parameter via Rotational Invariance Techniques (ESPRIT) algorithm [109-111]. These algorithms suffer significant performance degradation or even fail if the incoming signals are highly correlated or fully coherent [112]. However there are techniques that can make them robust to correlated signals. The most common technique is spatial smoothing [113-116]. However, due to the need to construct sub-arrays, the applications of the spatial smoothing techniques lead to a lower resolution due to the loss in the number of degrees of freedom and are also constrained to particular array configurations like uniform linear arrays (ULA) and uniform circular arrays (UCA).

In GPS applications, multipath error is one of the most significant causes of accuracy degradation in position estimation. As a result multipath signal detection and mitigation methods have been widely researched in the GPS area. For single antenna systems, the well-known narrow correlator [117], the strobe correlator [118, 119] and the double delta correlator [120] have been proposed to reduce distant multipath, but they are not effective in mitigating short delay multipath (close reflections) [121]. For antenna array applications, various methods and algorithms have been proposed and introduced into the GPS area, such as Maximum Likelihood (ML) [30], Alternating Projection (AP) [122], Space-Alternating Generalised EM (SAGE) [123-125] and statistical Constant False Alarm Rate (CFAR) multipath detector [126]. However these methods assume an ideal antenna array model, so their performance will drop in the presence of array errors such as mutual coupling between antennas.

Modern communication devices and systems tend to use smaller size antenna arrays. For conventional GPS receivers, there is often even less room for GPS antenna integration [125]. As a result, mutual coupling becomes a problem for these systems especially as the element separation in the antenna array is reduced below half of a wavelength [127]. Techniques for modelling, measuring and mitigating the mutual coupling effect between antennas are discussed in [78, 94-96, 127-134]. Multipath also affects the signal from the calibration sources. This will in turn have an impact on the resulting mutual coupling calibration accuracy. As a result it is important to model and account for mutual coupling within the calibration algorithm. A calibration algorithm that addresses this issue is the main focus of this chapter.

This chapter describes an algorithm that calibrates the mutual coupling effect in a GPS antenna array in the presence of multipath on the calibration sources. As in Chapter 3, the mutual coupling effects are modelled by a mutual coupling matrix based on the physical characteristics of the antenna array and the GPS signals are used as the disjoint calibration sources. The absolute DOAs of the GPS signals are known from their orbit models, however the DOAs of the GPS signals relative to the antenna array is not known due to the unknown orientation of the array. The calibration algorithm thus also estimates the array orientation error as part of the calibration process. The multipath signals of the calibration sources are incorporated into the calibration process by using a maximum likelihood approach and including the maximum number of expected multipath signals as additional signals in the likelihood function. The DOAs of the additional GPS multipath signals are estimated by Alternating Projection (AP) [104] which turns a multi-dimensional optimisation problem into an iterative process of one dimensional search.

The remainder of this chapter is structured as follows: The assumed calibration signal model is described in Section 4.2. In Section 4.3, the proposed calibration algorithm is outlined and simulation results are given in

Section 4.4. In Section 4.5, experimental results are presented. Finally, conclusion is given in Section 4.6.

4.2 Signal Model

4.2.1 Ideal Array Model

Following Chapter 3, consider an array of *M* elements with no mutual coupling and orientation errors. The vector form of the *M* sensor outputs is

$$\underline{x}(t) = \underline{v}(\theta, \varphi)s(t) + \underline{n}(t) \tag{4.2.1}$$

where $\underline{x}(t) = [x_1(t), x_2(t), \dots, x_M(t)]^T$, $\underline{v}(\theta, \varphi) = [e^{-j\omega\tau_1}, e^{-j\omega\tau_2}, \dots, e^{-j\omega\tau_M}]^T$ ($\underline{v}(\theta, \varphi)$ is the steering vector) and $\underline{n}(t) = [n_1(t), n_2(t), \dots, n_M(t)]^T$.

4.2.2 Mutual Coupling Model

The mutual coupling effects are described by matrices based on their physical models and included in the algorithm error minimisation process to parameterise the array model and hence reduce the number of parameters that need to be estimated to calibrate the array. This in turn reduces the number of calibration sources required to calibrate the array compared with other calibration algorithms that do not assume any underlying error model.

The mutual coupling model tries to describe the behaviour of the coupling between the antennas according to the shape of the antenna array using a matrix model. As discussed in Chapter 3, appropriate matrix models for the cases of uniformly spaced linear and circular arrays are given based on the assumption that the coupling between any two equally spaced antennas is

the same. If the array is a uniformly spaced linear array, the mutual coupling matrix will be banded symmetric Toeplitz matrix. If the array is a uniformly spaced circular array, the mutual coupling matrix will be a circulant symmetric matrix.

In this chapter, a uniformly spaced circular array with an additional antenna element in the centre to help reduce sidelobes was chosen. This array structure is used in [47] and [83]. To model the mutual coupling effect in this array configuration, the same assumptions as in [78] and [57] are used. The proposed mutual coupling matrix is shown by an example in figure 4.2.1. Note that this is different to Chapter 3 as this was what was used in the following experiment.

This example shows the modelled mutual coupling matrix for the array with 7 equally spaced circular antennas with an additional antenna in the centre, where *c1, c2, c3* and *c4* are the mutual coupling coefficients for the four antenna distances in the array.

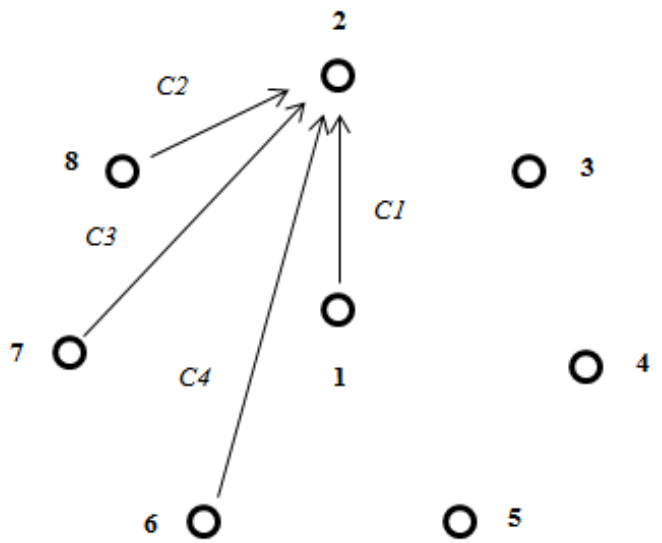

Figure 4.2.1: 8 elements array geometry – 7 element uniform circular array with 1 additional element in the centre.

If all the mutual coupling effects from all the antennas are included, the matrix is

$$\mathbf{C} = \begin{pmatrix} 1 & c1 & c1 & c1 & c1 & c1 & c1 & c1 \\ c1 & 1 & c2 & c3 & c4 & c4 & c3 & c2 \\ c1 & c2 & 1 & c2 & c3 & c4 & c4 & c3 \\ c1 & c3 & c2 & 1 & c2 & c3 & c4 & c4 \\ c1 & c4 & c3 & c2 & 1 & c2 & c3 & c4 \\ c1 & c4 & c4 & c3 & c2 & 1 & c2 & c3 \\ c1 & c3 & c4 & c4 & c3 & c2 & 1 & c2 \\ c1 & c2 & c3 & c4 & c4 & c3 & c2 & 1 \end{pmatrix} \quad (4.2.2)$$

Based on preliminary experimental measurements the mutual coupling of elements separated by greater than $\lambda/2$ could be ignored and only the mutual coupling effects from the adjacent antennas are considered, in this case the matrix is

$$\mathbf{C} = \begin{pmatrix} 1 & c1 & c1 & c1 & c1 & c1 & c1 & c1 \\ c1 & 1 & c2 & 0 & 0 & 0 & 0 & c2 \\ c1 & c2 & 1 & c2 & 0 & 0 & 0 & 0 \\ c1 & 0 & c2 & 1 & c2 & 0 & 0 & 0 \\ c1 & 0 & 0 & c2 & 1 & c2 & 0 & 0 \\ c1 & 0 & 0 & 0 & c2 & 1 & c2 & 0 \\ c1 & 0 & 0 & 0 & 0 & c2 & 1 & c2 \\ c1 & c2 & 0 & 0 & 0 & 0 & c2 & 1 \end{pmatrix} \quad (4.2.3)$$

The proposed matrix is similar to the mutual coupling model of uniformly spaced circular array, but has additional entries in the first column and the first row to describe inclusion of the centre antenna.

4.2.3 Array Model with Errors

The vector form of the antenna array outputs at the time *t* for a GPS satellite signal in the presence of an unknown array orientation error, mutual coupling, a single direct path signal and *P* multipath signals from the same source, *s(t),* is given by

$$\underline{x}(t) = \mathbf{CV}\underline{s}(t) + \underline{n}(t) \quad (4.2.4)$$

where,

$\underline{x}(t)$ is the antenna array outputs at the time *t*;

$\mathbf{C}$ is the mutual coupling matrix which is described in the above mutual coupling model section;

$\mathbf{V} = [\underline{v}(\theta + \theta_e, \varphi), \underline{v}(\theta_1, \varphi_1), \ldots, \underline{v}(\theta_P, \varphi_P)]$, $\underline{v}$ is the steering vector derived from the array geometry, θ and φ are the azimuth and elevation angles of the direct path signal which can be obtained based on the GPS almanac data and the user position, θ_e is the array orientation error which affects the azimuth angle estimation of the direct path signal, θ_p and φ_p are the azimuth and elevation angles of the p^{th} multipath signal;

$\underline{s}(t) = [s(t), s_1(t), s_2(t), \ldots, s_P(t))]^T$, $s(t)$ is the direct path signal at time t, $s_p(t) = A_p e^{j\varphi_p} s(t)$ is the p^{th} multipath signal at time t with an amplitude of A_p and a phase delay of φ_p;

$\underline{n}(t)$ is additive uncorrelated White Gaussian Noise in the array channels at time t.

The covariance matrix of this received signal is

$$\mathbf{R} = E\{\underline{x}(t)\underline{x}^H(t)\} \tag{4.2.5}$$

Once the covariance matrices are obtained, the array orientation error and the mutual coupling effects will be estimated by minimising a formulated cost function with respect to these errors.

4.2.4 Solution Existence Condition

This section considers the number of calibration signals that are required to ensure the existence of a solution. A simple example that assumes one multipath signal for each direct path signal is used to show how to determine the number of calibration sources required.

Consider an *M* (*M* is an even number) sensor array with *N* disjoint calibration sources. The array has *M-1* elements forming an *M-1* element uniformly spaced circular array and 1 element in the centre of the circular array. For each calibration source one multi-path signal is assumed to exist as well.

Based on the above model, there are *2(M/2)* mutual coupling parameters, 1 array orientation error parameter and *2N* multipath DOA parameters in the *M* sensor array. *N* disjoint sources give *2N(M-1)* least squares equations. Please note, if joint sources are used, this will be *2N(M-N)* and thus, the maximum number of calibration sources will be limited by the number of antennas in the array [91]. Hence, the solution exists when *2(M/2)+2N+1<= 2N(M-1)*, that is *N >= (M+1)/(2M-4)*. For example if the sensor number *M = 8*, the number of calibration sources *N* must *>= 1*.

4.3 Calibration Algorithm

The array manifold is the locus of steering vectors in a multidimensional space. If the parameters of the array are correctly estimated, the array manifold and the signal should span the same subspace at the signal bearings. This concept is adopted by the algorithm to construct the cost function. The array parameters are estimated by minimising the cost function until convergence is achieved.

4.3.1 Cost Function

Consider N disjoint GPS calibration sources, the estimated post-correlation covariance matrix for the n^{th} disjoint source is

$$\widehat{\mathbf{R}}_n = \frac{1}{T}\sum_{t=1}^{T} \underline{x}_n(t)\underline{x}_n{}^H(t) \tag{4.3.1}$$

where $\underline{x}_n(t)$is the vector of the M post-correlation sensor outputs for the n^{th} GPS source.

The noise is assumed to be uncorrelated White Gaussian Noise (WGN). The eigen decomposition of the n^{th} estimated covariance matrix $\widehat{\mathbf{R}}_n$ gives the estimated signal subspace $\widehat{\mathbf{E}}_n$ and the estimated noise subspace $\widehat{\mathbf{F}}_n$ as indicated in equation 4.3.2. In this Chapter, the multipath signals are assumed to be highly correlated or fully coherent with the direct path signal which means there is only one obvious large eigen-value, so the signal subspace $\widehat{\mathbf{E}}_n$ is a column vector. In the case of low correlation multipath signals, the signal subspace $\widehat{\mathbf{E}}_n$ will be a matrix and thus the vector $\underline{s}_n$ in equation 4.3.3 will become a matrix.

$$\widehat{\mathbf{R}}_n = \left[\widehat{\mathbf{E}}_n \vdots \widehat{\mathbf{F}}_n\right] \begin{bmatrix} \mathbf{\Lambda}_{s_n} + {\sigma_n}^2\mathbf{I} & \vdots & 0 \\ \cdots & \vdots & \cdots \\ 0 & \vdots & {\sigma_n}^2\mathbf{I} \end{bmatrix} \begin{bmatrix} {\widehat{\mathbf{E}}_n}^{\mathrm{H}} \\ \cdots \\ {\widehat{\mathbf{F}}_n}^{\mathrm{H}} \end{bmatrix} \tag{4.3.2}$$

The formulated cost function for an *M* element antenna array with *N* disjoint calibration sources and P_n multipath signals on the n^{th} calibration source is thus given by

$$\mathrm{Q} = \sum_{n=1}^{N} \left\| \underline{\hat{E}}_n - \mathbf{C}\mathbf{V}_{\boldsymbol{n}}\underline{S}_n \right\|^2_F \tag{4.3.3}$$

where,

Q is the value of the cost function;

$\mathbf{C}$ is the mutual coupling matrix described in the mutual coupling model section;

$\mathbf{V}_{\boldsymbol{n}} = [\underline{v}(\theta_n + \theta_e, \varphi_n), \underline{v}(\theta_{1_n}, \varphi_{1_n}), \ldots, \underline{v}(\theta_{P_n}, \varphi_{P_n})]$, $\underline{v}$ is the steering vector derived from the array geometry, θ_n and φ_n are the known azimuth and elevation angles of the n^{th} direct path signal which can be obtained based on

the GPS almanac data and the user position, θ_e is the unknown array orientation error of the horizontal array which affects the azimuth angle estimation of the direct path signal, θ_{p_n} and φ_{p_n} are the unknown elevation and azimuth angles of the p^{th} multipath signal for the n^{th} calibration source;

$\underline{s}_n$ is a complex vector that linearly combines array manifold vectors for the n^{th} calibration source. The values of the elements of $\underline{s}_n$ are not necessarily the signal amplitude and phase values (unlike $\underline{s}(t)$ in the signal model), but rather relate the array manifold $\mathbf{CV_n}$ to the signal subspace $\hat{\underline{\mathbf{E}}}_n$. The relative amplitude ratios and phase differences of the complex elements are the amplitude ratios and phase differences of the direct path and multipath signals. It is similar to the normalised post correlation signals which lose the absolute amplitude and phase information but the relative relationships are kept.

Note that the cost function in equation 4.3.3 is different to that used Chapter 3 due to the necessity of having to estimate both the DOAs and relative amplitudes of the multipath components.

4.3.2 Calibration Algorithm Flow Chart

As shown in figure 4.3.1, the proposed algorithm iterates between four steps:

- Step 1, the array orientation error is estimated using the estimated array parameters in the last round.
- Step 2, the DOAs of the multipath signals are estimated using the array orientation angle obtained from step 1 and the mutual coupling matrix from the last round.
- Step 3, the complex numbers which fit the array manifold to the signal subspace are estimated using the array orientation error obtained from step 1, the DOAs of multipath signals from step 2 and the mutual coupling matrix from last iteration.

- Step 4, the mutual coupling matrix is estimated by using the array orientation error obtained from step 1, the DOAs of the multipath signals from step 2 and the fitting complex numbers from step 3. The process will complete when the cost function converges. The final array orientation error and the mutual coupling matrix are the estimated results.

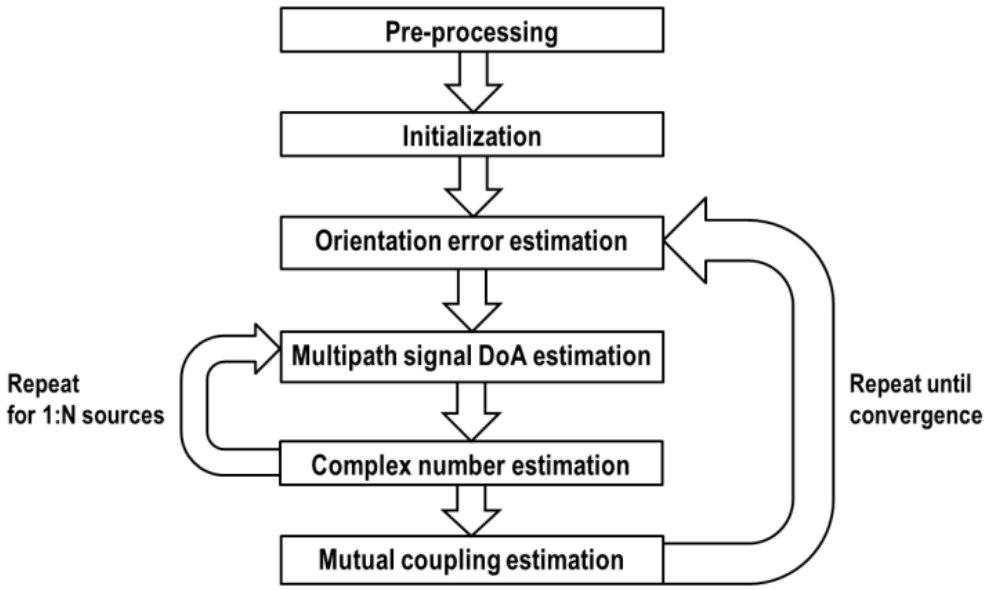

Figure 4.3.1: Calibration algorithm flow chart.

4.3.3 Pre-processing

In the pre-processing step, the gain/phase responses with respect to the different frequencies in the system bandwidth of each channel are measured using a spectrum analyser with the inputs of each channel terminated. A Wiener filter is applied to the received data to match the gain/phase responses of all the channels to the reference channel which is chosen to be channel 1 in this chapter and corresponds to the central element of the array.

After applying the above gain/phase calibration on the received data, the covariance matrix of each GPS signal across the antenna array is extracted separately by cross correlating the CA code with that particular GPS signal

and integrating. As the GPS signals can be separated in this way, the post-correlation covariance matrices for each GPS satellite can be treated as resulting from disjoint sources, although the GPS satellites are actually transmitting at the same time.

4.3.4 Initialization

The initial values of the mutual coupling matrix **C** can be selected based on prior knowledge. If there is no prior knowledge, **C** will be initialised to be the identity matrix $\mathbf{I}_M$.

The DOAs of the calibration sources (direct path signals) are calculated from the constellation of the satellites and the location of the antenna array. If the array orientation error θ_e can be estimated a-priori, this angle will be included to calculate the azimuth angles of the direct path signals.

4.3.5 Array Orientation Error Estimation

The values of the DOAs of multipath signals and the mutual coupling matrix **C** from the last round are used as the current values and fixed in the cost function. If this is the first iteration, the initial value of **C** is used and the estimation assumes an absence of multipath signals. The complex vector $\underline{s}_n$ is not involved in the steering vector parameter estimations in this and the next sections, because it becomes a scalar in the projection operation.

The array orientation error θ_e at the k^{th} iteration is estimated using a maximum-likelihood approach

$$\hat{\theta}_e^{\,k} = arg\,\max_{\theta_e} \sum_{n=1}^{N} \left\| \mathbf{P}_{\mathbf{C}^{k-1}\mathbf{V}_n(\theta_e)} \hat{\underline{E}}_n \right\|_F^2 \qquad (4.3.4)$$

where $\mathbf{V_n} = [\underline{v}(\theta_n + \theta_e, \varphi_n), \underline{v}(\theta_{1_n}{}^{k-1}, \varphi_{1_n}{}^{k-1}), \ldots, \underline{v}(\theta_{P_n}{}^{k-1}, \varphi_{P_n}{}^{k-1})]$ and **P** is the projection operator defined as $\mathbf{P_A} = (\boldsymbol{A}^H\boldsymbol{A})^{-1}\boldsymbol{A}^H$, *H* is the Hermitian transpose. In the first iteration, where multipath is assumed to be absent, $\mathbf{V_n} = \underline{v}(\theta_n + \theta_e, \varphi_n)$ and $\mathbf{P_A} = \{[\mathbf{C}\underline{v}(\theta_n + \theta_e, \varphi_n)]^H\mathbf{C}\underline{v}(\theta_n + \theta_e, \varphi_n)\}^{-1}[\mathbf{C}\underline{v}(\theta_n + \theta_e, \varphi_n)]^H$.

The maximisation defined by the equation above is performed by a grid (0.01° step size) search over the space of θ_e. The corresponding angle at which the maximum occurs is the estimated orientation error.

4.3.6 Multipath DOA Estimation

The values of the array orientation error estimated from this iteration and the mutual coupling matrix **C** from the last iteration are used as the current values and fixed in the cost function.

Consider P_n multipath signals exist for the *n*th calibration source. The $p_n{}^{\text{th}}$ multipath signal's DOA is estimated by using the DOAs of the 1st, 2nd, … , $(p-1)_n{}^{\text{th}}$ multipath signals estimated in this iteration and the DOAs of the $(p+1)_n{}^{\text{th}}$, …, $P_n{}^{\text{th}}$ multipath signals estimated from the last iteration.

The azimuth and elevation angles θ_{p_n} and φ_{p_n} of the $p_n{}^{\text{th}}$ multipath signal for the n^{th} calibration source at the *k*th iteration are estimated by

$$(\hat{\theta}_{p_n}, \hat{\varphi}_{p_n})^k = arg \max_{\theta_{p_n}, \varphi_{p_n}} \left\| \mathbf{P}_{\mathbf{C}^{k-1}\mathbf{V}_n(\theta_{p_n}, \varphi_{p_n})} \underline{\hat{\mathrm{E}}}_n \right\|_{\boldsymbol{F}}^{\mathbf{2}} \qquad (4.3.5)$$

where

$\mathbf{V_n} = [\underline{v}(\theta_n + \theta^k{}_e, \varphi_n), \underline{v}(\theta_{1_n}{}^k, \varphi_{1_n}{}^k), \ldots, \underline{v}(\theta_{p_n}, \varphi_{p_n}), \ldots, \underline{v}(\theta_{P_n}{}^{k-1}, \varphi_{P_n}{}^{k-1})]$ and **P** is the projection operator defined as $\mathbf{P_A} = (\boldsymbol{A}^H\boldsymbol{A})^{-1}\boldsymbol{A}^H$.

The maximisation is performed by a grid (0.01° step size) search over the space of the azimuth and elevation angles of the multipath signals. The corresponding angle at which the maximum occurs is the estimated DOAs. The multipath DOA estimation iterates through the multipath signals of all the calibration sources using Alternating Projection.

4.3.7 Complex Number Estimation

The values of the array orientation error and DOAs of the multipath signals estimated from this round and the mutual coupling matrix **C** from the last round are used as the current values and fixed in the cost function.

The complex vector $\underline{s}_n$ for *n*th calibration source at k^{th} iteration is estimated by the linear least squares estimator as follows

$$\underline{\hat{s}}_n{}^k = \left[\left(\mathbf{C}^{k-1}\mathbf{V_n}{}^k\right)^H\left(\mathbf{C}^{k-1}\mathbf{V_n}{}^k\right)\right]^{-1}\left(\mathbf{C}^{k-1}\mathbf{V_n}{}^k\right)\underline{\hat{\mathrm{E}}}_n \qquad (4.3.6)$$

where $\mathbf{V_n} = [\underline{v}(\theta_n + \theta_e{}^k, \varphi_n), \underline{v}(\theta_{1_n}{}^k, \varphi_{1_n}{}^k), \ldots, \underline{v}(\theta_{P_n}{}^k, \varphi_{P_n}{}^k)]$ and *H* is the Hermitian transpose.

4.3.8 Mutual Coupling Matrix Estimation

In this step, the mutual coupling matrix is estimated by minimising the cost function with respect to the mutual coupling matrix. The values of the orientation error θ_e, the DOAs of the multipath signals and the complex vector $\boldsymbol{s}_n$ estimated by the latest previous steps are used as the current values and are fixed in the cost function. If the current iteration number is *k*, the cost function is given by

$$Q^k = \sum_{n=1}^{N} \left\| \underline{\widehat{\mathrm{E}}}_n - \mathbf{C}\mathbf{V}_n{}^k \underline{S}_n{}^k \right\|_F^2 \tag{4.3.7}$$

Consider an *M* sensor antenna array with *M-1* sensors forming a uniformly spaced circular array and 1 additional antenna in the centre of the circle. The mutual coupling matrix which describes this array configuration is given in Section 4.2.2. There are *M/2* unknown complex parameters in the mutual coupling matrix if *M* is an even number or *(M+1)/2* unknown complex parameters in the mutual coupling matrix if *M* is an odd number. Assume *M* is an even number. The cost function in equation 4.3.7 can be rewritten as

$$Q^k = \sum_{n=1}^{N} \left\| \underline{\widehat{\mathrm{E}}}_n - \boldsymbol{\alpha}_n{}^k \, \underline{c} \right\|_F^2 \tag{4.3.8}$$

where $\underline{c}$ is a *(M/2+1)×1* vector containing all the unknown parameters in the mutual coupling matrix and $\underline{\mathrm{c}} = [c1, 1, c2, c3, \dots, c_{M/2}]^T$, $\boldsymbol{\alpha}_n{}^k$ is a *M×(M/2+1)* matrix created from the matrix product $\mathbf{V}_n{}^k \underline{S}_n{}^k$, the expression for $\boldsymbol{\alpha}_n{}^k$ is given below

$$[\boldsymbol{\alpha}_n{}^k]_{pq} = \begin{cases} \sum_{i=2}^{M} [\underline{d}]_i, & p = 1, q = 1 \\ [\underline{d}]_1, & p = 1, q = 2 \\ 0, & p = 1, q \neq 1\&2 \\ [\underline{d}]_1, & q = 1 \\ \sum_{i=1}^{4} [\boldsymbol{W_i}]_{pq}, & otherwise \end{cases} \tag{4.3.9}$$

where $\underline{d} = \mathbf{V}_n{}^k \underline{S}_n{}^k$**,** and matrices $\boldsymbol{W_1}, \boldsymbol{W_2}, \boldsymbol{W_3}, \boldsymbol{W_4}$ are given as

$$\begin{aligned} [\boldsymbol{W_1}]_{pq} &= \begin{cases} [\underline{d}]_{p+q-2,} & p+q \leq M+3 \\ 0, & otherwise \end{cases} \\ [\boldsymbol{W_2}]_{pq} &= \begin{cases} [\underline{d}]_{p-q+2,} & p \geq q \geq 3 \\ 0, & otherwise \end{cases} \\ [\boldsymbol{W_3}]_{pq} &= \begin{cases} [\underline{d}]_{M+1+p-q,} & p < q \leq M/2 \\ 0, & otherwise \end{cases} \end{aligned} \tag{4.3.10}$$

$$[\boldsymbol{W_4}]_{pq} = \begin{cases} [\underline{d}]_{p+q-M-1,} & 3 \le q \le M/2\,, p+q \ge M+4 \\ 0, & otherwise \end{cases}$$

Combine *N* sources into one least squares solution,

$$Q^k = \left\| \hat{\mathbf{E}} - \boldsymbol{\gamma}^k \underline{\mathrm{c}} \right\|_F^2 \tag{4.3.11}$$

where $\hat{\mathbf{E}} = \left[\underline{\hat{\mathrm{E}}}_1{}^{\mathrm{T}}, \underline{\hat{\mathrm{E}}}_2{}^{\mathrm{T}}, \ldots, \underline{\hat{\mathrm{E}}}_N{}^{\mathrm{T}} \right]^{\mathrm{T}}$ and $\boldsymbol{\gamma} = [\boldsymbol{\alpha}_1{}^{\mathrm{T}}, \boldsymbol{\alpha}_2{}^{\mathrm{T}}, \ldots, \boldsymbol{\alpha}_N{}^{\mathrm{T}}]^{\mathrm{T}}$**.**

The minimisation problem becomes to be a linear least squares problem with linear constraints $\underline{w}^{\mathrm{H}}\, \underline{\hat{\mathrm{c}}}^k = 1$, where $\underline{w} = [0, 1, 0 \ldots, 0]^T$. The solution to this problem is

$$\underline{\hat{\mathrm{c}}}^k = \underline{\hat{\mathrm{c}}}_{\mathrm{u}}^k - \left(\boldsymbol{\gamma}^{k\mathrm{H}} \boldsymbol{\gamma}^k \right)^{-1} \underline{w} \left[\underline{w}^{\mathrm{H}} \left(\boldsymbol{\gamma}^{k\mathrm{H}} \boldsymbol{\gamma}^k \right)^{-1} \underline{w} \right]^{-1} (\underline{w}^{\mathrm{H}}\, \underline{\hat{\mathrm{c}}}_{\mathrm{u}}^k - 1) \tag{4.3.12}$$

where $\underline{\hat{\mathrm{c}}}_{\mathrm{u}}^k = (\boldsymbol{\gamma}^{k\mathrm{H}} \boldsymbol{\gamma}^k)^{-1} \boldsymbol{\gamma}^{k\mathrm{H}}\, \underline{\hat{\mathrm{E}}}$ is the linear least squares solution with no constraints.

4.3.9 Convergence Check

The cost function value Q^k is calculated at the end of each round. If the difference in the previous and current cost function value is larger than a pre-set threshold ε, ie.

$$Q^{k-1} - Q^k > \varepsilon \tag{4.3.13}$$

another iteration of the algorithm is performed, otherwise the calibration algorithm will stop and the current array orientation error and mutual coupling matrix are taken to be the estimated results.

4.4 Simulation Results

In the simulations, no prior knowledge of the array parameters was assumed. The antenna array configuration is shown in figure 4.2.1. It had 8 omni-directional antennas, 7 of them forming a uniformly distributed circular array with a radius of 1.25λ and one additional antenna in the centre of the circle.

There were 12 far-field narrow band GPS calibration sources. Each GPS signal had a SNR of -20dB and a data length of 300,000 samples. The DOAs of the 12 GPS calibration sources are in table 4.4.1. After the correlation and integration, the SNR of each source was 20dB and the number of available snapshots was 30. In all simulations, the calibration sources were assumed to have 1 multipath signal with an SNR of 10dB after correlation.

Source number	**01**	**02**	**03**	**04**	**05**	**06**
Azimuth angle	230.00º	223.86º	43.73º	241.49º	308.59º	268.60º
Elevation angle	48.41º	11.55º	36.40º	19.77º	29.70º	44.32º
Source number	**07**	**08**	**09**	**10**	**11**	**12**
Azimuth angle	137.99º	77.28º	73.47º	90.26º	289.47º	16.37º
Elevation angle	22.22º	43.48º	12.74º	13.79º	30.94º	23.96º

Table 4.4.1: DOAs of the 12 GPS calibration sources.

The array parameters are:

- The antenna array orientation: 10^0.
- Mutual coupling effect between antennas as shown in table 4.2.2.

	C 1	C 2	C 3	C 4
Gain (amplitude)	0.2	0.22	0.15	0.1
Phase (degrees)	174.27^0	-133.01^0	82.06^0	19.33^0

Table.4.4.2: Mutual coupling coefficients for the fixed distances between two antennas.

As shown in figure 4.4.1, the calibration algorithm converges after 12 iterations.

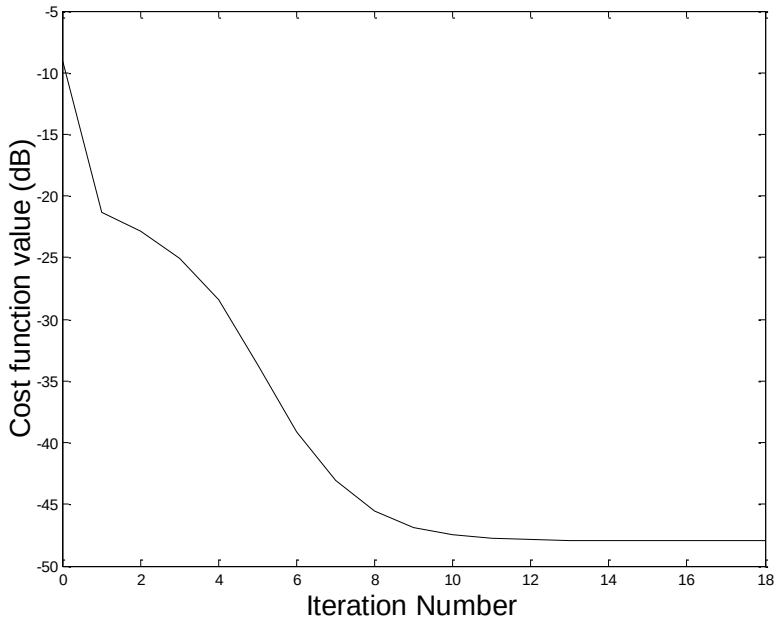

Figure.4.4.1: Cost function value versus iterations.

The estimated array orientation error and mutual coupling coefficients are:

- The estimated antenna array orientation: 10^0.
- Estimated mutual coupling effect between antennas.

	C 1	C 2	C 3	C 4
Gain (amplitude)	0.2015	0.2199	0.1469	0.0987
Phase (degrees)	174.20^0	-132.68^0	82.38^0	18.88^0

Table.4.4.3: Estimated mutual coupling coefficients.

The calibration results are very accurate. The array orientation error is identical to the simulation value and the mutual coupling coefficients are within 2.5% of the correct values. The accuracy of the calibration can be seen by comparing the resulting beampatterns of the calibrated array with that of an ideal, perfectly calibrated array.

Figure 4.4.2 and figure 4.4.3 show the ideal beampattern and the beampattern before and after the proposed calibration scheme is applied. The beampatterns are those of the conventional beamformer.

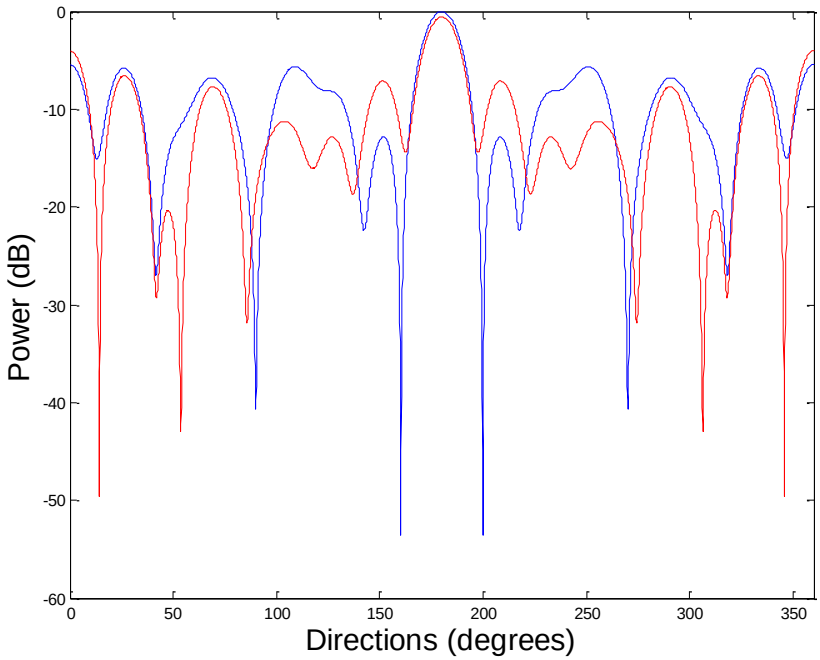

Figure 4.4.2: Ideal beampattern (blue) and beampattern without calibration (red), main beam steering direction: 180^0, elevation angle = 0^0.

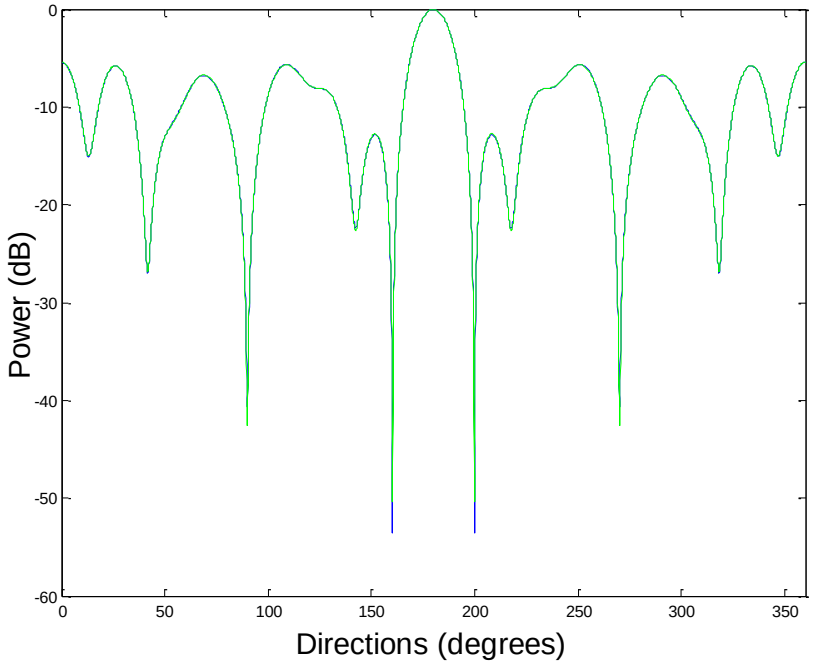

Figure 4.4.3: Ideal beampattern (blue) and beampattern with calibration (green), main beam steering direction: 180^0, elevation angle = 0^0.

Before calibration, the main beam of the beampattern without calibration is attenuated slightly and the highest sidelobe level increases. After calibration, the beampattern is very close to the ideal beampattern. Although there are still some very small differences in the null and sidelobe structure, the main beam is the same as the ideal main beam and can be easy distinguished from the sidelobes.

4.5 Experimental Results

4.5.1 Experiment Setup

An experiment was carried out with a 7 element equally spaced circular monopole antenna array with one monopole antenna in the centre. The

radius of the circular array was 25cm (1.3129λ). The actual array picture is shown in figure 4.5.1.

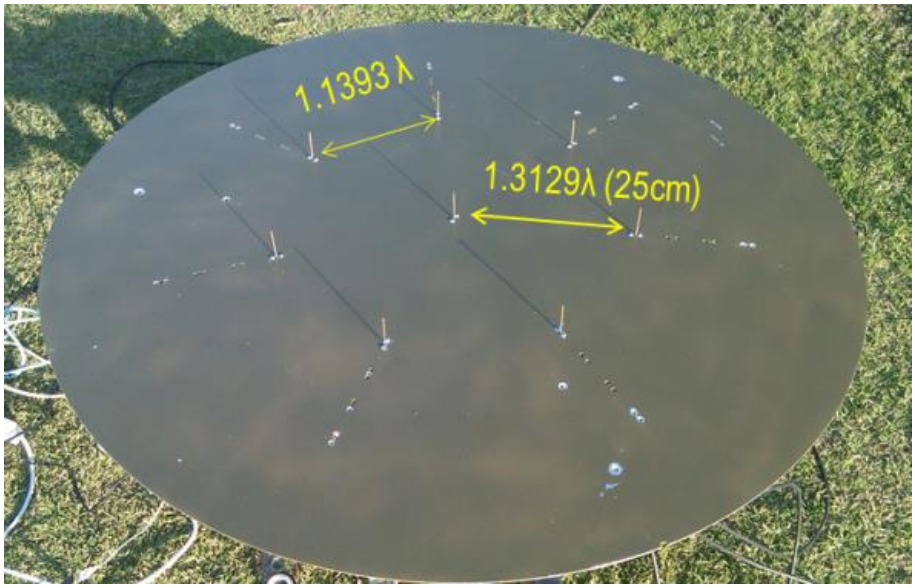

Figure 4.5.1: The antenna array used in the experiment. It is part of the GNSS Environmental Monitoring System (GEMS) [83].

The number of data points per channel that were used in the cross-correlation to extract the GPS signal was 2,291,520; this corresponds to a total time length of 143 ms at a sampling frequency of 16 MHz. The antenna array orientation was roughly measured to be 52^0 to initialise the calibration algorithm. This angle was estimated manually using a magnetic compass and then correcting for the magnetic declination in Adelaide. The manual compass reading was expected to be accurate to within a few degrees. The terminated gain/phase errors in each channel were measured by a spectrum analyser and a Wiener filter was applied to equal the gain/phase responses of the eight channels.

After cross-correlation processing, 5 satellites SV 11, 20, 23 30, 32 were obtained and used as the calibration sources. The SNR of each was about 18dB after integration. By referring to the GPS almanac, the azimuth and elevation angles of the satellites are as follows:

SV	11	20	23	30	32
Azimuth	314.3^0	226^0	279.5^0	52.6^0	194^0
Elevation	48.1^0	44.4^0	35^0	10.1^0	64.8^0

Table 4.5.1: DOAs of the satellites.

4.5.2 Calibration Performance Analysis

The calibration is carried out with the assumption that there is one multipath existing for each calibration source. However the technique still works if there is less than one multipath signal. In this case the second largest value in the complex number vector, $\underline{s_n}$ for *n*th calibration source will be much smaller than the largest value. After 10 iterations, the calibration converges as shown in figure 4.5.2. The estimated array orientation error and mutual coupling coefficients, when only the adjacent mutual coupling effects are considered, are in table 4.5.2.

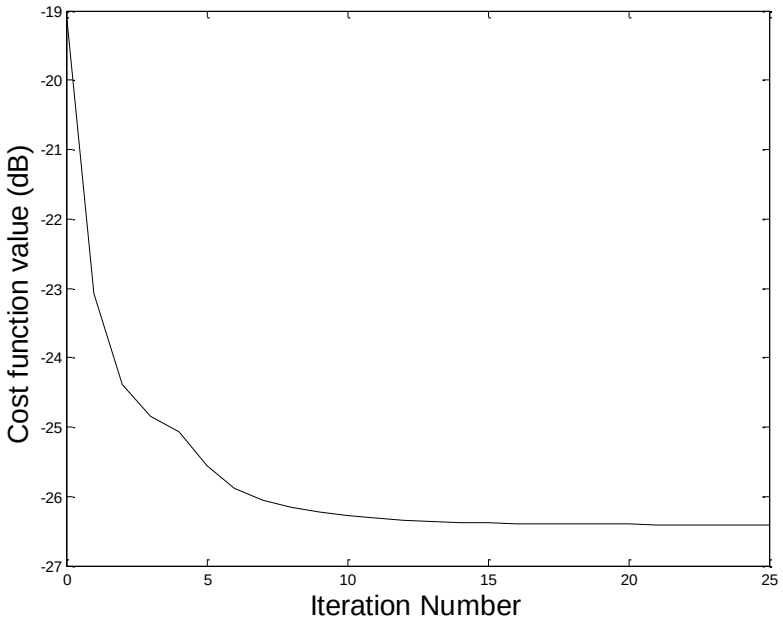

Figure 4.5.2: Cost function value versus the iterations

Array orientation				
51.71^0				
Mutual coupling coefficients				
	C 1	C 2	C 3	C 4
Gain (amplitude)	0.1085	0.0944	0	0
Phase	-165.54º	-15.72º	0	0

Table 4.5.2: Estimated parameters for the antenna array.

The estimated array orientation is 51.71^0 which is close to the measured value 52^0. This comparison is to give the accuracy of the experimental setup but is not intended to be an estimate of the accuracy of the algorithm. The estimated mutual coupling gains are 0.1085 (-19.29dB) and 0.0944 (-20.50dB) for C1 and C2 respectively. These values are very close to the values measured by the network analyser, which were C1 = C2 = -20dB.

The magnitudes of complex number $\underline{s}_n$ which indicate the existence of multipath signals for each calibration source are shown in table 4.5.3.

	SV 11	SV 20	SV 23	SV 30	SV 32
$\lvert\underline{s}(1)\rvert$	0.3536	0.3143	0.3088	0.2836	0.3043
$\lvert\underline{s}(2)\rvert$	0.0826	0.1502	0.1001	0.1324	0.1006
$\lvert\underline{s}(2)\rvert/\lvert\underline{s}(1)\rvert$	0.2336	**0.4779**	0.3242	**0.4669**	0.3306

Table 4.5.3: Magnitudes of $\underline{s}$.

Because the algorithm cannot estimate the number of multipath signals, so the multipath signal detecting threshold is set to be at most 8dB lower than the direct path signal which is a higher threshold than the normal multipath power level. That is if $|\underline{s}(2)|/|\underline{s}(1)|$ value is lower than 0.3981 in magnitude, no multipath is assumed to be in that calibrating signal. Based on this threshold, SV 20 and SV 30 are detected to have multipath signals as shown in table 4.5.3.

The elevation angle of SV 30 is only 10.1^0, so the multipath could be caused by the ground reflection. The elevation angle of SV 20 is 44.4^0 and the azimuth angle is 226^0. Therefore, there may be a possible multipath reflector nearby the antenna array. The calibration algorithm estimates the DOA information for the multipath signal of SV 20 is: azimuth angle 145.2^0 (compensated by the estimated array orientation error in table 4.5.2) and elevation angle 48.5^0. Figure 4.5.3 shows the investigation of a possible multipath reflector based on the location of the antenna array and the estimated azimuth DOA of the multipath signal. As the measurement suggests at the azimuth direction of 143.23^0, there is a large metal court lamp, which is close to the estimated value of 145.2^0 and could be the possible multipath reflection source. However the DOA estimation of multipath signals could be inaccurate because of the lack of knowledge of the number of the signals, which will affect the parameter estimation.

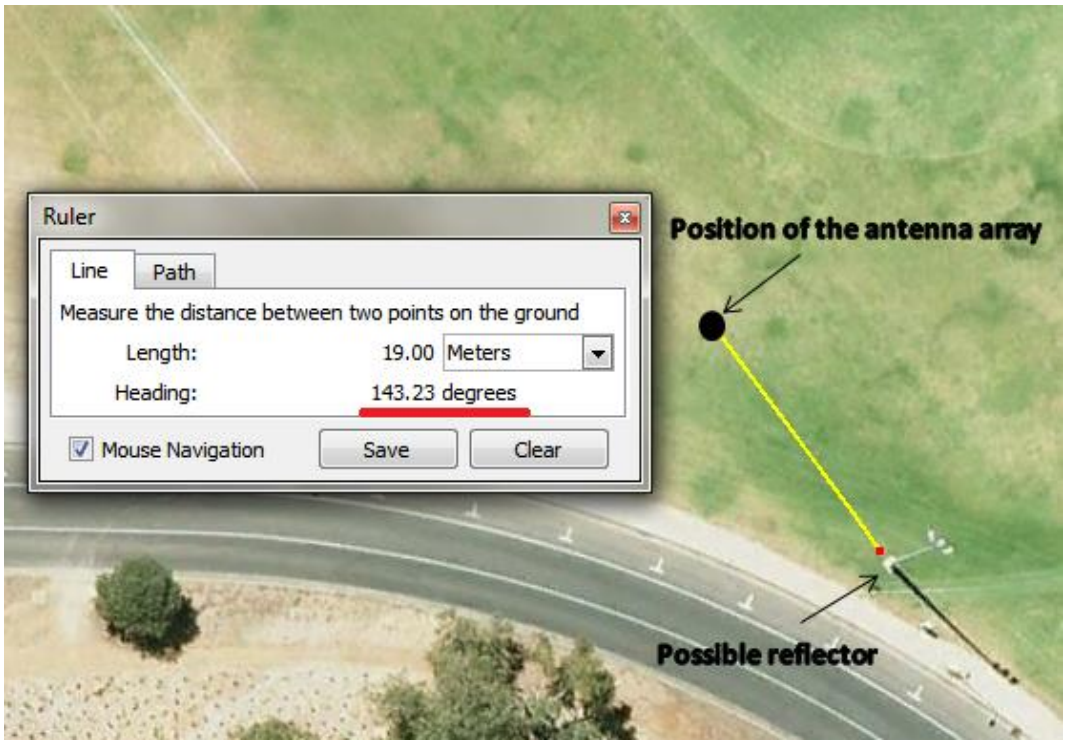

Figure 4.5.3: The possible multipath reflector for SV 20.

4.5.3 Performance Comparison between the Calibration Algorithms with and without Multipath Assumptions

One of the important features of the proposed calibration algorithm in this chapter is that it assumes the calibration sources have multipath signals and includes these multipath components into the signal model and the calibration cost function. Therefore, it is interesting to compare the performance of the calibration algorithms with and without multipath assumptions.

The antenna array calibration without multipath was implemented by removing the multipath signal components from the signal model and the multipath DOA estimation step in the calibration process. The estimated parameter values are in table 4.5.4. Comparing with parameter values estimated with multipath assumption, the array orientation estimation is 0.36º higher and all the mutual coupling coefficients are estimated to be higher. These higher mutual coupling coefficients may be due to the compensations of no multipath calibration.

Array orientation				
52.07º				
Mutual coupling coefficients				
	C 1	C 2	C 3	C 4
Gain (amplitude)	0.1142	0.1083	0	0
Phase	-123.57º	-35.96º	0	0

Table 4.5.4: Estimated parameters for the antenna array with no multipath calibration.

The performance of the two calibration algorithms were evaluated by estimating the DOAs of the GPS signals on the other recorded GPS data at a

different time. 4 strong GPS signals were obtained. The GPS signals were correlated and integrated in each array channel. The final processed received data for each GPS source had a SNR of about 20dB with 100 snapshots. The DOAs of the GPS signals were estimated by the MUSIC algorithm applied with the estimated calibration parameters in table 4.5.2 and table 4.5.4.

SV	Almanac azimuth angle	Calibration without multipath	Calibration with multipath
04	208.26^0	206.6^0 (-1.66^0)	207.82^0 (-0.44^0)
16	56.87^0	55.6^0 (-1.27^0)	56.72^0 (-0.15^0)
08	289.23^0	287.9^0 (-1.33^0)	288.92^0 (-0.31^0)
20	15.69^0	14.8^0 (-0.89^0)	15.23^0 (-0.46^0)

Table 4.5.5: GPS signal azimuth angle estimations. The angle estimation errors are in brackets.

	Almanac elevation angle	Calibration without multipath	Calibration with multipath
04	13.12^0	11.1^0 (-2.02^0)	11.6^0 (-1.52^0)
16	36.12^0	33.2^0 (-2.92^0)	33.2^0 (-2.92^0)
08	31.56^0	29.1^0 (-2.46^0)	27.4^0 (-4.16^0)
20	25.28^0	22.6^0 (-2.68^0)	24.4^0 (-0.88^0)

Table 4.5.6: GPS signal elevation angle estimations. The angle estimation errors are in brackets.

As shown in table 4.5.5 and table 4.5.6, the DOA estimation errors of the calibration algorithm without multipath assumption are worse than the algorithm with multipath assumption for all the azimuth angles and most of the elevation angles. Without multipath calibration, the Root Mean Squared Error (RMSE) of the azimuth angle estimation is 1.32º. With multipath calibration, the RMSE reduces to 0.36º. Due to the array geometry limitation, the elevation angle estimation has a large variance, so the calibration algorithm with multipath calibration is only marginally better than the calibration algorithm without multipath calibration.

As shown in figure 4.5.4 and figure 4.5.5, the MUSIC spectrum with multipath calibration has a higher target response and a cleaner pattern than the one without multipath calibration. This indicates the calibration algorithm with multipath calibration has a better estimation of the mutual coupling matrix and thus the array manifold than the one without multipath calibration.

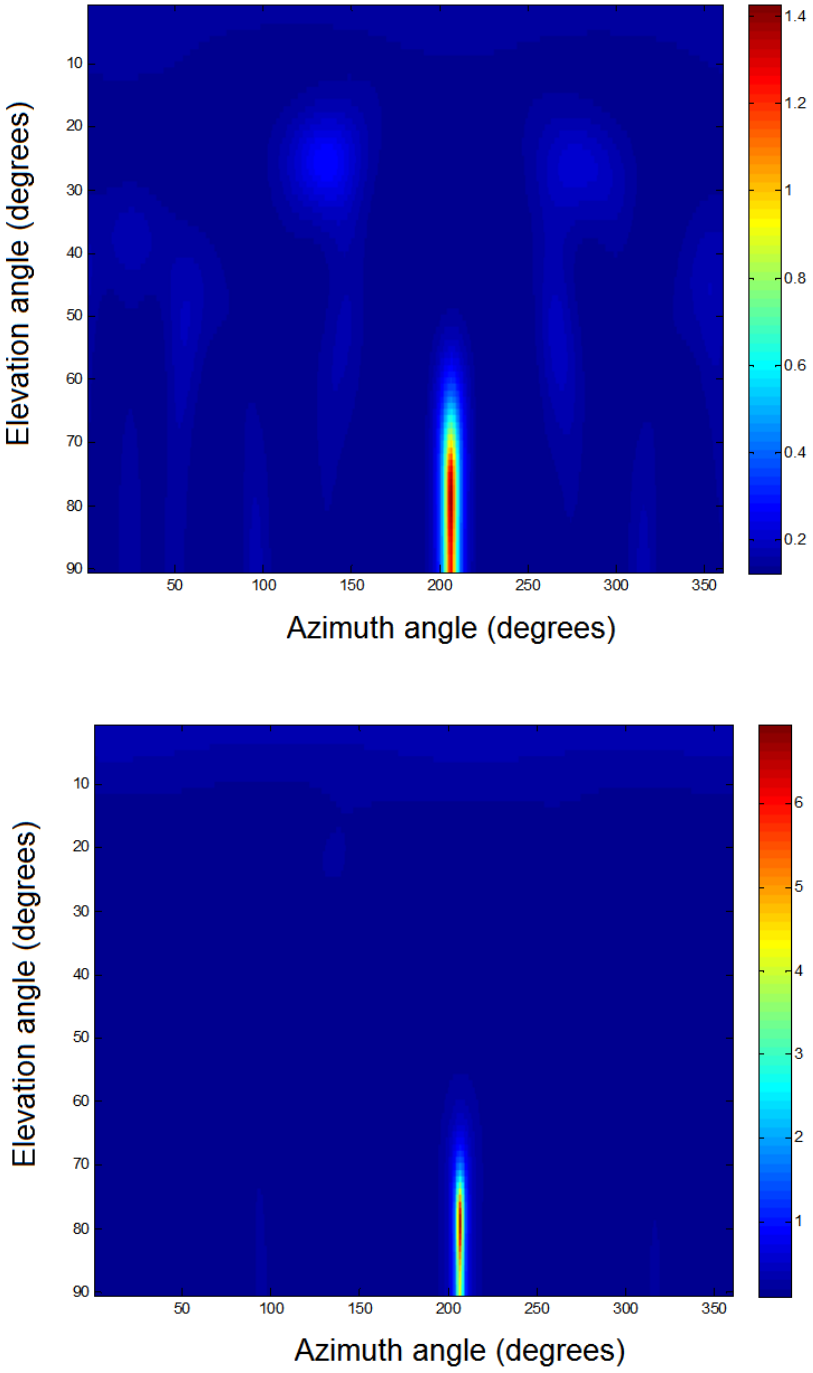

Figure 4.5.4: MUSIC spectrums for SV04 without multipath calibration (upper) and with multipath calibration (lower).

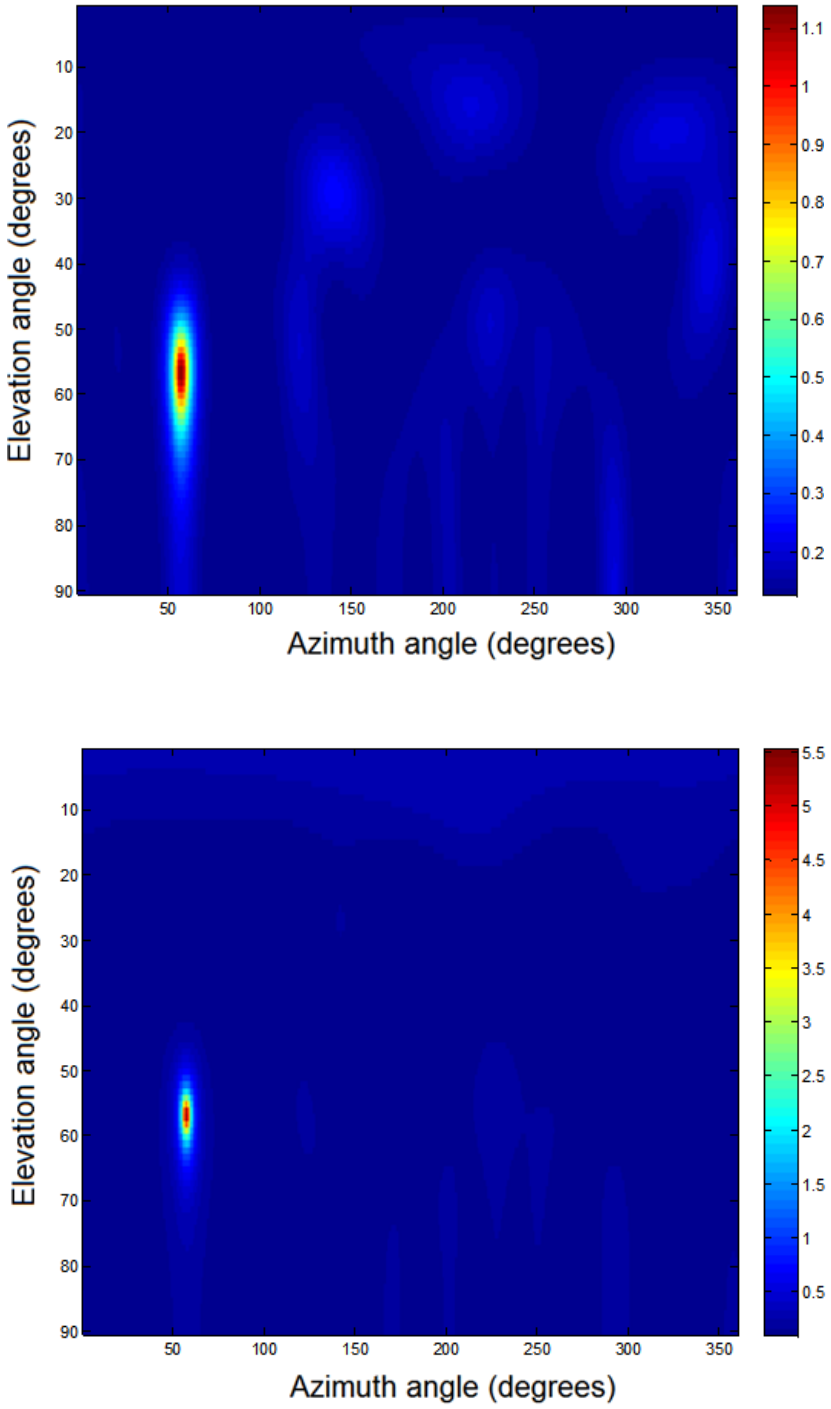

Figure 4.5.5: MUSIC spectrums for SV16 without multipath calibration (upper) and with multipath calibration (lower).

4.5.4 Performance Comparison between One and Two Multipath Assumptions

In Section 4.5.2, the calibration was performed with one multipath assumption. Similar to the discussions in Section 4.5.3, it is also very interesting to compare the performance of the proposed calibration algorithm using one and two multipath assumptions.

The estimated parameter values using two multipath assumption are in table 4.5.7 and table 4.5.8. As shown in table 4.5.7, the magnitudes of the complex number of the second multipath components *s*(3) are about 3 to 6 times lower than those of the first multipath components *s*(2). The small magnitudes of the second multipath components indicate that the signal model with two multipath may overfit the calibration data by expanding the dimension of the signal structure. Comparing the results in table 4.5.8 with the parameter estimated with one multipath assumption, the array orientation estimation is 0.09º higher and the mutual coupling coefficients are slightly different.

	SV 11	SV 20	SV 23	SV 30	SV 32
$\lvert\underline{s}(1)\rvert$	0.3612	0.3124	0.3076	0.2963	0.3172
$\lvert\underline{s}(2)\rvert$	0.0751	0.1259	0.0992	0.1304	0.0641
$\lvert\underline{s}(3)\rvert$	0.0271	0.0363	0.0296	0.0206	0.0225

Table 4.5.7: Magnitudes of $\underline{s}$.

Array orientation				
51.80º				
Mutual coupling coefficients				
	C 1	C 2	C 3	C 4
Gain (amplitude)	0.1036	0.0960	0	0
Phase	-169.18º	-13.69º	0	0

Table 4.5.8: Estimated parameters for the antenna array with two multipath assumption.

The performance is compared by DOA estimation accuracy using the same validation GPS sources in Section 4.5.3. As shown in table 4.5.9, for azimuth angles, the RMSE of two multipath assumption is 0.51° whilst the RMSE of one multipath assumption is 0.36°. One multipath assumption is better than two multipath assumption but the difference is very limited. This indicates two multipath assumption may only slightly overfit the calibration data. As discussed in Section 4.5.3, due to the array geometry limitation, the elevation angle estimation showed in table 4.5.10 has a large variance but one multipath assumption is still marginally better than two multipath assumption.

SV	Almanac azimuth angle	Calibration with one multipath	Calibration with two multipath
04	208.26^0	207.82º (-0.44º)	207.99° (-0.27°)
16	56.87^0	56.72º (-0.15º)	56.38° (-0.49°)
08	289.23^0	288.92º (-0.31º)	288.65° (-0.58°)
20	15.69^0	15.23º (-0.46º)	15.01° (-0.68°)

Table 4.5.9: GPS signal azimuth angle estimations. The angle estimation errors are in brackets.

	Almanac elevation angle	Calibration with one multipath	Calibration with two multipath
04	13.12^0	11.6º (-1.52º)	11.2º (-1.92º)
16	36.12^0	33.2º (-2.92º)	32.6º (-3.52º)
08	31.56^0	27.4º (-4.16º)	28.3º (-3.26º)
20	25.28^0	24.4º (-0.88º)	24.6º (-0.68º)

Table 4.5.10: GPS signal elevation angle estimations. The angle estimation errors are in brackets.

4.6 Conclusion

In this chapter, a calibration algorithm for array orientation error and mutual coupling parameters in the presence of multipath for a GPS antenna array is proposed. This algorithm uses GPS signals as the disjoint calibration sources to iteratively estimate the array orientation error, the parameters of mutual

coupling matrix and the DOAs of multipath signals based on the assumption that if the estimates of these parameters are correct, the model should be able to make the array manifold and the signal span the same subspace at the signal bearings. The DOAs of multipath signals are estimated by Alternating Projection which turns a multi-dimensional optimisation problem into an iterative process of one dimensional search in each iteration.

The simulations show the estimated array parameters are very close to the true values resulting in an improved beampattern after the calibration. The algorithm was also applied to a limited amount of the real data and the experimental results showed the estimated DOAs of the GPS signals using the calibrated parameters were close to the true DOAs. The experimental results also indicate that the calibration algorithm resolves possible multipath reflection sources but the performance is limited by the unknown number of multipath signals. Comparing with the calibration algorithm without multipath assumptions, the proposed calibration algorithm is more accurate in terms of DOA estimates and array manifold estimation.

Chapter 5: GPS Signal Cancellation

5.1 Introduction

As discussed in Chapter 1, there are four main issues that affect the DOA estimation accuracy of the antenna array for weak interferences. They are:

1. Errors in the antenna array model.
2. GPS signals acting as interference sources.
3. Weak interference non-coherent integration length.
4. Coloured noise and other interference in the system.

Errors in the antenna array model are addressed by the two GPS antenna array calibration algorithms proposed in Chapters 3 and 4. These algorithms calibrate the antenna array orientation error, channel gain/phase mismatches and mutual coupling effects between antennas in the presence of calibration sources that also have a multi-path component. This chapter will propose a method to solve the issue 2 by cancelling the GPS signals using a Multiple Subspace Projection (MSP) method.

5.1.1 The Need to Cancel GPS Signals

Typically the power of the GPS L1 C/A code signals are below the total receiver noise power, i.e., GPS pre-correlation signal SNRs range from -15dB to -30dB, so they usually have no or very limited effect on the DOA estimation of a strong interference. However, if the INR of the interference is at level of -15dB or lower, the GPS signals are now stronger than the

interference and will affect the estimation of the DOA of the interference. The following figure shows this effect.

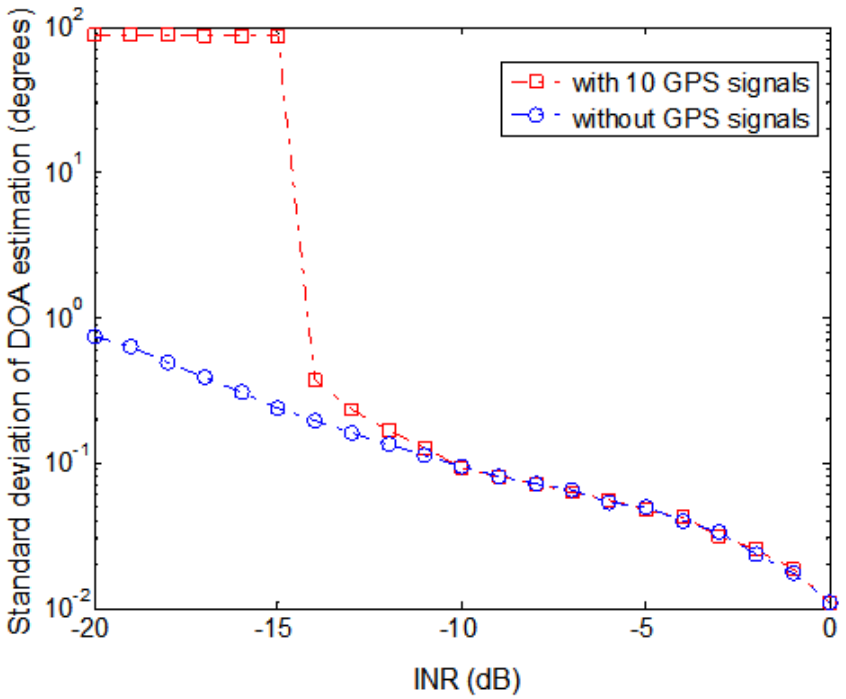

Figure 5.1.1: Standard Deviation of the GPS interference DOA estimation using the MUSIC algorithm in the presence of 10 GPS signals (red) and without GPS signals (blue).

Figure 5.1.1 shows the simulation results of the standard deviation of the interference DOA estimates using the MUSIC (MUltiple SIgnal Classification algorithm) algorithm with and without GPS signals. The grid step size of MUSIC is 0.01°. The interference is a simulated CW interference. This simulation is based on an 8 element half wavelength uniformly spaced linear array (ULA), the number of snapshots K = 10000 and 10 GPS signals are uniformly distributed from 0 to 180 degrees with an SNR of -20dB. Each standard deviation is estimated using 200 independent simulations. From Figure 5.1.1, the DOA estimation accuracy of the interference is basically unaffected for an INR is above -10dB. When the INR is between -10dB and -14dB, the interference DOA variance is clearly affected by the GPS signals, while below -14dB the MUSIC algorithm fails completely in estimating the DOA of the interference. Thus the GPS signals need to be cancelled if the

DOAs of interferences with an INR of less than -20 dB need to be accurately estimated. Although GPS interference with an INR of -20dB or lower at the receiver end does not interfere with far field high precision surveying receivers according to the results in [135], it is still highly important to be able to accurately estimate its DOA for the purpose of interference localisation as it may still be a problem for nearby receivers.

5.1.2 Current GPS Signal Cancellation Methods

Several GPS signal cancellation methods have been proposed in both the adaptive antenna array processing area and the GPS area.

In the adaptive antenna array processing area, spatial filtering [50] and subspace projection based techniques [136] have been used to reject GPS signals from certain directions, but these methods reduce the array processing gain for the intended signal as one spatial degree of freedom is required to mitigate each interference. Furthermore, if the number of antennas is less than the number of GPS signals, array processing is not capable of rejecting these signals as the least squares equations become underdetermined.

In the GPS area, several methods have been proposed to cancel the unwanted GPS signals from the input data in order to detect a much weaker signal. The classical problem is the near-far problem where a strong GPS signal masks a much weaker one. This is also known as the CA code cross correlation or GPS civilian signal self-interference problem. In [137], a Successive Interference Cancellation (SIC) technique was proposed to subtract strong GPS signals by reconstructing the strong GPS signals using CA code information derived from the tracking loops of a conventional detector. A Partitioned Subspace Projection (PSP) method [48, 49], removes the unwanted GPS signals by projecting the received signal onto the orthogonal subspace of the strong GPS signals. Compared with [137], the

PSP method uses a least squares filter to produce a better amplitude estimate of strong signals. The PSP method was further studied in [138, 139] and proved to be independent of the received signal phase which was convenient for non-coherent receivers. To solve the quantization problem when using a low-end GPS receiver with a one or two bit ADC, adaptive orthogonalization using the constraints method [140, 141] and the Delayed Parallel Interference Cancellation (DPIC) method [142-144] were proposed. Adaptive orthogonalization, using a constraint method, reconstructs the despreading codes making them orthogonal to the strong GPS signals and nearly parallel to the weak GPS signals, but it cannot be used to cancel the GPS signals directly. The Delayed Parallel Interference Cancellation (DPIC) method subtracts the cross correlation of the strong GPS signals from the correlation output at the post-correlation stage. The performance of DPIC is slightly worse than PSP because it is designed to have a lower computational burden [143]. However, due to their single rank least mean squares estimation structure, both PSP and DPIC methods can only cancel a line of sight (LOS) GPS signal and thus are unable to cancel multipath components of the unwanted GPS signals or distortions due to a non-ideal frequency response of the GPS front end filters.

In this chapter, the subspace projection concept in [48] and [49] is extended to a Multiple Subspace Projection (MSP) method. This MSP method assumes the received GPS L1 C/A signal is received after it is transformed by a Finite Impulse Response (FIR) filter, and thus its signal subspace becomes multi-dimensional while in the PSP method it is assumed to be rank one. Due to its multi-dimensional subspace structure, MSP achieves better cancellation of the received GPS signal if the signal is band-limited, has multipath components, or has fractional delays.

The remainder of the chapter is structured as follows: The Multiple Subspace Projection (MSP) method is proposed in Section 5.2; its performance analysis is presented in Section 5.3; in Section 5.4, experimental results are described. Finally conclusions are given in Section 5.5.

5.2 GPS Signal Cancellation Using Multiple Subspace Projection

5.2.1 GPS Signal Model

The vector form of a single channel down-converted baseband received signal $\underline{x}(n)$ with *K* GPS L1 C/A signals and a single GPS interference is

$$\underline{x}(n) = \sum_{k=1}^{K} \underline{q}_k(n) + \underline{v}(n) + \underline{w}(n) \tag{5.2.1}$$

where $\underline{q}_k(n) = [q_k[n],\ q_k[n-1], \dots, q_k[n-c_L+1]]^T$ is the k^{th} GPS L1 C/A code signal which is orthogonal to other GPS signals, c_L is the code length, $\underline{v}(n) = [v[n], v[n-1], \dots, v[1]]^T$ is the interfering signal whose DOA is to be estimated, $\underline{w}(n) = [w[n], w[n-1], \dots, w[1]]^T$ is Additive White Gaussian Noise (AWGN), and n denotes sample number.

For the k^{th} GPS L1 C/A signal, the code phase, Doppler frequency and the data modulation are obtained through software GPS acquisition and are used to construct the signal $\underline{s}_k$ which is the k^{th} transmitted baseband GPS L1 C/A signal with unity gain. The transmitted signal $s_k[n]$ is given by

$$s_k[n] = c_k[n-\tau_k] \cdot D_k \cdot e^{j2\pi f_k n} \tag{5.2.2}$$

where $c_k[n]$ is the Direct-Sequence Spread Spectrum (DS-SS) signal (the C/A code), τ_k is the code phase, D_k is the data modulation and f_k is the Doppler frequency.

In many practical situations, there are multipath arrivals which can be modelled as the delayed versions of the direct path signal $s_k[n]$. As these are treated as interferences, they can be modelled as the output of an FIR filter and this is discussed in the following section.

5.2.2 Cancellation Algorithm

In order to cancel the k^{th} GPS signal $\underline{q_k}(n)$ in the received data $\underline{x}(n)$, the relationship between the unknown signal $\underline{q_k}(n)$ and the known signal $\underline{s_k}(n)$ need to be modeled. In [49] and [48], it is modeled as:

$$\underline{q_k}(n) = A_k e^{j\varphi_k} \underline{s_k}(n) \tag{5.2.3}$$

where A_k is the amplitude of the k^{th} GPS signal and φ_k is the carrier phase mismatch between the two signals. This simple but effective model assumes that in the received data $\underline{x}(n)$, the only parameters of the k^{th} GPS signal, $\underline{q_k}(n)$, that need be estimated are the amplitude and carrier phase difference. However, if the GPS signal has multipath components, fractional delays or is band-limited due to the receiver front end filters, this model will be mismatched.

In order to cancel the GPS signals even if they have multipath components, fractional delays or are band-limited, an L^{th} order Finite Impulse Response (FIR) model to describe the relationship between $\underline{q_k}(n)$ and $\underline{s_k}(n)$ is proposed as shown in figure 5.2.1.

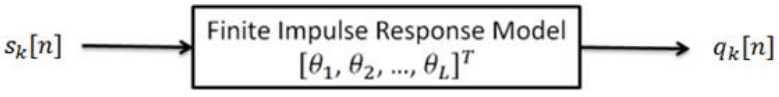

$$\theta_1 s_k[n] + \theta_2 s_k[n-1] + \cdots + \theta_L s_k[n-L+1] = q_k[n]$$

Figure 5.2.1: Finite Impulse Response (FIR) model.

This model is a linear model, so the vector form of this model can be expressed as

$$\underline{q_k}(n) = \mathbf{S}_k(n)\underline{\theta_k} \tag{5.2.4}$$

where $\underline{\theta}_k$ are the weights of the FIR system for the k^{th} GPS signal and $\mathbf{S}_k(n)$ is given by

$$\mathbf{S}_k(n) = [\underline{s}_k(n), \quad \underline{s}_k(n-1), \quad \cdots \quad \underline{s}_k(n-L+1)] \tag{5.2.5}$$

where L is the order of the FIR system. In practice, L is set to be from 15 to 100 taps.

For the k^{th} GPS L1 C/A code signal where $\underline{q}_k(n) = \mathbf{S}_k(n)\underline{\theta}_k$, the received signal $\underline{x}(n)$ can be rewritten as

$$\underline{x}(n) = \mathbf{S}_k(n)\underline{\theta}_k + \mathbf{S}_o(n)\underline{\theta}_o + \underline{v}(n) + \underline{w}(n) \tag{5.2.6}$$

where $\mathbf{S}_o = [\mathbf{S}_1\, \mathbf{S}_2 \ldots \mathbf{S}_{k-1}\, \mathbf{S}_{k+1} \ldots \mathbf{S}_K]$ are the other GPS signals and their respective FIR system weights are $\underline{\theta}_o = [\underline{\theta}_1{}^T\, \underline{\theta}_2{}^T \ldots \underline{\theta}_{k-1}{}^T\, \underline{\theta}_{k+1}{}^T \ldots \underline{\theta}_K{}^T]^T$.

In order to cancel the k^{th} GPS signal, the subspace principle is utilised. The subspace orthogonal to that spanned by the k^{th} GPS signal is

$$\mathbf{P}_k = \mathbf{I} - \mathbf{S}_k\left(\mathbf{S}_k{}^H\mathbf{S}_k\right)^{-1}\mathbf{S}_k{}^H \tag{5.2.7}$$

The rank of $\mathbf{S}_k{}^H\mathbf{S}_k$ is the order of the FIR system L even if the sampling rate is higher than the chip rate, so the orthogonal subspace $\mathbf{P}_k$ is a multi-dimensional subspace while it is only rank one in the PSP method [48, 49]. The received data $\underline{x}(n)$ now is projected onto $\mathbf{P}_k$ to cancel the k^{th} GPS signal $\mathbf{S}_k\underline{\theta}_k$

$$\begin{aligned}\mathbf{P}_k\underline{x} &= \left(\mathbf{I} - \mathbf{S}_k\left(\mathbf{S}_k{}^H\mathbf{S}_k\right)^{-1}\mathbf{S}_k{}^H\right)\left(\mathbf{S}_k\underline{\theta}_k + \mathbf{S}_o\underline{\theta}_o + \underline{v} + \underline{w}\right) \\ &= \mathbf{S}_o\underline{\theta}_o + \underline{v} + \underline{w} - \mathbf{S}_k\left(\mathbf{S}_k{}^H\mathbf{S}_k\right)^{-1}\mathbf{S}_k{}^H\left(\mathbf{S}_o\underline{\theta}_o + \underline{v} + \underline{w}\right)\end{aligned} \tag{5.2.8}$$

In equation 5.2.8, the received k^{th} GPS signal $\mathbf{S}_k(n)\underline{\theta}_k$ is fully cancelled and $\mathbf{S}_o(n)\underline{\theta}_o + \underline{v}(n) + \underline{w}(n)$ is the desired projection result which only includes the other GPS signals $\mathbf{S}_o(n)\underline{\theta}_o$, the GPS interference $\underline{v}(n)$ and the noise $\underline{w}(n)$. So the projection error is

$$e_k(n) = \mathbf{S}_k\left(\mathbf{S}_k{}^H\mathbf{S}_k\right)^{-1}\mathbf{S}_k{}^H\left(\mathbf{S}_o(n)\underline{\theta}_o + \underline{v}(n) + \underline{w}(n)\right) \quad (5.2.9)$$

So,

$$\mathbf{P}_k\underline{x}(n) = \mathbf{S}_o(n)\underline{\theta}_o + \underline{v}(n) + \underline{w}(n) + e_k(n) \quad (5.2.10)$$

In equation 5.2.9, due to the CDMA structure of the GPS signals, the GPS signal is uncorrelated with the interference $\underline{v}(n)$ and the white Gaussian noise $\underline{w}(n)$, so $E\{\boldsymbol{S}_k(n)^H\underline{v}(n)\} = 0$ and $E\{\boldsymbol{S}_k(n)^H\underline{w}(n)\} = 0$. Also because of the limited GPS gold code cross-correlation dynamic range, which is about 23.9 dB within 1ms[1], $\mathbf{S}_k{}^H\mathbf{S}_o$ is not strictly but approximately 0. This means the projection error is very small and can be approximated by 0 ($e_k \approx 0$). Furthermore, as discussed below, the cancellation is iteratively applied on all the GPS signals, so this error will be even smaller after all the GPS signals are subtracted.

The projection result is

$$\mathbf{P}_k\underline{x}(n) \approx \mathbf{S}_o\underline{\theta}_o + \underline{v}(n) + \underline{w}(n) \quad (5.2.11)$$

where the k^{th} GPS signal $\underline{q}_k(n) = \mathbf{S}_k(n)\underline{\theta}_k$ is cancelled from the received signal $\underline{x}(n)$.

Multiple GPS signals are able to be cancelled by applying the individual projection multiple times, or by combining matrices $\mathbf{S}_k$ and $\mathbf{S}_o$ into $\mathbf{S} = [\mathbf{S}_k\ \mathbf{S}_o]$ and being included in the projection matrix to be cancelled. These GPS signal cancellations are applied on all the antenna array receiver channels whilst the GPS acquisition information can be obtained from only one antenna, or a beam steered at the GPS satellite.

This multiple dimensional subspace structure based on the FIR system model has some important benefits in GPS signal cancellation, as it will accurately subtract the GPS signals even if the GPS signal has unknown

[1] Known as the CA code cross correlation problem, the GPS civilian signal self-interference or the GPS near-far effect.

amplitude and carrier phase, multipath components, fractional delays or is band-limited due to the receiver front end filters.

There is a potential implementation issue, as the orthogonal subspace matrix $\mathbf{P}_k$ may be too large to be calculated directly, due to the memory requirements. So when implementing$\mathbf{P}_k\underline{x} = \left(\mathbf{I} - \mathbf{S}_k\left(\mathbf{S}_k{}^H\mathbf{S}_k\right)^{-1}\mathbf{S}_k{}^H\right)\underline{x}$, instead of trying to obtain the orthogonal subspace $\mathbf{P}_k = \mathbf{I} - \mathbf{S}_k\left(\mathbf{S}_k{}^H\mathbf{S}_k\right)^{-1}\mathbf{S}_k{}^H$ first, it is better to change this equation to be

$$\mathbf{P}_k\underline{x} = \underline{x} - \mathbf{S}_k\left(\mathbf{S}_k{}^H\mathbf{S}_k\right)^{-1}\mathbf{S}_k{}^H\underline{x} \tag{5.2.12}$$

Then the following 1-4 steps can be calculated in sequence to reduce the memory requirements during the computation.

1. $\mathbf{S}_k{}^H\underline{x}$,
2. $\left(\mathbf{S}_k{}^H\mathbf{S}_k\right)^{-1}\mathbf{S}_k{}^H\underline{x}$,
3. $\mathbf{S}_k\left(\mathbf{S}_k{}^H\mathbf{S}_k\right)^{-1}\mathbf{S}_k{}^H\underline{x}$,
4. $\underline{x} - \mathbf{S}_k\left(\mathbf{S}_k{}^H\mathbf{S}_k\right)^{-1}\mathbf{S}_k{}^H\underline{x}$

In this sequence, the result of each operation has a maximum memory requirement of $L \times N$, where L is the order of the system and N is the number of samples, and thus avoided the problem to store the massive $N \times N$ orthogonal subspace matrix $\mathbf{P}_k$.

5.3 Performance Analysis

In order to evaluate the GPS cancellation performance of the Multiple Subspace Projection method, Matlab was used to simulate the different cancellation scenarios. The GPS code phase and data modulation were assumed to be accurately estimated and this estimation step was not

included in the simulations. The sampling rate was 4MHz and the FIR model of the MSP method has *L* = 60 taps.

In this section, the cancellation performance comparison between the MSP and the PSP method is evaluated by using the ratio between the cross correlation peak before the cancellation and the cross correlation peak after cancellation, which is defined as

$$GPS\ cancellation\ performance = 10log_{10}(\frac{crosscorrelation\ peak\ after\ cancellation}{crosscorrelation\ peak\ before\ cancellation})^2 \quad (dB) \qquad (5.3.1)$$

where the cross correlation is computed between the received signal (before or after cancellation) and the ideal received signal defined in equation 5.2.2 with no errors in it.

An example of this ratio calculation is given below:

- If a GPS signal's cross correlation peak before cancellation was 1×10^4.
- After applying the MSP cancellation method, the cross correlation peak value became 1×10^3.
- After applying PSP cancellation method, the cross correlation peak value became 2.5×10^3.

The GPS cancellation performance of the MSP method and PSP method were -20dB and -12dB respectively. In this case, MSP method has a better performance than PSP method. Please note the GPS cancellation performance numbers are only comparable in the same scenario between the two algorithms, because they are not only determined by the performances of the algorithms, but also determined by the SNRs of the GPS signals and the correlation length used in the cross correlation process.

5 different scenarios were simulated to compare performance. The rest of this section will discuss and compare the cancellation performance of the MSP method and the PSP method in these scenarios. The 5 scenarios were:

1. One GPS signal in thermal noise
2. One GPS signal with a Doppler frequency demodulation error in thermal noise
3. One GPS signal with fractional delay in thermal noise
4. One GPS signal with one multipath signal in thermal noise
5. One band limited GPS signal in thermal noise

5.3.1 Scenario 1: one GPS signal

In this simulation, there is only one GPS signal (PRN 1) and thermal noise in the received data. The GPS signal (PRN 1) is intended to be cancelled. This scenario shows the cancellation performance in the ideal conditions (no errors), so the two algorithms should have very similar performances and are able to cancel the GPS signal.

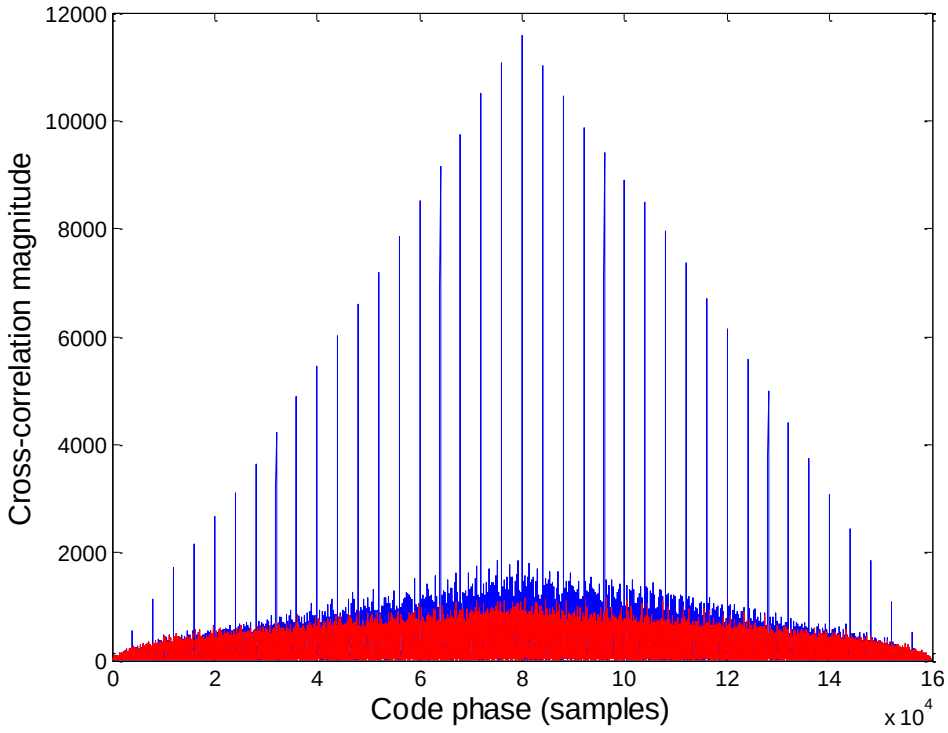

Figure 5.3.1: Cross correlation results before the MSP cancellation (blue) and after the MSP cancellation (red). The data length is 20ms, the GPS (PRN 1) signal has a SNR of -20dB.

As shown in figure 5.3.1, after applying MSP cancellation on the received data, the peak of the cross-correlation is significantly reduced and even lower than the original noise floor. The cancellation performance is -19.5dB. This indicates the MSP method can reject the GPS signal very effectively in the ideal conditions.

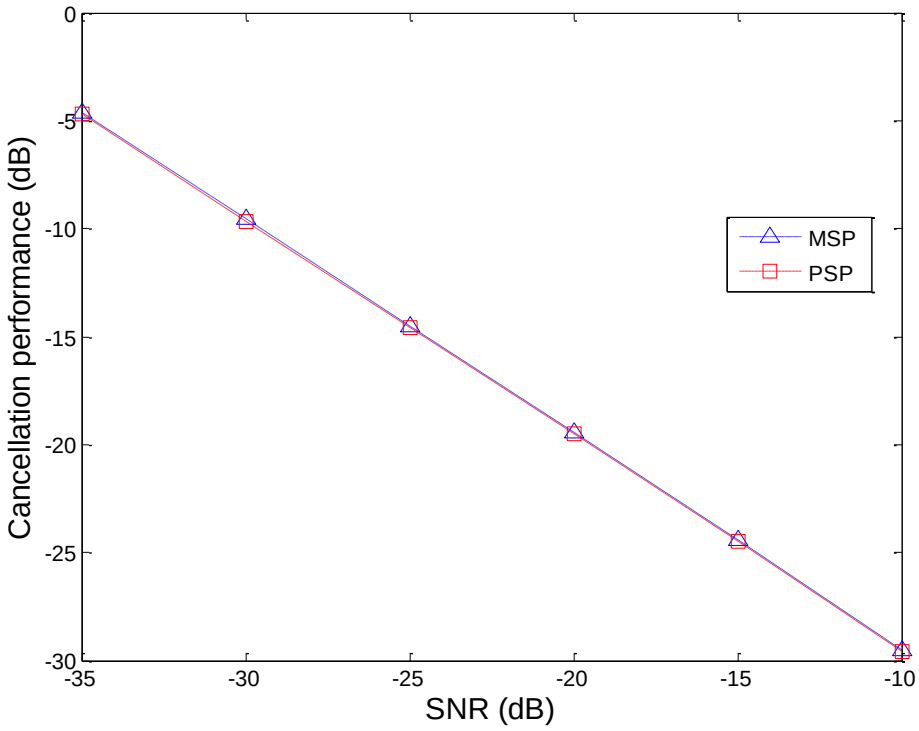

Figure 5.3.2: The cancellation performance comparison between MSP (blue) and PSP (red) using GPS (PRN 1) signal. The data length is 20ms, each cancellation performance point is estimated using 100 simulations.

Figure 5.3.2 shows the cancellation performance comparisons of MSP and PSP against the SNR of the GPS signal from -35dB to -10dB. As expected, the two algorithms have almost the same performance and both are able to cancel the GPS signal well. They are able to achieve about -29.5dB cancellation when the GPS signal has -10dB SNR. As the SNR of the GPS signal drops to -35dB, the two algorithms have about -4.7dB cancellation.

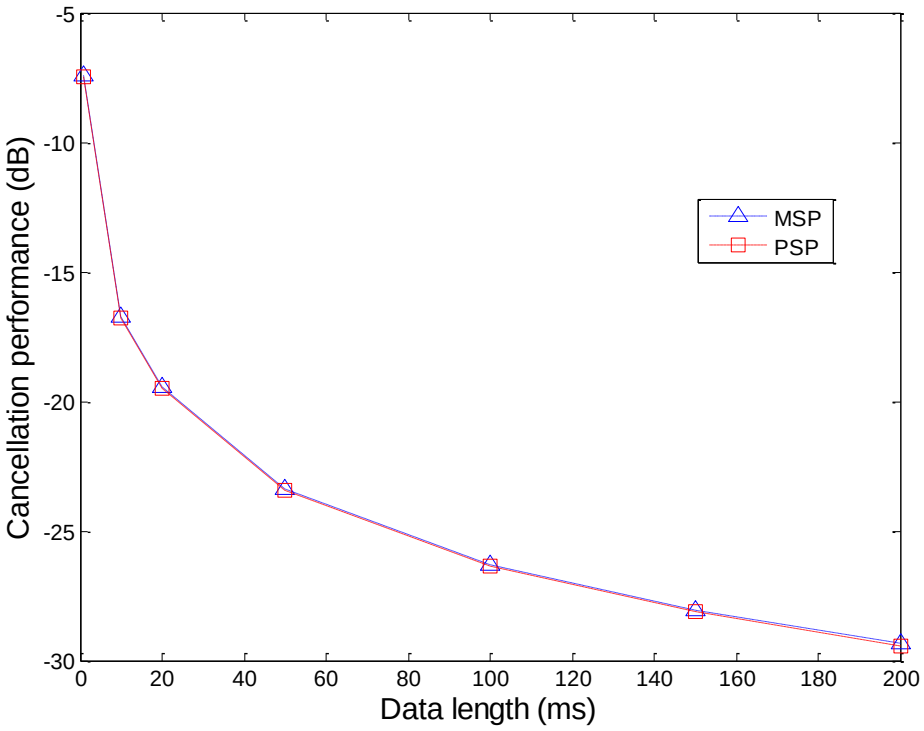

Figure 5.3.3: The cancellation performance comparison between MSP (blue) and PSP (red) using GPS (PRN 1) signal. The SNR of the GPS (PRN 1) signal is -20dB, each cancellation performance point is estimated using 100 simulations.

Figure 5.3.3 shows the cancellation performance comparisons of MSP and PSP against data length from 1 ms (1 period) to 200ms (200 periods). Again, the two algorithms have almost the same performance and both are able to cancel the GPS signal well. They are able to achieve -29.5dB cancellation when the data length is 200ms. As the data length drops to 1ms, the two algorithms give -7.5dB cancellation. This figure also shows that the cancellation performance improvement rate reduces as the data length increases.

Although MSP has greater complexity and the noise subspace is smaller than that of PSP, no performance degradation ensures.

5.3.2 Scenario 2: one GPS signal with Doppler error

In this simulation, there was only one GPS signal (PRN 1) and thermal noise in the received data. The GPS signal (PRN 1) had a residual Doppler frequency. The GPS signal (PRN 1) is intended to be cancelled. The signal models of the MSP and PSP methods do not include the Doppler frequency error, so they are not supposed to be able to cancel the GPS signal well or even fail in this condition.

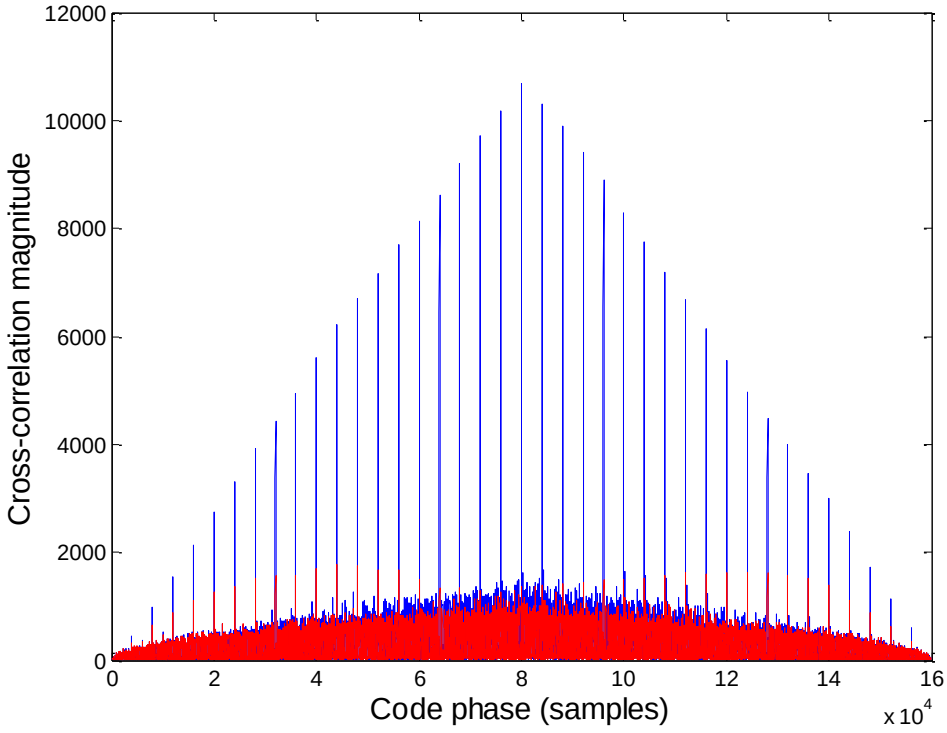

Figure 5.3.4: Cross-correlation results before the MSP cancellation (blue) and after the MSP cancellation (red). The residual Doppler frequency is 10Hz, the data length is 20ms, the GPS signal (PRN 1) has a SNR of -20dB.

Figure 5.3.4 shows the GPS signal with 10Hz residual Doppler frequency. The MSP method is still able to partially cancel the GPS signal. The cancellation performance is -15.7dB. Comparing with -19.5dB cancellation performance in the ideal condition, the cancellation performance drops by 3.8dB.

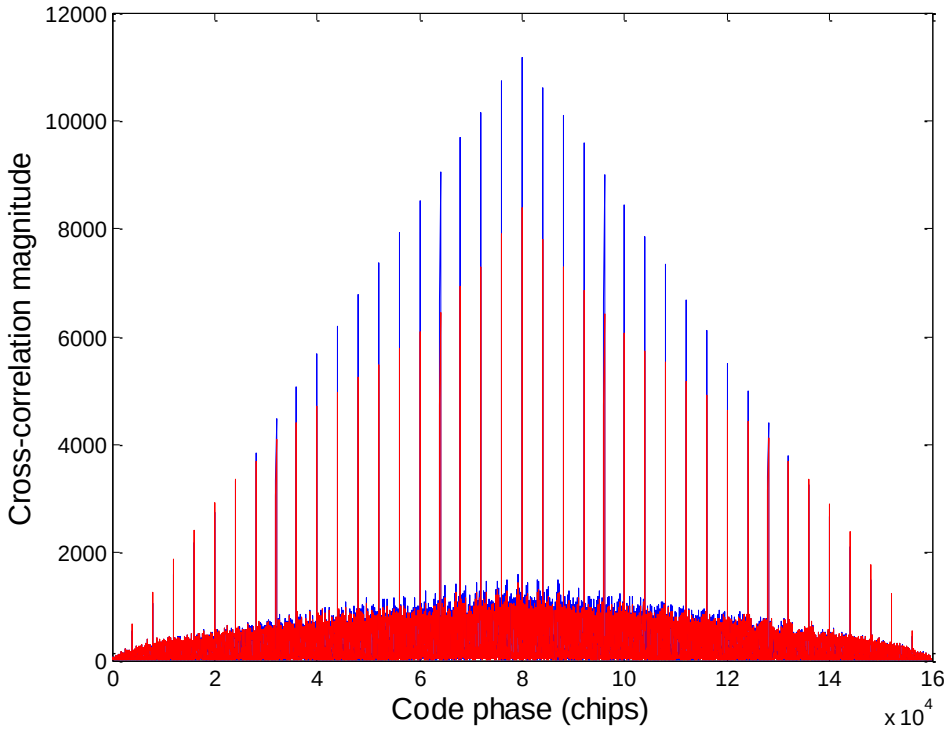

Figure 5.3.5: Cross-correlation results before the MSP cancellation (blue) and after the MSP cancellation (red). The residual Doppler frequency is 30Hz, the data length is 20ms, the GPS signal (PRN 1) has a SNR of -20dB.

As shown in figure 5.3.5, as the Doppler frequency error increases to 30Hz, the cancellation performance of the MSP method degrades dramatically. The cancellation performance value is -2.6dB comparing with -15.7dB when the Doppler frequency error is 10Hz. Compared with -19.5dB cancellation performance in the ideal condition, the cancellation performance drops by 16.9dB. It almost fails to cancel the GPS signal.

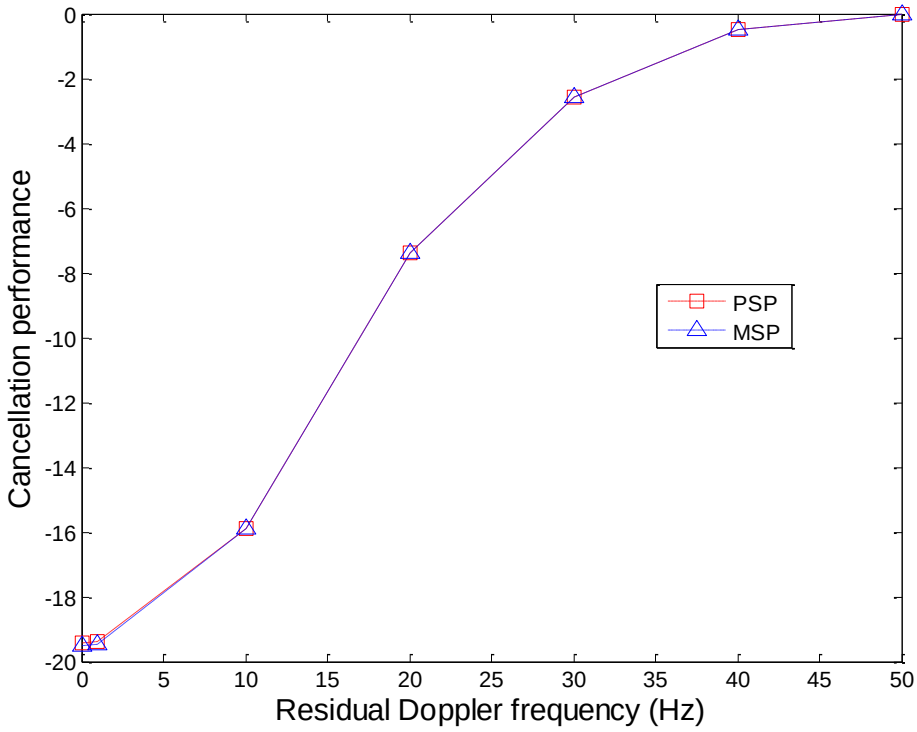

Figure 5.3.6: Cancellation performance comparison between MSP (blue) and PSP (red) using GPS (PRN 1) signal. The SNR of the GPS (PRN 1) signal is -20dB, the data length is 20ms, each cancellation performance point is estimated using 100 simulations.

Figure 5.3.6 shows that the MSP and PSP algorithms have the same cancellation performance in the presence of residual Doppler frequency. When there is no residual Doppler frequency, the cancellation performance is -19.5dB. As the Doppler frequency increases, the cancellation performance decreases. When the residual Doppler frequency increases to 50Hz, both MSP and PSP algorithms fail to cancel this GPS signal as Doppler error is not included in the signal model.

The main factor affecting the tolerable Doppler error is actually the data length to be processed. A longer data length will require a more accurate estimation of the Doppler frequency.

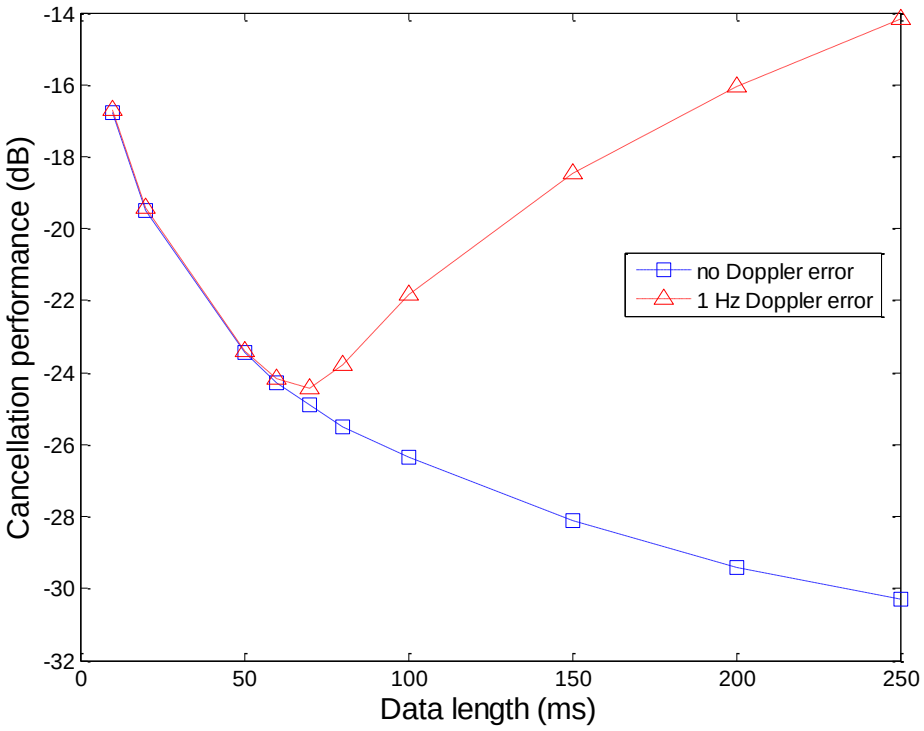

Figure 5.3.7: The MSP cancellation performance comparison between no Doppler error (blue) and 1Hz Doppler error (red). The SNR of the GPS (PRN 1) signal is -20dB, each cancellation performance point is estimated using 100 simulations.

Figure 5.3.7 shows that for a 1Hz Doppler frequency error, the MSP algorithm has a small cancellation performance loss when the data length is less than 60ms (60 periods), but has a significant loss when the data length is larger than 100ms (100 samples). This is due to the increase in Doppler error when larger block of data is used. In practice, the data would be split into smaller blocks and cancellation is done by block basis.

5.3.3 Scenario 3: one GPS signal with fractional delay

In this simulation, there is only one GPS signal (PRN 1) and thermal noise in the received data. The GPS signal (PRN 1) has a fractional delay varying from 1 to 2 samples corresponding to ¼ and ½ chip delay. The GPS signal

(PRN 1) is intended to be cancelled. Due to the multiple dimensional subspace structure, the MSP method should be able to cancel the GPS signal whilst the PSP method will perform worse or even fail.

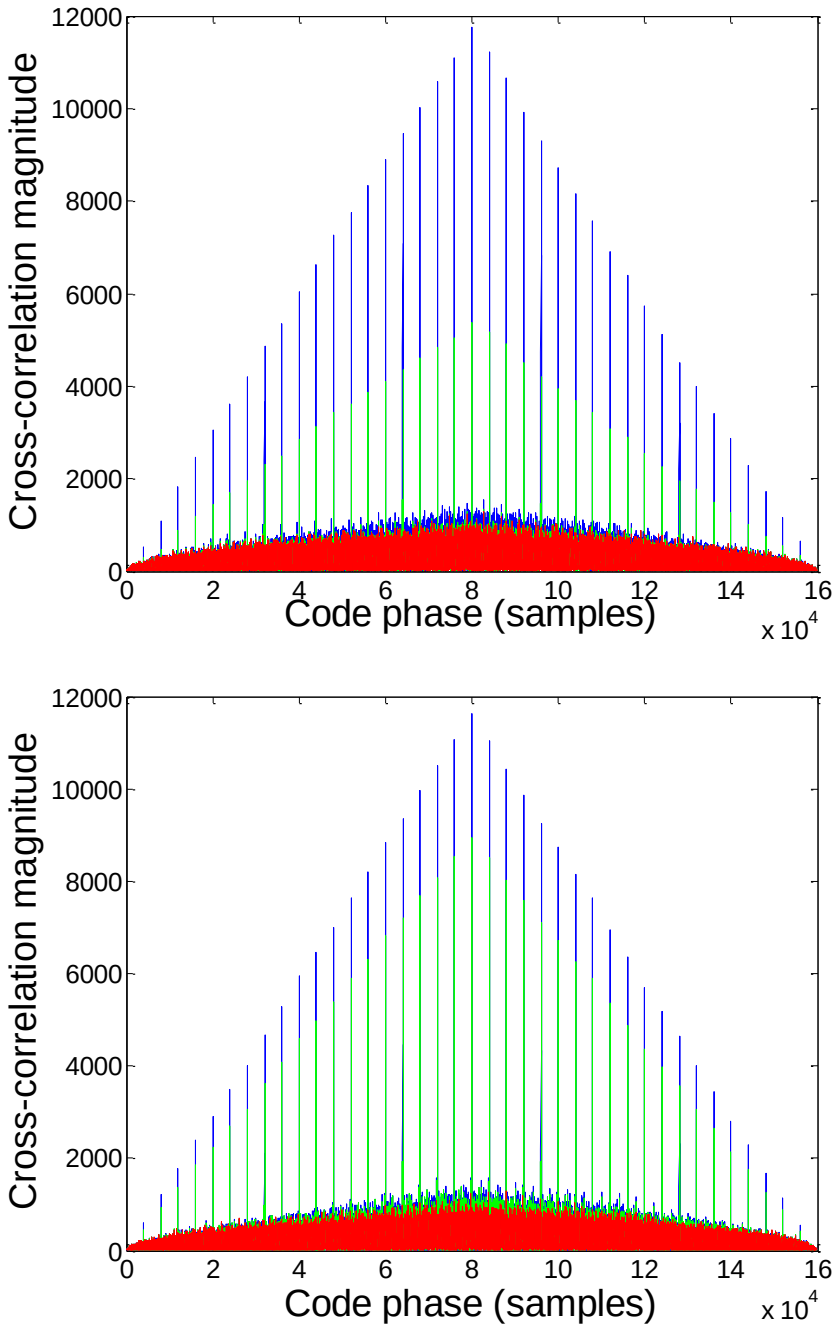

Figure 5.3.8: Cross correlation results comparison between the MSP cancellation (red) and the PSP cancellation (green) with a fraction delay. The data length is 20ms, the GPS (PRN 1) signal has a SNR of -20dB. The fractional delays are 1/4 chip (upper) and 1/2 chip (lower).

As shown in figure 5.3.8, the MSP method is able to cancel the GPS signal with the cancellation performance of -19.5dB for 1/4 chip (1 sample) and 1/2 chip (2 samples) delays. The cancellation performance of the PSP method decreases to -7.1dB (1/4 chip delay) and -2.4dB (1/2 chip delay).

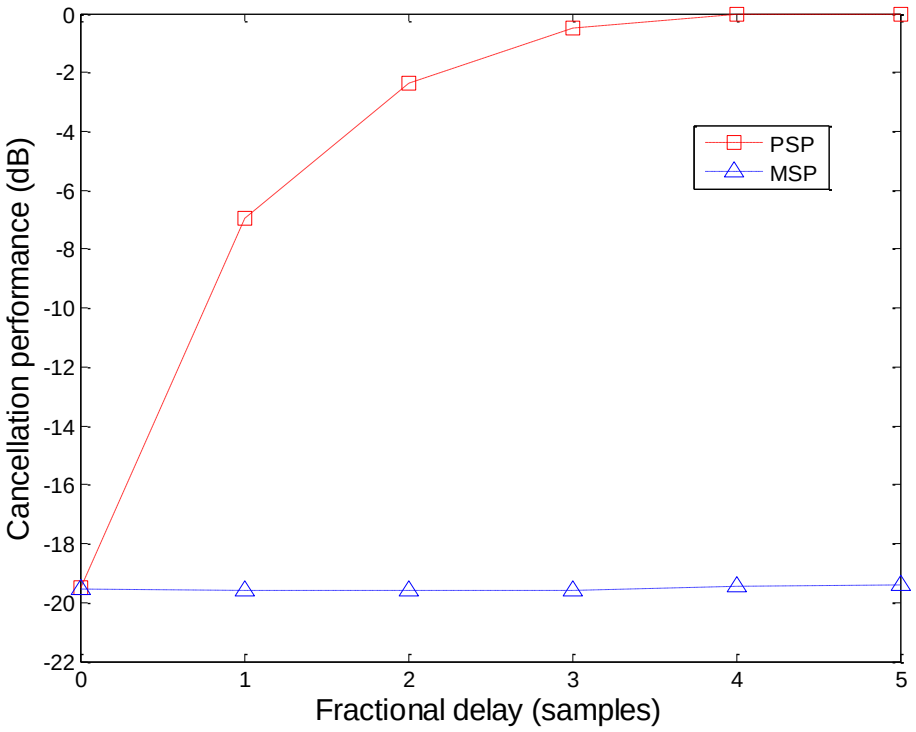

Figure 5.3.9: The cancellation performance comparison between MSP (blue) and PSP (red) using GPS (PRN 1) signal. The SNR of the GPS (PRN 1) signal is -20dB, the data length is 20ms, each cancellation performance point is estimated using 100 simulations

The simulation in Figure 5.3.9 assumes the fractional delay is able to be larger than half chip space (2 samples), but this rarely happens in real GPS applications. The result shows that the cancellation performance of the MSP method is -19.5dB in all the fractional delay conditions. The PSP method performs worse in the presence of any fractional delay, and it will fail when the delay is one chip (4 samples).

5.3.4 Scenario 4: one GPS signal with one multipath signal

In this simulation, there is only one GPS signal (PRN 1) and thermal noise in the received data. The GPS signal (PRN 1) has multipath components. The GPS signal (PRN 1) is intended to be cancelled. Due to the multiple dimensional subspace structure, the MSP method should still be able to cancel the GPS signal whilst the PSP method will perform worse or even fail.

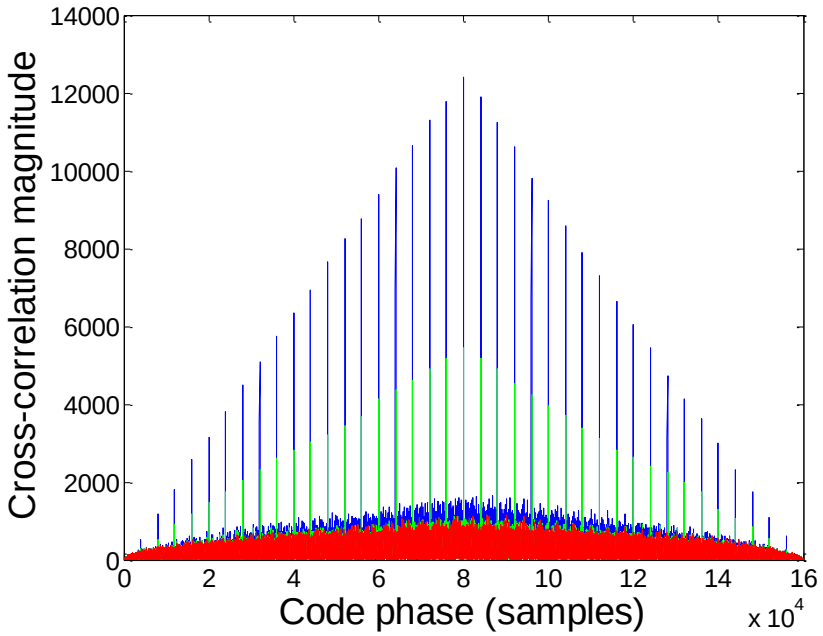

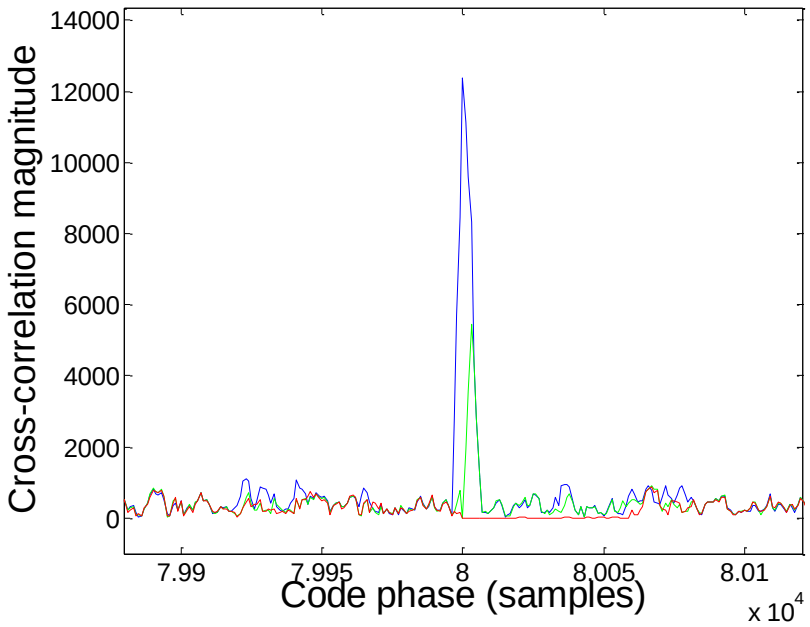

Figure 5.3.10: Cross correlation results comparison between the MSP cancellation (red) and the PSP cancellation (green) with a multipath signal. The blue curve is the cross-correlation result before cancellation. The data length is 20ms, the GPS (PRN 1) signal has a SNR of -20dB, the multipath signal has 3 sample delay and SNR of -26dB.

In figure 5.3.10, the upper graph shows the cross-correlation results for 39 correlation peaks, the lower graph shows the cross-correlation results for the highest (centre) peak, the data length is 20ms, the GPS (PRN 1) signal has a SNR of -20dB and the multipath signal has 3 sample delay and SNR of -26dB. The results show the MSP method is still able to cancel the GPS signal with the cancellation performance of -20.2dB. The cancellation performance of the PSP method decreases to -7.6dB.

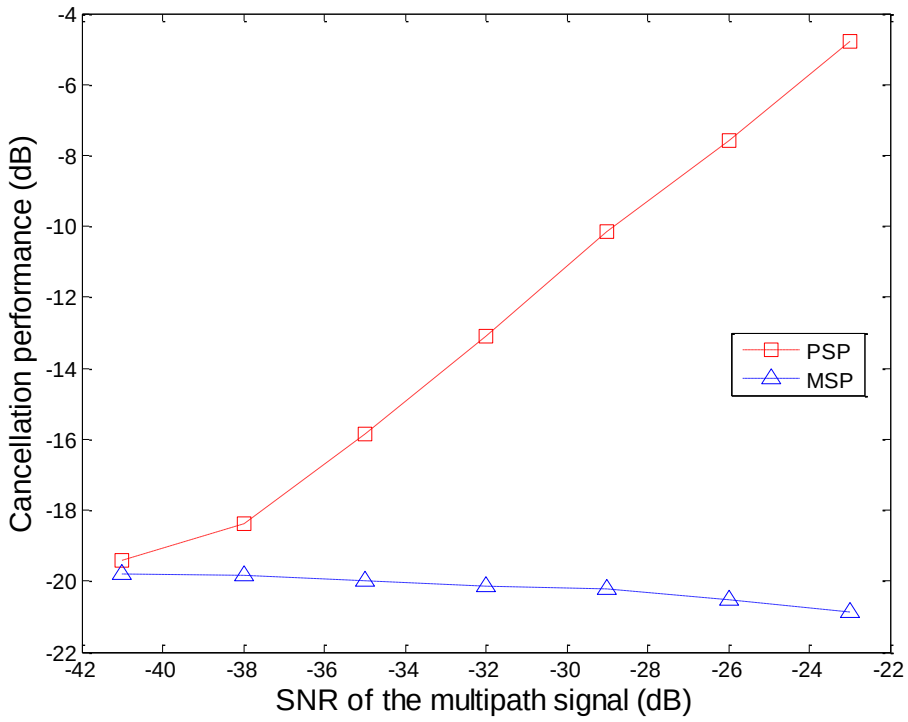

Figure 5.3.11: The cancellation performance comparison between MSP (blue) and PSP (red) using GPS (PRN 1) signal. The SNR of the GPS (PRN 1) signal is -20dB, the multipath signal has a 3 sample delay, the data length is 20ms, each cancellation performance point is estimated using 100 simulations.

Figure 5.3.11 shows the cancellation performance in the presence of one multipath signal with SNR from -26dB to –41dB. The cancellation performance of the MSP method is about -20dB in all the SNR conditions. The PSP method performs worse in the presence of multipath. The stronger (higher SNR) the multipath signal is, the larger the degradation is.

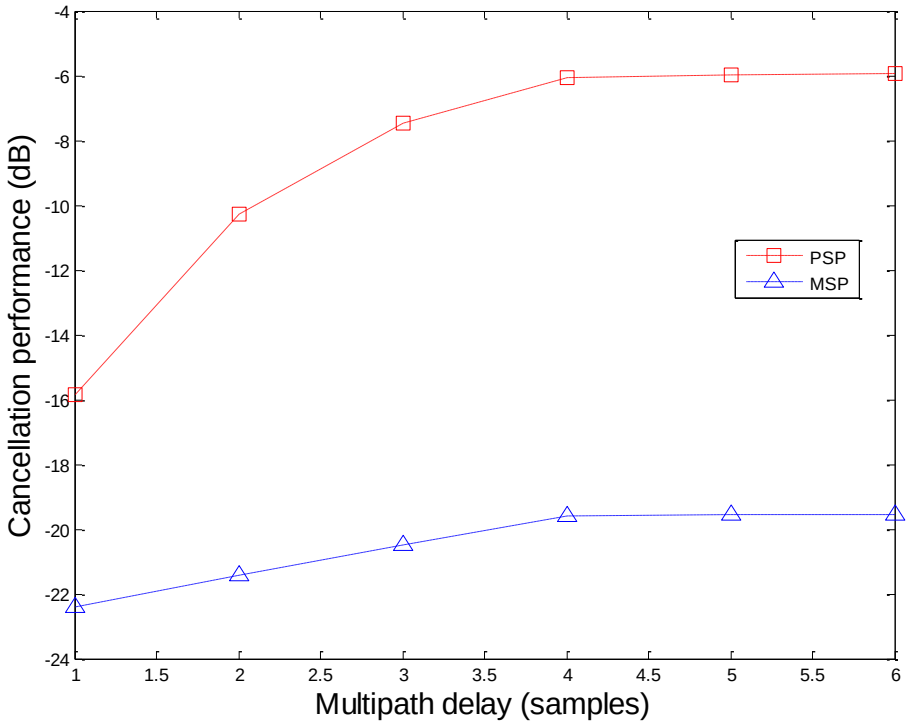

Figure 5.3.12: The cancellation performance comparison between MSP (blue) and PSP (red) using GPS (PRN 1) signal. The SNR of the GPS (PRN 1) signal is -20dB, the multipath signal has SNR of -26dB, the data length is 20ms, each cancellation performance point is estimated using 100 simulations.

Figure 5.3.12 shows the cancellation performance in the presence of one multipath signal with delay from 1 sample to 6 samples. The cancellation performance of the MSP method is about -20dB in all the SNR conditions. The cancellation performance of the PSP method degrades as the multipath delay increases. But when the multipath delay is larger than 4 samples (1 chip), the PSP cancellation performance stays at about -6 dB.

5.3.5 Scenario 5: one band-limited GPS signal

In this simulation, there is only one GPS signal (PRN 1) and thermal noise in the received data. The received data is filtered by a band pass filter. The GPS signal (PRN 1) is intended to be cancelled. Due to the multiple dimensional subspace structure, the MSP method should still be able to cancel the GPS signal whilst the PSP method will perform worse.

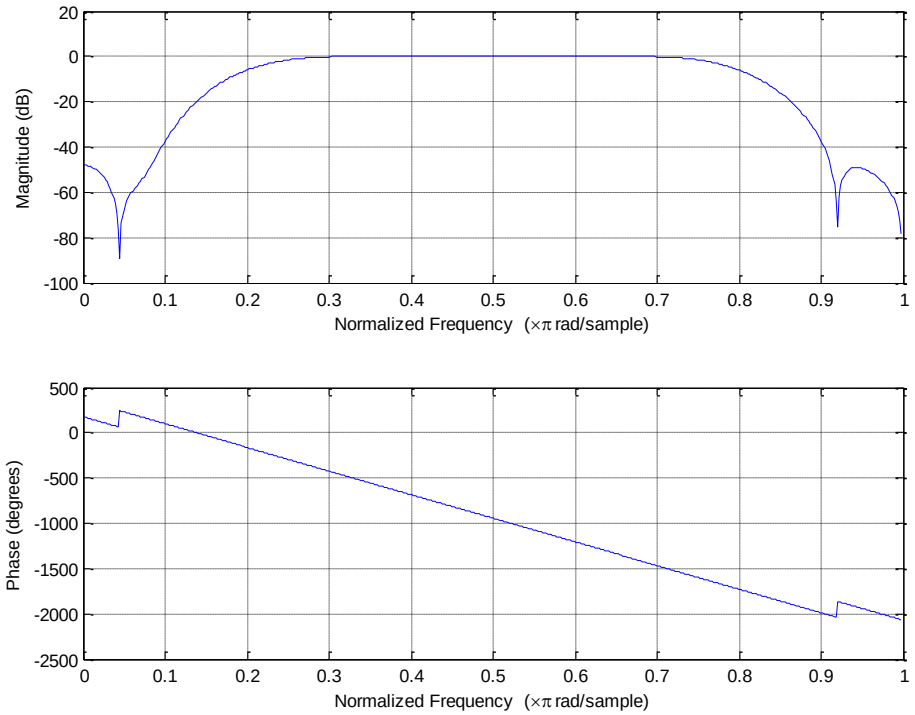

Figure 5.3.13: The frequency spectrum of the band pass filter.

Figure 5.3.13 shows the spectrum of this band pass filter. It is a 31 tap FIR filter with a group delay of 15 samples and it emulates the filter spectrum response in the GPS front-end. The pass band frequencies are [0.2 0.8] of fs/2, where fs is the 4MHz sampling frequency.

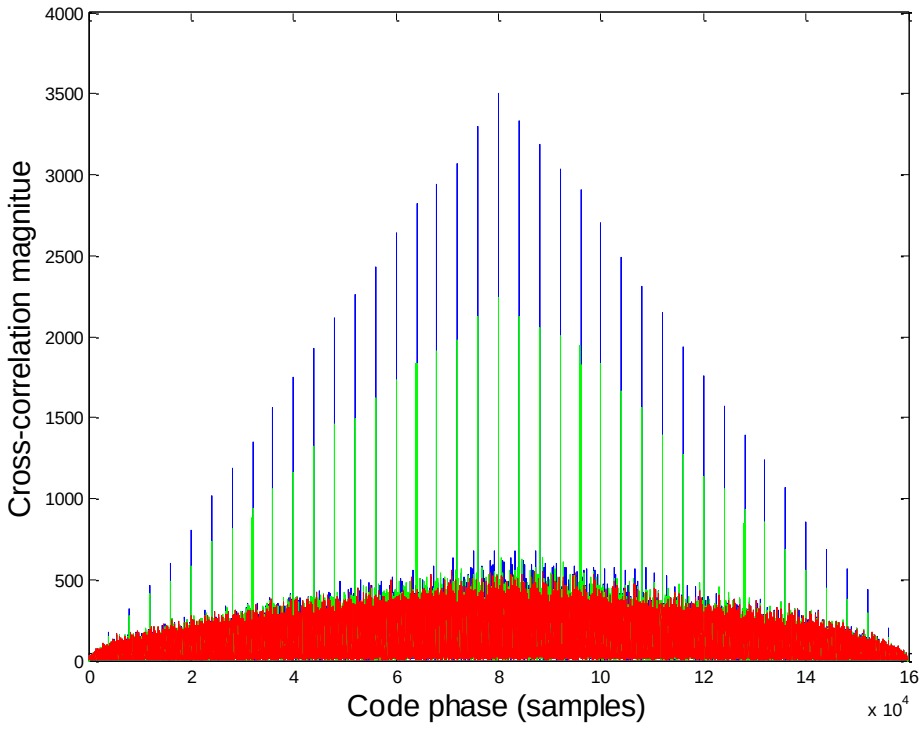

Figure 5.3.14: Cross correlation results comparison between the MSP cancellation (red) and the PSP cancellation (green) with a band limited GPS signal. The data length is 20ms, the GPS (PRN 1) signal has a SNR of -20dB.

Figure 5.3.14 shows the PSP method only has a cancellation performance of -4 dB because it cannot re-construct the shape the signal which is distorted by the front-end filter. Due to the multiple dimensional subspace structure, the MSP method is able to estimate this linear transfer system, linearly reconstruct the signal and cancel the band limited GPS signal.

5.3.6 Summary of Performance Analysis

As summarised in table 5.3.1, in the ideal condition with no errors, both the MSP and PSP are able to cancel the GPS signal effectively. If there is residual Doppler frequency in the GPS signal, the cancellation performances of the two algorithms degrade as the residual Doppler frequency increases. If the GPS signal has fractional delay error or multipath components, the

MSP method is still able to cancel this GPS signal whilst the PSP method provides less cancellation or even fails. If the GPS signal is distorted due to a band limiting filter, the PSP method fails to cancel the GPS signal whilst the MSP method is still able to cancel it.

Error type	Algorithm	
	PSP	MSP
Residual Doppler frequency	No	No
Fractional delay	No	Yes
Multipath	No	Yes
Band limiting	No	Yes

Table 5.3.1: Comparisons of the cancellation capability of PSP and MSP methods.

5.4 Experimental Results

An experiment was performed using the antenna array of the GNSS Environment Monitoring System (GEMS) [44, 45, 83]. The antenna array consisted of 7 equally spaced circular monopole antennas with one monopole antenna in the centre. Although the GPS signal cancellations were performed on all the channels, only the reference channel (channel 1, the centre antenna) result is presented in this section. The GEMS original sampling rate was 16MHz, but it was down sampled to 4MHz by software decimation in this experiment. The data length was 50ms (50 CA code periods). The MSP cancellation used 60 taps as it enables the filter response to be well modelled without incurring the losses associated with either too small or too many taps.

8 GPS signals were obtained after GPS acquisition. The MSP and PSP cancellation performance is summarised in table 5.4.1. MSP method has a better cancellation performance than PSP method for all the GPS signals. For PRN 16, 18, 19 and 21, MSP method is about 1.3dB better than PSP

method on average. For PRN 03, 06, 14 and 22, MSP method is 5.3dB better than PSP method on average. For PRN 21, MSP method is 0.96dB better than PSP method. For PRN 14, MSP method is 7.03dB better than PSP method.

PRN	**03**	**06**	**14**	**16**
MSP	-22.38	-22.63	-20.66	-17.54
PSP	-17.60	-16.23	-13.63	-16.42
PRN	**18**	**19**	**21**	**22**
MSP	-19.52	-21.45	-19.91	-20.60
PSP	-18.21	-20.08	-18.95	-17.11

Table 5.4.1: MSP and PSP cancellation performance comparison, the unit is in dB.

The cross-correlation results of PRN 14 and PRN 21 are shown in figure 5.4.1 and 5.4.2. MSP cancellation residues are almost in the noise floor for both cases but PSP cancellation has large residue peaks for PRN 14.

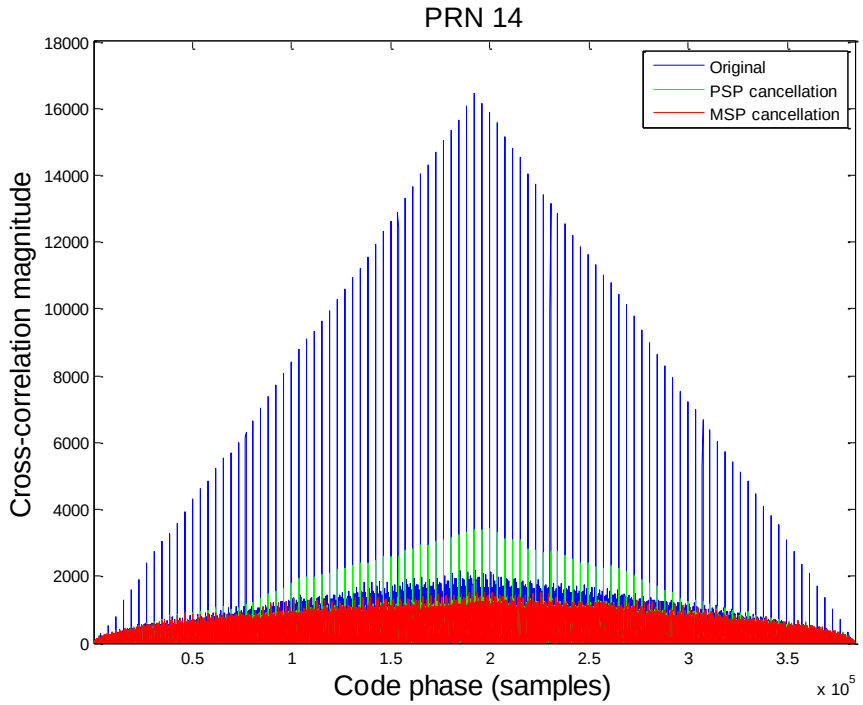

Figure 5.4.1: Cross correlation results comparison between the MSP cancellation (red) and the PSP cancellation (green) for PRN 14.

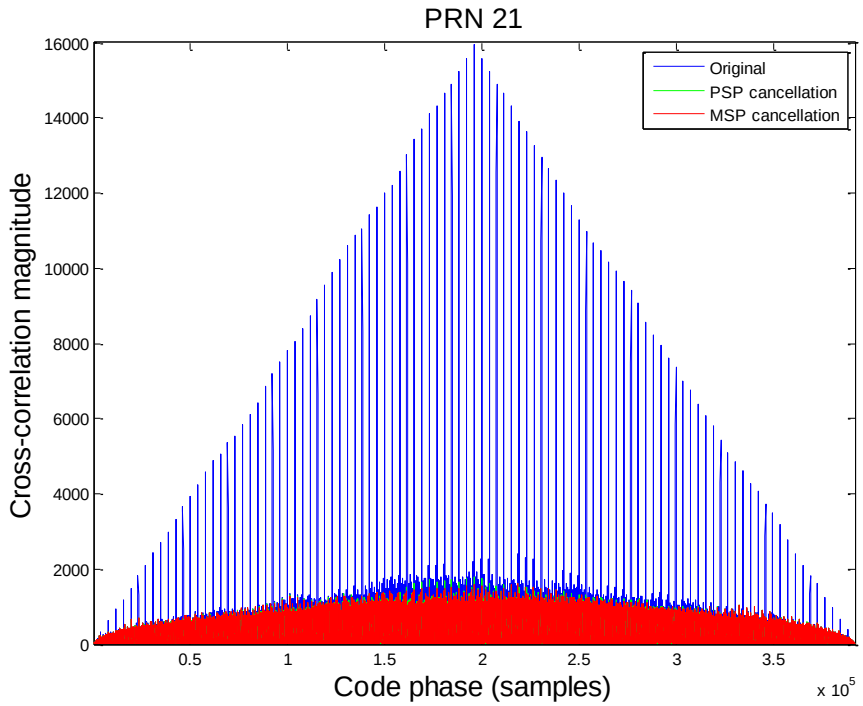

Figure 5.4.2: Cross correlation results comparison between the MSP cancellation (red) and the PSP cancellation (green) for PRN 21.

5.5 Conclusion

In this chapter, a Multiple Subspace Projection (MSP) method is proposed to cancel the GPS signals in the received data of a GPS antenna array to enable accurate DOA estimation of weak GPS interferences. The simulations show this method is capable of subtracting the GPS signals even if the GPS signal has unknown amplitude and carrier phase, multipath components, fractional delays or is band-limited due to the receiver front end filters. The experiment result shows the GPS signals in the real received data are effectively cancelled.

Chapter 6: Weak GPS Interference DOA Estimation

6.1 Introduction

This chapter first considers the effect of the number of snapshots used in the covariance matrix estimation and the effect of coloured noise on weak interference direction of arrival estimation. An experiment and the use of the collected data to estimate the direction of arrival (DOA) of a weak interference in the GPS L1 band using antenna array calibration, GPS signal cancellation and coloured noise whitening techniques are then discussed.

The remainder of this chapter is structured as follows. The received signal models for direction of arrival estimation with and without model errors are introduced in Section 6.2. Based on the signal model without errors, a CRLB analysis is conducted to investigate the effect of the number of snapshots used in covariance matrix estimation on the DOA estimation variance in Section 6.3. The effect of coloured noise and its mitigation are discussed in Section 6.4. An experiment set up to estimate the DOA of a weak interference and the results obtained are presented in Section 6.5, and the conclusions are given in Section 6.6.

6.2 Signal Model of Weak GPS Interference DOA Estimation

In this section, the signal model used for weak interference DOA estimation is described. In Section 6.2.1 the signal model of an ideal antenna array in

the presence of a single far-field interference is presented. Due to errors in the antenna array, when estimating the DOA of weak interference, the real signal model is unlikely to be the same as the ideal signal model. So an alternative signal model taking into account such errors is proposed in Section 6.2.2.

6.2.1 Ideal Signal Model

Consider an ideal GPS antenna array of M elements in the presence of a single far-field interference in the GPS L1 frequency band. To provide a useful bound to estimation accuracy it has been assumed, on this ideal case, that there are no GPS signals present or alternatively all GPS signals have been removed by the techniques outlined in Chapter 5. The vector form of the M sensor outputs $\underline{x}$ at the time *t* is

$$\underline{x}(t) = \underline{v}_s s(t) + \underline{n}(t) \tag{6.2.1}$$

where $\underline{v}_s \equiv \underline{v}_s(\theta_s\,,\,\varphi_s)$ is the M×1 signal steering vector which is derived based on the antenna array geometry, the azimuth angle θ_s and the elevation angle φ_s of the interference, $s(t)$ is the transmitted interference at time *t*, $\underline{n}(t)$ is the M×1 additive receiver noise which is assumed to be uncorrelated Additive White Gaussian Noise (AWGN).

The covariance matrix $\mathbf{R}$ of the received signal is

$$\mathbf{R} = E\{\underline{x}(t)\underline{x}^H(t)\} = \mathbf{R}_s + \mathbf{R}_n = {\sigma_s}^2 \underline{v}_s {\underline{v}_s}^H + {\sigma_n}^2 \mathbf{I} \tag{6.2.2}$$

where H is the Hermitian transpose, $\mathbf{R}_s$ is the M×M interference covariance matrix, $\mathbf{R}_n$ is the M×M noise covariance matrix, ${\sigma_s}^2$ is the interference power, ${\sigma_n}^2$ is the noise power and $\mathbf{I}$ is the M×M identity matrix.

The estimated covariance matrix $\widehat{\mathbf{R}}$ is

$$\hat{\mathbf{R}} = \frac{1}{N}\sum_{n=1}^{N} \underline{x}(n)\underline{x}^{H}(n) \qquad (6.2.3)$$

where *N* is the number of the snapshots.

In this ideal signal model, three factors are not considered, which need to be included when estimating the DOA of a very weak interference in the GPS frequency band with a signal to noise ratio lower than -15 dB.

Factor 1: Antenna array errors

The true array manifold may be different from the theoretical computed steering vector due to the mutual coupling between the antennas, gain/phase errors in each channel and the antenna array orientation error. The GPS antenna array calibration algorithms to estimate these errors have been proposed in Chapter 3 and Chapter 4.

Factor 2: Other directional signals in the GPS L1 frequency band

The GPS L1 frequency band is well protected by law. However navigation signals themselves are in the L1 frequency band. These navigation signals are: GPS L1 C/A code, GPS L1 P(Y) code and Galileo E1 code. These signals are very weak. For example, the SNR of the GPS L1 C/A code is -15 dB to -30 dB. As discussed in Chapter 5, if the INR of the intended interference is stronger than -10 dB, its DOA estimation is not influenced. However, if the INR is below -10 dB, the DOA estimation results are affected.

The Multiple Subspace Projection (MSP) method has been proposed in Chapter 5 to cancel the GPS L1 C/A signal. Because the GPS P(Y) code is encrypted, it will be very difficult to cancel them. But the SNR of the GPS L1 P(Y) signal is even weaker than GPS L1 C/A signal. The null to null bandwidth of the GPS L1 P(Y) signal is 20.46 MHz which is 10 times larger than the GPS L1 C/A signal which has a null to null bandwidth of 2.046MHz [2]. The typical power of the GPS L1 P(Y) signal is -163 dBW while the typical power of the GPS L1 C/A signal is -160 dBW. So the GPS L1 P(Y)

signal is about 10 dB lower than the GPS L1 C/A signal in a 4 MHz bandwidth which is the bandwidth used in this chapter. The SNR of the GPS L1 P(Y) signal is about -25 dB to -40 dB. This will have no or very limited effect on DOA estimation of an interference with an INR of -20 dB. Whilst the Galileo navigation system had 15 operational satellites in year 2016, there were only 2 operational satellites at the time of the experiment (May 2012), so it was not a problem. In the future, spatial filtering methods or MSP based subspace cancellation methods can be used to remove Galileo signals.

Factor 3: Correlated noise

The receiver noise may not be uncorrelated white Gaussian noise, so its covariance matrix may have values at non-diagonal positions (coloured) and needs to be whitened. The solution “coloured noise whitening” will be discussed in Section 6.4.

6.2.2 Signal Model with Errors

The following new signal model is proposed to include the above three factors.

Consider a GPS antenna array of M elements in the presence of single interference and N GPS L1 C/A code signals. The vector form of the M sensor outputs $\underline{x}$ at time t is

$$\underline{x}(t) = \mathbf{E}\underline{v}_s s(t) + \mathbf{E}\mathbf{V}_i \underline{s}_i(t) + \underline{n}(t) \tag{6.2.4}$$

where $\mathbf{E}$ is the M×M matrix describing the uncertainties in the antenna array, $\underline{v}_s$ is the M×1 steering vector derived from the antenna array geometry and the DOA of the interference, $s(t)$ is the transmitted interference at time t, $\mathbf{V}_i$ is the M×N matrix whose columns consist of the GPS signal steering vectors which are derived from the antenna array geometry and the DOA of the GPS

signals, $\underline{s_i}(t)$ is the N×1 transmitted GPS signals at time t and $\underline{n}(t)$ is the receiver coloured noise.

The array error matrix $\mathbf{E}$ is given by

$$\mathbf{E} = \mathbf{C\Gamma} \tag{6.2.5}$$

where $\mathbf{C}$ is the antenna mutual coupling matrix and $\mathbf{\Gamma}$ is the channel gain/phase error matrix. Calibration techniques based on of these matrices are discussed in Chapter 3 and 4.

The covariance matrix $\mathbf{R}$ of the received signal is

$$\mathbf{R} = E\{\underline{x}(t)\underline{x}^H(t)\} = \mathbf{R}_s + \mathbf{R}_i + \mathbf{R}_n \tag{6.2.6}$$

where $\mathbf{R}_s$ is the estimated M×M interference covariance matrix, $\mathbf{R}_i$ is the estimated M×M GPS signal covariance matrix and $\mathbf{R}_n$ is the estimated M×M coloured noise covariance matrix.

The estimated covariance matrix $\widehat{\mathbf{R}}$ of the received signal is

$$\widehat{\mathbf{R}} = \frac{1}{N}\sum_{n=1}^{N}\{\underline{x}(n)\underline{x}^H(n)\} \tag{6.2.7}$$

where *N* is the number of snapshots used to estimate the covariance matrix.

6.3 Cramer-Rao Lower Bound (CRLB) Analysis for DOA Estimation

The Cramer-Rao Lower Bond (CRLB) is defined as the negative of the second order derivative of the logarithm of the likelihood function at its peak [145]. The likelihood function is the probability density function of the data as a function of the unknown parameters [91]. The CRLB provides useful

engineering limits to the estimation accuracy of the unknown parameters of the likelihood function. In this section, the standard expression for the CRLB [67, 146] is applied to a circular array with an element in the centre.

6.3.1 CRLB Derivation for Ideal Signal Model

Consider a far-field single interference, the likelihood function of the complete received data set $\{\underline{x}(t)$, *t = 1, 2, … , T*$\}$ is given by

$$P\left[\underline{x}(1), \underline{x}(2), \dots, \underline{x}(T)|\underline{\Psi}\right] = \prod_{t=1}^{T} \frac{1}{\pi^M \|\mathbf{R}\|} \exp\left(-\underline{x}^H(t)\mathbf{R}^{-1}\underline{x}(t)\right) \quad (6.3.1)$$

where *T* is the number of snapshots, $\underline{\Psi}$ is the unknown parameter vector of the likelihood function, *M* is the number of antennas, $\mathbf{R}$ is the covariance matrix.

The unknown parameters $\underline{\Psi}$ of the likelihood function are given by

$$\underline{\Psi} = [\theta, \varphi]^T \quad (6.3.2)$$

where φ is the azimuth angle and φ is the elevation angle of the weak interference.

The covariance matrix of the ideal signal model is given by equation 6.2.2 in Section 6.2.1 as

$$\mathbf{R} = {\sigma_s}^2 \underline{v_s}\underline{v_s}^H + {\sigma_n}^2 \mathbf{I} \quad (6.3.3)$$

The unconditional CRLB [67, 146] can be shown to be

$$\mathbf{CRLB}(\mathbf{\Phi}) = \mathbf{J}^{-1}(\underline{\Psi}) \quad (6.3.4)$$

where the elements of the symmetric Fisher Information Matrix (FIM) are

$$J_{ij} = J_{ji} = T\ trace\left\{\mathbf{R}^{-1}\frac{\partial \mathbf{R}}{\partial \underline{\Psi}_i}\mathbf{R}^{-1}\frac{\partial \mathbf{R}}{\partial \underline{\Psi}_j}\right\} \tag{6.3.5}$$

Azimuth angle – azimuth angle terms is

$$J_{\theta,\theta} = T\ trace\left\{\mathbf{R}^{-1}\frac{\partial \mathbf{R}}{\partial \theta}\mathbf{R}^{-1}\frac{\partial \mathbf{R}}{\partial \theta}\right\} \tag{6.3.6}$$

$$J_{\theta,\theta} = T\sigma_s{}^4\left\{\mathbf{R}^{-1}(\underline{\dot{v}}_{s_\theta}\underline{v}_s{}^H + \underline{v}_s\underline{\dot{v}}_{s_\theta}{}^H)\mathbf{R}^{-1}(\underline{\dot{v}}_{s_\theta}\underline{v}_s{}^H + \underline{v}_s\underline{\dot{v}}_{s_\theta}{}^H)\right\} \tag{6.3.7}$$

where $\underline{\dot{v}}_{s_\theta} = \partial \underline{v}_s(\theta,\varphi)/\partial\theta$.

Elevation angle – elevation angle term is

$$J_{\varphi,\varphi} = T\ trace\left\{\mathbf{R}^{-1}\frac{\partial \mathbf{R}}{\partial \varphi}\mathbf{R}^{-1}\frac{\partial \mathbf{R}}{\partial \varphi}\right\} \tag{6.3.8}$$

$$J_{\varphi,\varphi} = T\sigma_s{}^4\left\{\mathbf{R}^{-1}(\underline{\dot{v}}_{s_\varphi}\underline{v}_s{}^H + \underline{v}_s\underline{\dot{v}}_{s_\varphi}{}^H)\mathbf{R}^{-1}(\underline{\dot{v}}_{s_\varphi}\underline{v}_s{}^H + \underline{v}_s\underline{\dot{v}}_{s_\varphi}{}^H)\right\} \tag{6.3.9}$$

where $\underline{\dot{v}}_{s_\varphi} = \partial \underline{v}_s(\theta,\varphi)/\partial\varphi$.

Azimuth angle – elevation angle term is

$$J_{\theta,\varphi} = T\ trace\left\{\mathbf{R}^{-1}\frac{\partial \mathbf{R}}{\partial \theta}\mathbf{R}^{-1}\frac{\partial \mathbf{R}}{\partial \varphi}\right\} \tag{6.3.10}$$

$$J_{\theta,\varphi} = T\sigma_s{}^4\left\{\mathbf{R}^{-1}(\underline{\dot{v}}_{s_\theta}\underline{v}_s{}^H + \underline{v}_s\underline{\dot{v}}_{s_\theta}{}^H)\mathbf{R}^{-1}(\underline{\dot{v}}_{s_\varphi}\underline{v}_s{}^H + \underline{v}_s\underline{\dot{v}}_{s_\varphi}{}^H)\right\} \tag{6.3.11}$$

Finally, the FIM is given by

$$\mathbf{J} = \begin{bmatrix} J_{\theta,\theta} & J_{\varphi,\theta} \\ J_{\theta,\varphi} & J_{\varphi,\varphi} \end{bmatrix} \tag{6.3.12}$$

6.3.2 The Antenna Array and CRLB Analysis

The antenna array used for DOA estimation was an 8 element monopole antenna array shown in figure 6.3.1. It was a 7 element uniformly spaced

circular array with an additional 1 element in the center. The radius of the circular array was 10cm.

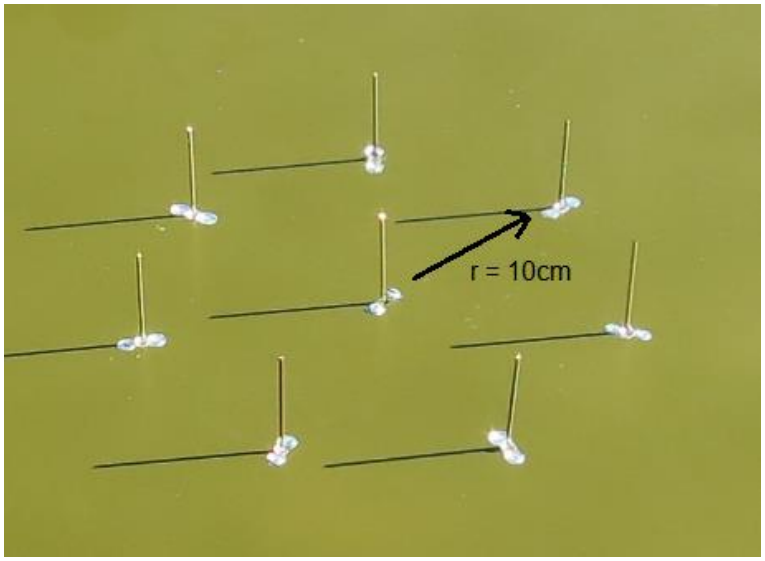

Figure 6.3.1: The 8 element monopole antenna array.

The Cramer-Rao Lower Bound (CRLB) of the ideal signal model of this antenna array is numerically analysed in this section due to its highly complex analytical solutions. Unless specified otherwise, the default parameter values used in the CRLB calculations are: target SNR = -20dB, azimuth angle = 180º, elevation angle = 85º, the number of snapshots is 1×10^6. For example, when analysing CRLB for azimuth angle variation with azimuth angle, SNR = -20dB and elevation angle = 85º are used in the calculations; when analysing CRLB for azimuth angle variation with elevation angle, SNR = -20dB and azimuth angle = 180º are used in the calculations.

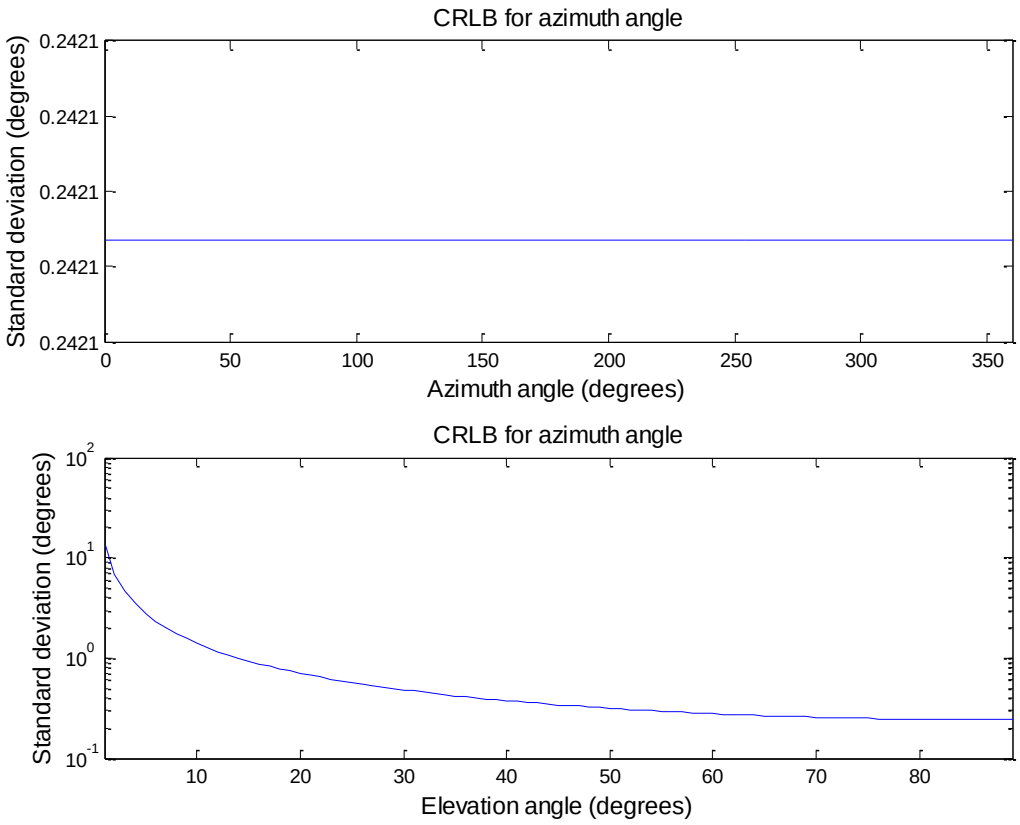

Figure 6.3.2: CRLB for azimuth angle variation with azimuth angle (upper) and elevation angle (lower).

As shown in figure 6.3.2, this antenna array has a uniform azimuth angle estimation standard deviation (STD), but the azimuth angle estimation STD for the same azimuth angle increases as the elevation angle decreases. This is as expected because the antenna array elements are uniformly distributed along the azimuth direction but not along the elevation direction.

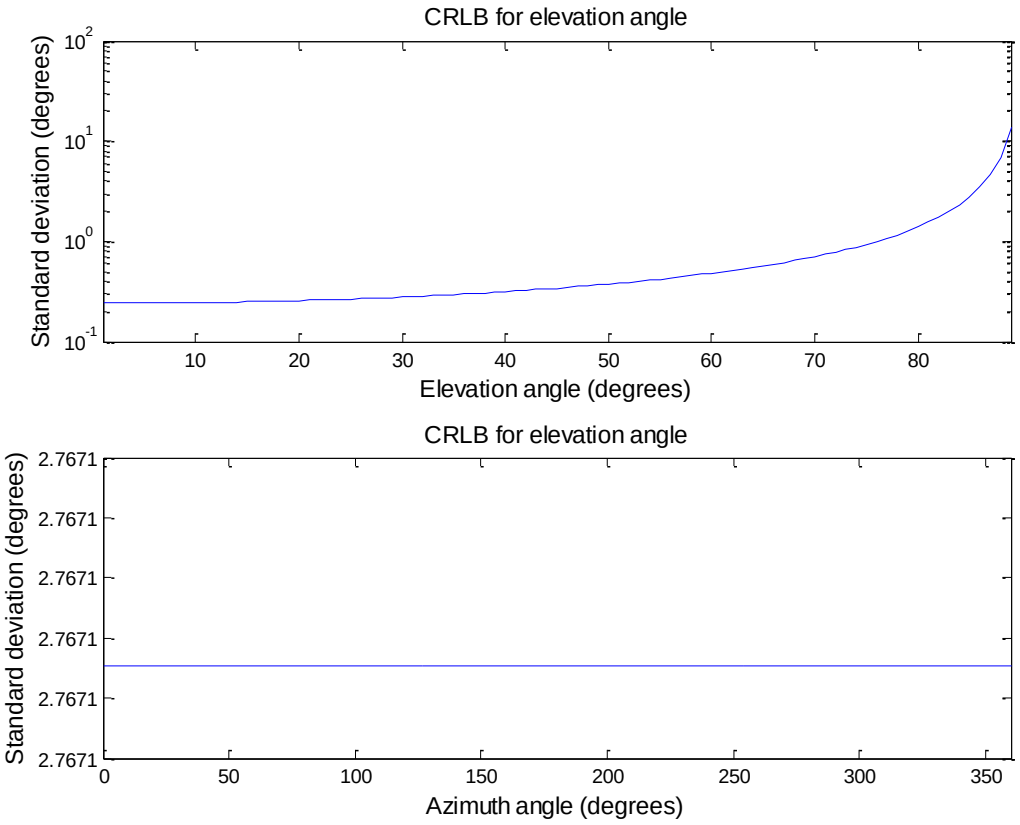

Figure 6.3.3: CRLB for elevation angle variation with elevation angle (upper) and azimuth angle (lower).

Figure 6.3.3 shows the similar results as above, as the elevation angle decreases, the elevation angle estimation STD decreases, but the elevation angle estimation for the same elevation angles does not vary with azimuth angle.

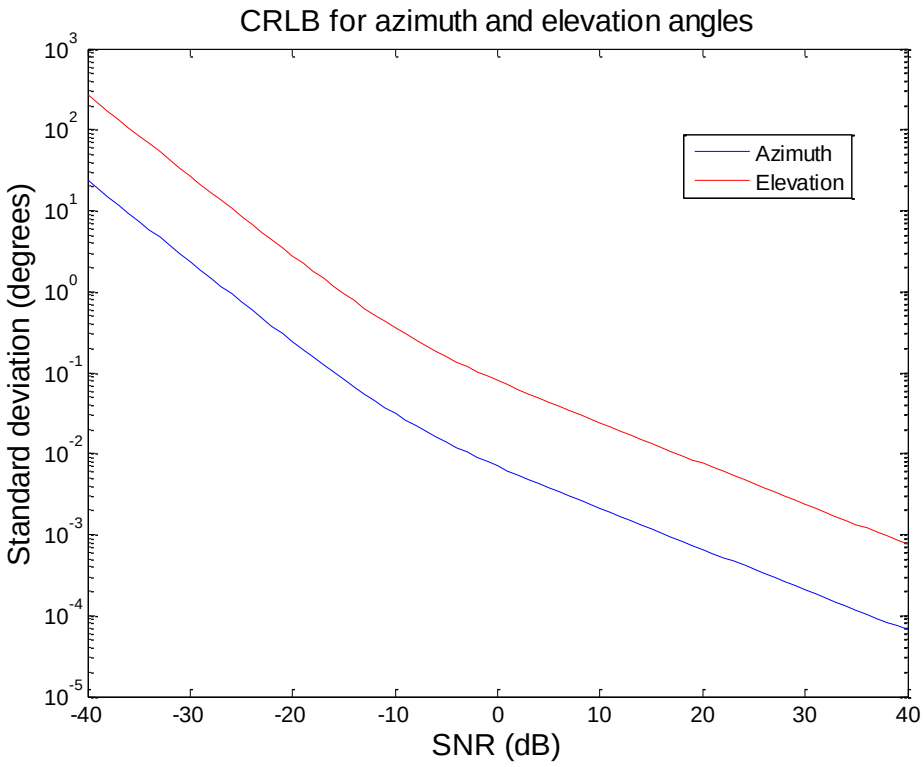

Figure 6.3.4: CRLB for azimuth angle variation with SNR (blue) and CRLB for elevation angle variation with SNR (red).

Figure 6.3.4 shows both azimuth and elevation angle estimation STD decreases as the signal SNR increases. However, azimuth angle estimation STD is about 10 times lower than elevation estimation STD for the same SNR.

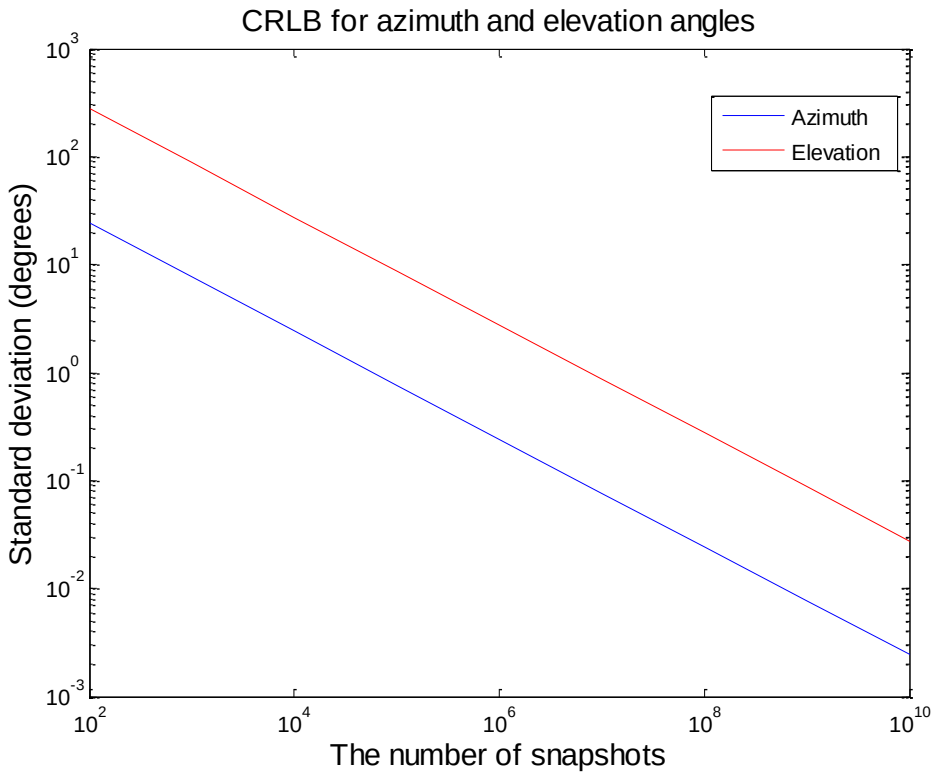

Figure 6.3.5: CRLB for azimuth angle variation with the number of snapshots (blue) and CRLB for elevation angle variation with the number of snapshots (red).

As shown in figure 6.3.5, both azimuth and elevation angle estimation STDs decrease as the number of snapshot increases, however the azimuth angle estimation STD is still about 10 times lower than elevation estimation variance for the same SNR. If the standard deviation of the azimuth DOA estimate is required to be lower than 1º, the number of snapshots in the covariance matrix estimation must be larger than 100,000. In this chapter, the number of snapshots is selected to be 1,000,000, which corresponds to a azimuth angle standard deviation of 0.248 degrees and a ± 9 m location error at a 1 km range as shown in table 6.3.6. For a 4MHz sampling rate, 1,000,000 samples is equivalent to 0.25 seconds. This time duration is effective against short time interferences.

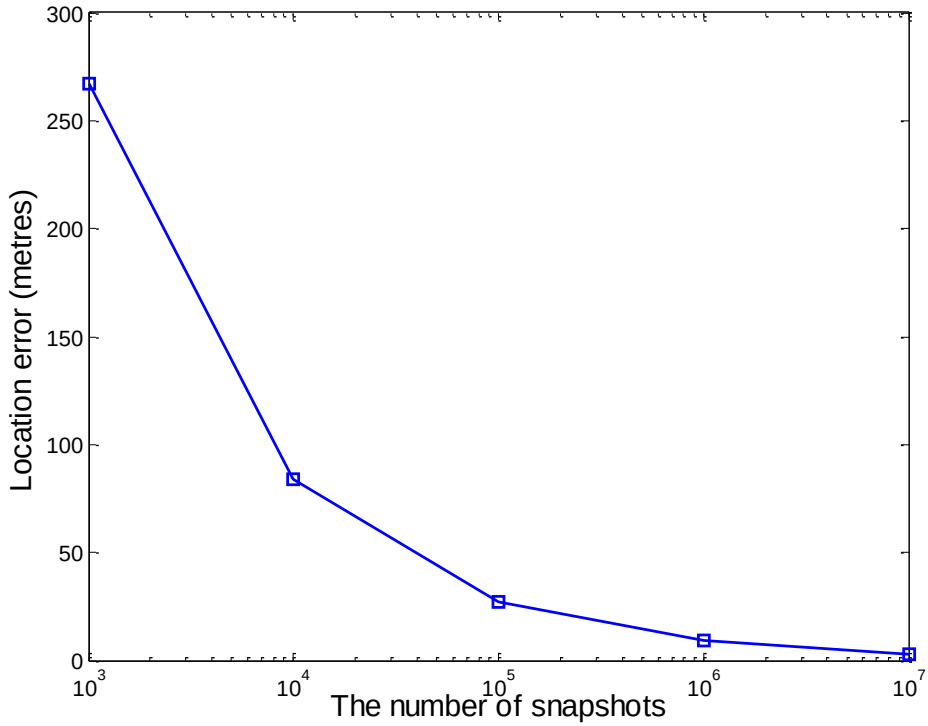

Figure 6.3.6: The number of snapshots and the predicted location errors based on CRLB. The location error assumes 1 km distance from the array and is estimated by 2 STD of azimuth DOA estimation.

6.4 Coloured Noise Mitigation

This section discusses the coloured noise whitening method and a potential Galileo satellite interference mitigation method.

Adaptive antenna array techniques such as MUSIC assume the noise within the system is uniformly distributed spatially uncorrelated White Gaussian Noise with the a noise covariance matrix $\mathbf{R}_n = {\sigma_n}^2\mathbf{I}$, where ${\sigma_n}^2$ is the noise power and $\mathbf{I}$ is the identity matrix. However, due to low level spurious oscillations in the front-end electronics, channel coupling and near-field interferences, the noise in the system is non-uniformly distributed and its covariance matrix is not diagonal.

An example of the covariance matrix of the noise-only data in GNSS Environmental Monitoring System (GEMS) antenna array is shown in figure 6.4.1. The (2, 5)th value of the covariance matrix is 0.22 whilst the diagonal values are around 0.93. There will thus be a significant noise model error if $\mathbf{R}_n = {\sigma_n}^2\mathbf{I}$ is used.

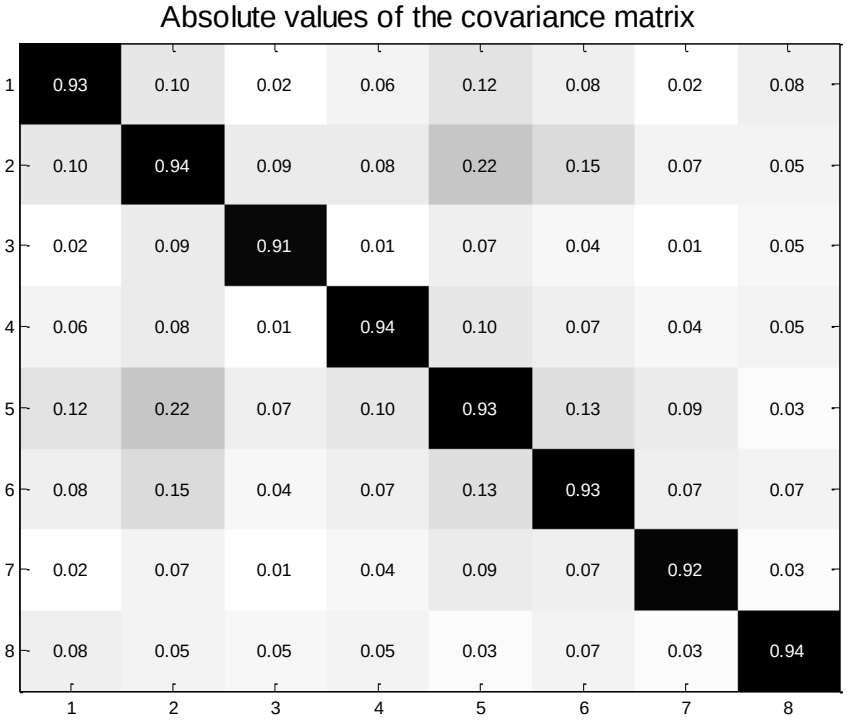

Figure 6.4.1: The covariance matrix of the noise-only data.

The Minimum Variance Distortionless Response algorithm (MVDR) estimated power spectrum of the above noise-only data in figure 6.4.1 is shown in figure 6.4.2. The standard deviation of the MVDR estimated power spectrum was 0.0098, the average estimated power was 0.1103. This non-uniform angular distribution of noise power indicated by the peak around 150 degrees azimuth and 90 degrees elevation will behave as strong interference and mask weak interferences.

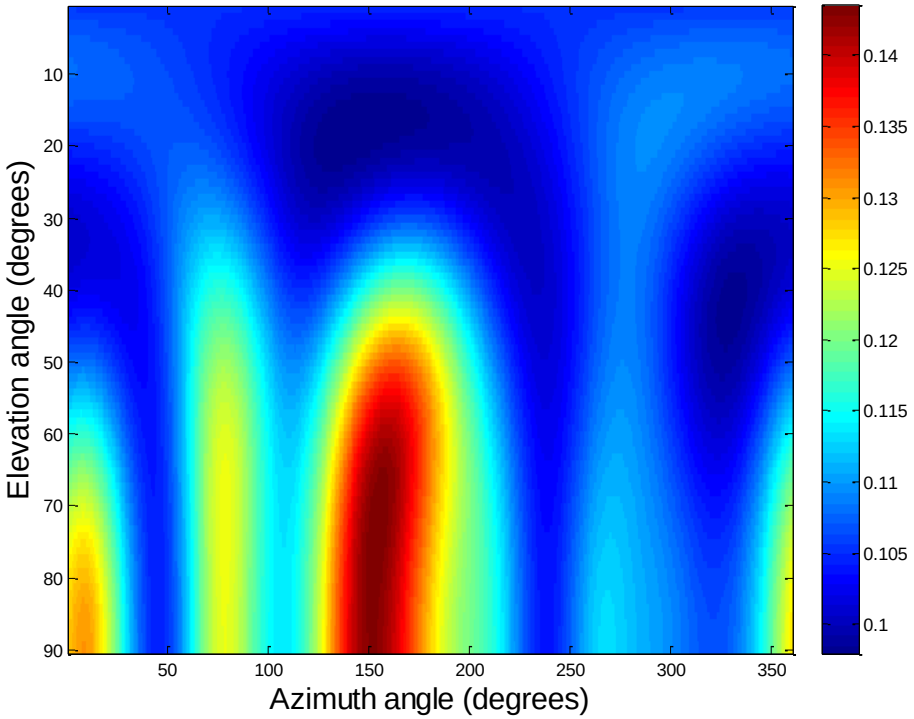

Figure 6.4.2: MVDR estimated power spectrum of the noise-only data.

Various methods for coloured noise whitening or DOA estimation in the presence of coloured noise are discussed in [147-159]. This chapter uses the coloured noise whitening method introduced in [145].

This method assumes a previously recorded noise-only calibration data $\mathbf{R}_c$ has been obtained. Assuming the noise is stationary, then

$$\mathbf{R}_c \approx \mathbf{R}_n \tag{6.4.1}$$

The decomposition

$$\mathbf{R}_c{}^{-1} = \mathbf{D}^H\mathbf{D} \tag{6.4.2}$$

Is used to project $\mathbf{R}_n$ onto the subspace spanned by **D** and the following equation is obtained

$$\mathbf{D}\mathbf{R}_n\mathbf{D}^H \approx \mathbf{D}\mathbf{R}_c\mathbf{D}^H = \mathbf{D}\mathbf{D}^{-1}\mathbf{D}^{H\,-1}\mathbf{D}^H = \mathbf{I} \tag{6.4.3}$$

So the coloured noise $\mathbf{R}_n$ is whitened.

The above noise-only data in figure 6.4.1 and figure 6.4.2 was whitened by the noise-only data which was captured 40 minutes earlier. Figure 6.4.3 shows the maximum non-diagonal value was reduced to 0.093 and the diagonal values were increased to about 1.0 resulting in a noise model that is significantly closer to $\mathbf{R}_n = {\sigma_n}^2\mathbf{I}$.

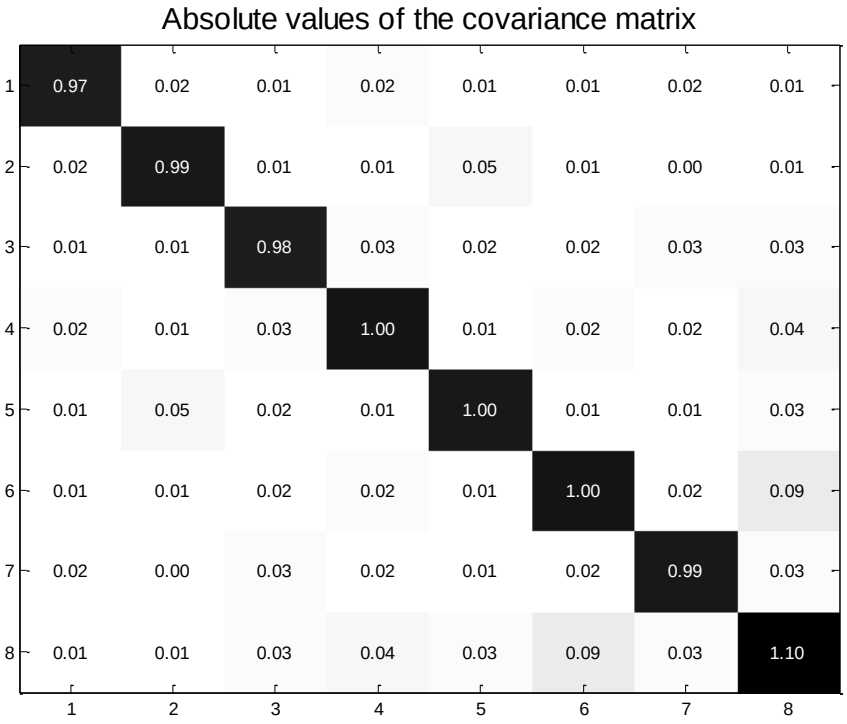

Figure 6.4.3: The covariance matrix of the whitened noise.

The MVDR estimated power spectrum of the whitened noise in figure 6.4.3 is shown in figure 6.4.4. The standard deviation of the MVDR estimated power spectrum was reduced to 0.0033, and the average power was increased to 0.1248. The noise power mismatch in spatial domain is reduced.

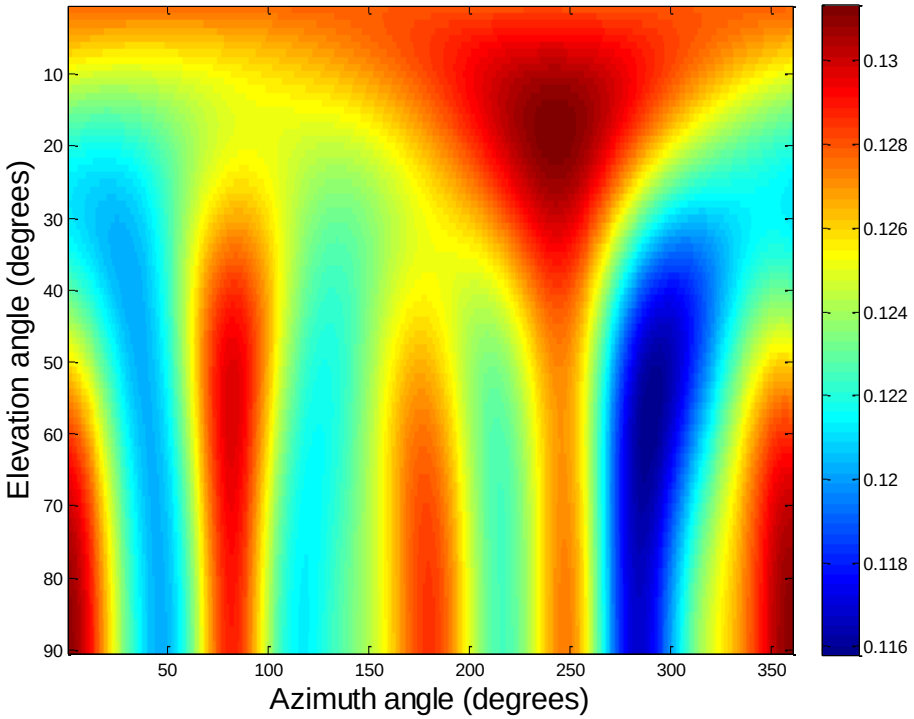

Figure 6.4.4: MVDR estimated power spectrum of the whitened noise.

6.5 Experimental Results

Before the experiment, the antenna array was calibrated using the calibration algorithm proposed in Chapter 4 to obtain estimates of the antenna array orientation and the mutual coupling matrix.

The received data was processed in 5 steps:

1. Cancel the GPS signals from the data using MSP method proposed in Chapter 5.
2. Construct the covariance matrix with 1×10^6 samples (250 CA code periods).
3. Whiten the constructed covariance matrix using the noise only data as described in Section 6.4.

4. Correct the array manifold using the estimated calibration parameters by the calibration algorithm in Chapter 4. The estimated mutual coupling matrix of the antenna array is shown in figure 6.5.1.

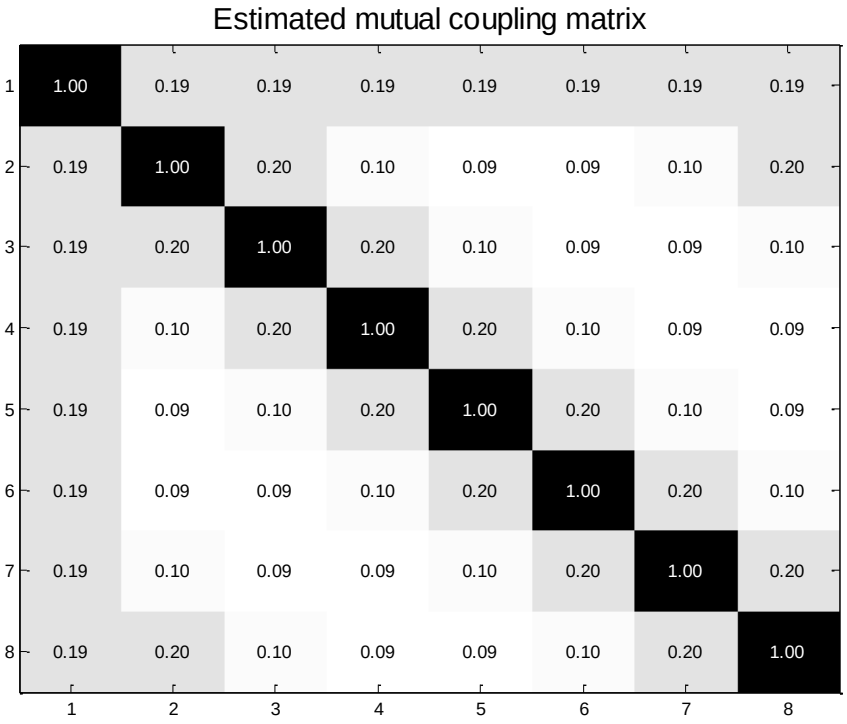

Figure 6.5.1: Estimated mutual coupling matrix using the calibration algorithm in Chapter 4.

5. Estimate the DOA of the interference using MUltiple Signal Classification algorithm (MUSIC).

6.5.1 Hardware Description

The antenna array hardware consisted of an 8 element antenna array followed by an 8 channel down converter followed by an Analogue to Digital Converter (ADC) and an FPGA board that buffered the data prior to transferring it to the computer. The basic structure is shown in figure 6.5.2.

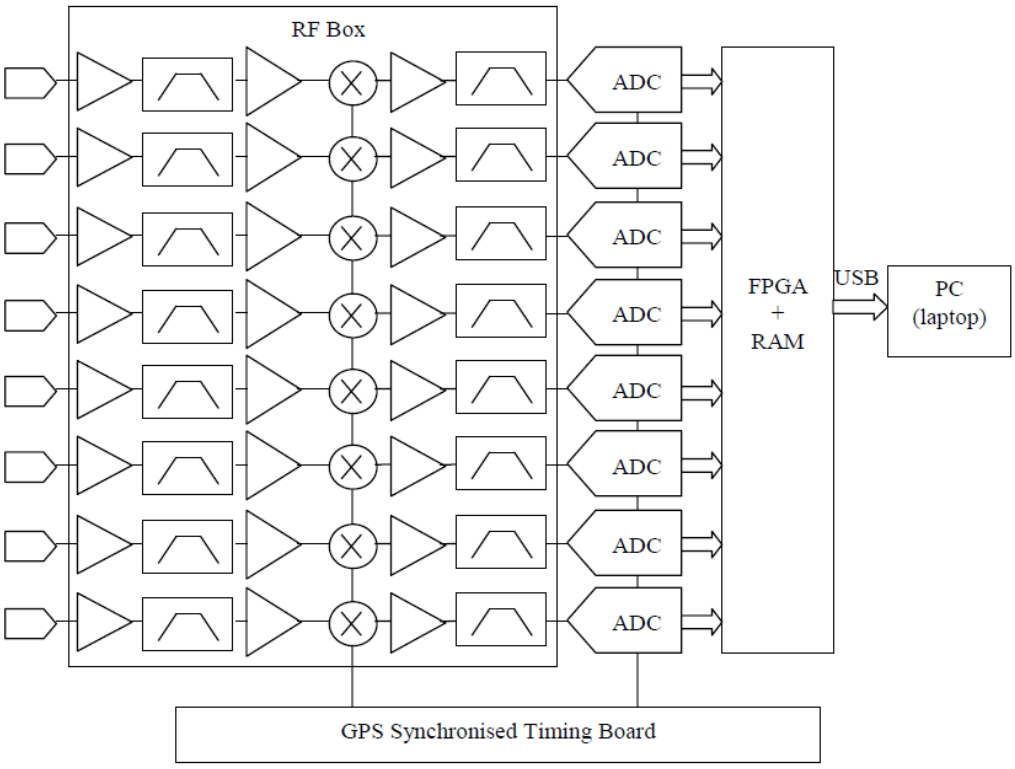

Figure 6.5.2: Antenna array data recording system.

The final sample rate of the ADC was chosen to be 32 MHz, although the ADC chip can actually go to 125 MHz. This gave a usable bandwidth of up to 16 MHz, although the final band-pass filters were slightly narrower than 16 MHz to reduce aliasing. The initial band-pass filter was centred at the GPS carrier frequency of 1.57542GHz, while the final band-pass filter was centred at 56MHz with a bandwidth slightly less than 16MHz, so that the signal would alias down to 0-16MHz when sampled at 32MHz. The final sampling rate used in the experiment was 4 MHz.

A picture of the antenna array hardware is shown in figure 6.5.3. The ADC and RF boards were custom designed, while the FPGA board was a COTS board that plugs onto the ADC board and included an FPGA as well as 64MB of RAM to capture continuous blocks of data in real time that could be transferred to the computer via USB in a slower time.

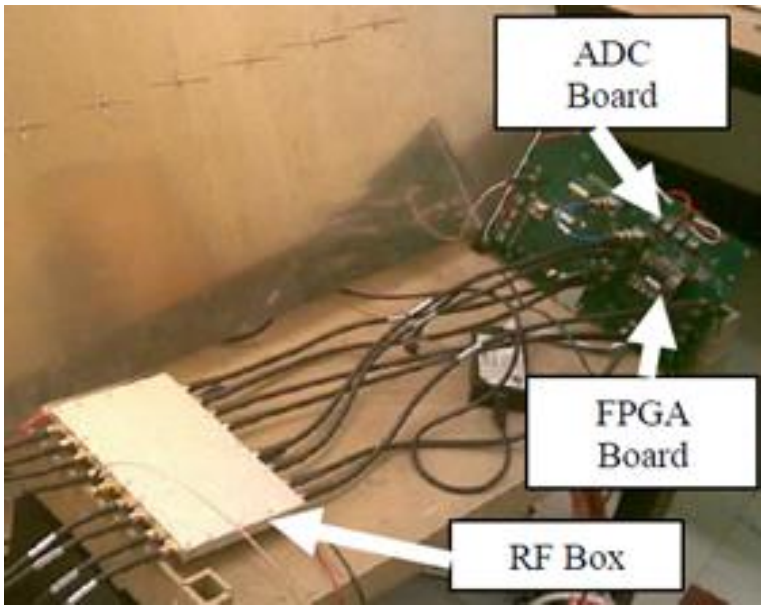

Figure 6.5.3: Picture of the antenna array data recording system.

6.5.2 DOA Estimation Results

Because it is prohibited to transmit signal in the GPS L1 frequency band, it was hard to find a proper interference source. In the experiment, the interference source was a desktop computer. As shown in figure 6.5.4, this desktop computer generated a narrowband interference in GPS L1 frequency band during its startup period. The interference to noise ratio was about -22dB and the distance was about 7 meters from the antenna array, so it was not capable of interfering with the GPS signals during the experiment. Although it was narrowband interference, the DOA estimation during this experiment was using a wideband signal assumption and processed the entire signal bandwidth.

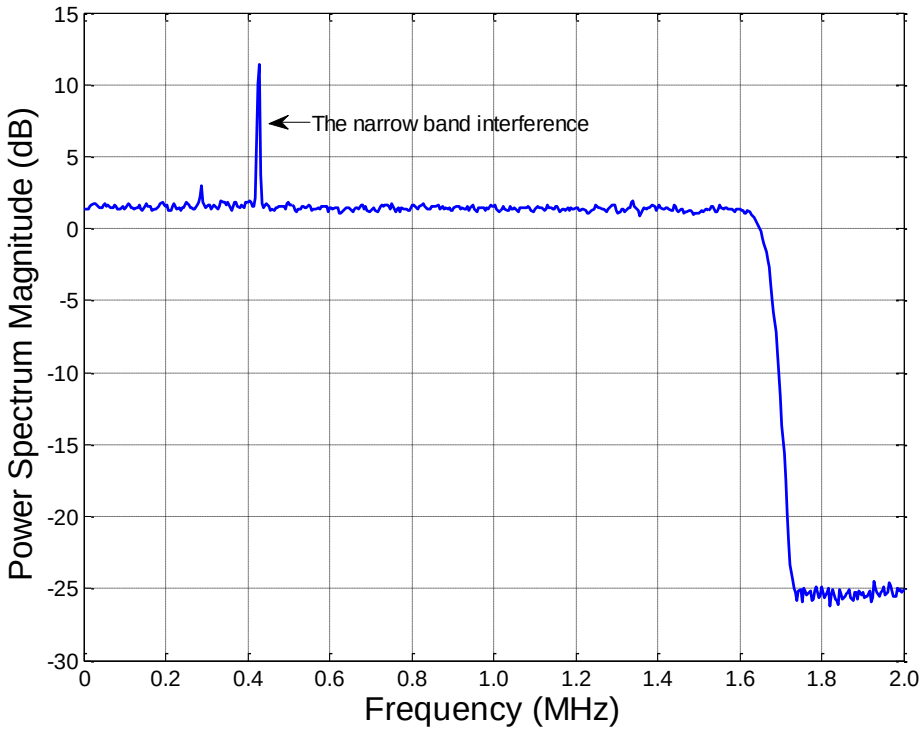

Figure 6.5.4: The power spectrum of channel 1 received data after GPS signal subtraction. The peak value of the spike (narrowband interference) is 11.4dB, the noise floor is at 1.5dB, the processing gain is 31.9dB, so the power of the narrowband interference is 11.4dB - 1.5dB – 31.9dB = -22dB.

The interference DOA was estimated by the MUSIC algorithm where the two eigenvectors corresponding to the largest two eigenvalues were chosen as the signal subspace because this gave a less noisy MUSIC spectrum than just using a single eigenvalue. The DOA estimation result is shown in figure 6.5.5. The estimated azimuth angle of the interference was 179.4^0 compared with a true value of 180^0. The clean MUSIC spectrum suggested a good estimation result.

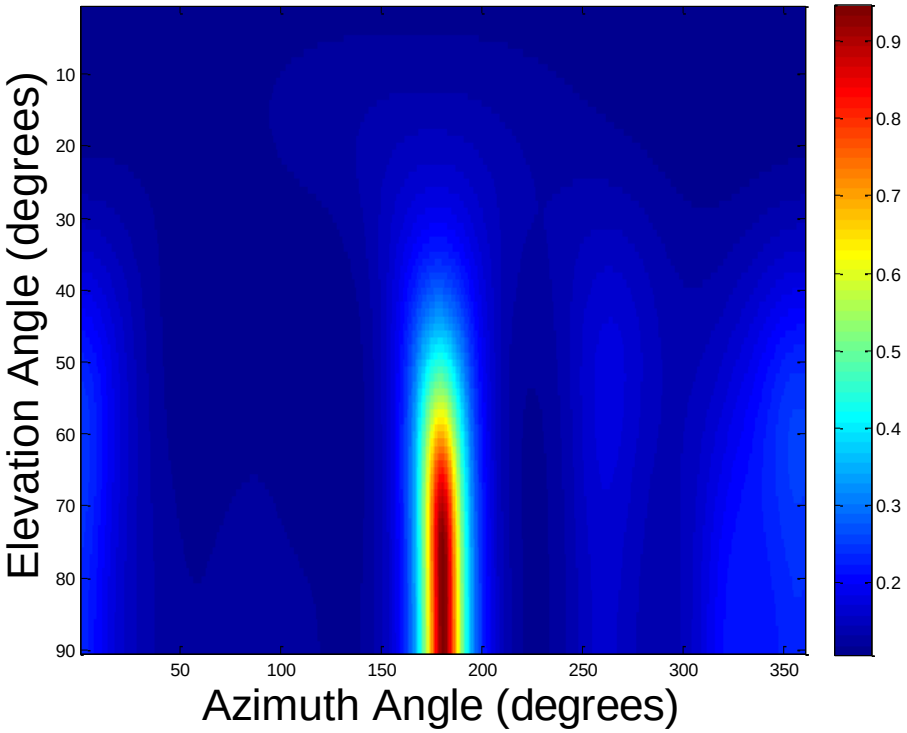

Figure 6.5.5: Interference DOA estimation using MUSIC.

6.6 Conclusion

In this chapter, the requirement of the number of snapshots of the received signal and a method to mitigate the coloured noise has been discussed. The CRLB analysis for the ideal signal model shows the number of snapshots needs to be larger than 1×10^6 to ensure that a lower bound for the accuracy of the azimuth DOA estimation is within 0.5º for an interference with a SNR of -22dB. The coloured noise in the system was effectively whitened by using the projections of the noise only covariance matrix.

By applying the GPS signal cancellation, the coloured noise mitigation and the array calibration parameters, the experimental result shows the DOA of an interference with SNR of -22dB in the GPS L1 band was accurately estimated by MUSIC algorithm.

Chapter 7: Conclusion

7.1 Summary

The work in this thesis developed a GPS antenna array based technique to estimate the direction of arrival (DOA) of weak interferences in the GPS frequency band. Initially, the main issues which affect DOA estimation accuracy were addressed. They are

1. Errors in the antenna array model.
2. GPS signals acting as interference sources.
3. The number of snapshots requirement for DOA estimation.
4. Coloured noise in the system.

Two calibration algorithms were developed in Chapter 3 and Chapter 4 to calibrate GPS antenna arrays. In Chapter 3, the GPS antenna array is calibrated by a modelled eigenstructure based calibration algorithm using GPS signals as disjoint calibration sources. This algorithm described antenna array errors using their physical models, which reduces the number of unknown parameters in the cost function and thus reduces the minimum requirement of the number of calibration sources. The use of GPS signals as disjoint sources largely simplifies the computations required to estimate directions of arrival of calibration sources and also enables the number of calibration sources to be larger than the number of GPS antenna array elements. The unknown parameters are estimated by minimising the highly sensitive eigenstructure based cost function iteratively.

The calibration algorithm in Chapter 4 was developed to calibrate GPS antenna arrays when the calibration sources (GPS signals) have multipath components. The multipath signals from the calibration sources are modelled

in the subspace based calibration cost function as well as array orientation error and mutual coupling effects. This cost function is minimised by the Alternating Projection (AP) method based calibration algorithm which iteratively estimates the unknown parameters in the cost function.

In Chapter 5, it was found that the DOA estimation variance of a weak GPS interference increases significantly due to the presence of GPS signals, so GPS signals need to be cancelled in the received data to enable an accurate weak interference DOA estimation. A Multiple Subspace Projection (MSP) algorithm was proposed in this chapter to cancel the GPS signals. This algorithm projects the received data onto the orthogonal multi-dimensional subspace of the intended GPS signals to cancel them completely even if the signals are band-limited, have multipath components, or have fractional delays.

The last two issues, non-coherent integration length and coloured noise mitigation, are discussed in Chapter 6. The Cramer-Rao Lower Bound (CRLB) was derived and analysed for the antenna array DOA estimation. By using the CRLB, the number of snapshots required for weak interference non-coherent spatial integration was determined. Coloured noise in the system was pre-whitened by using noise-only calibration data. Experimental results using an eight-element GPS antenna array showed that the DOA of a weak GPS interference with a signal to noise ratio (SNR) of -22dB could be accurately estimated.

7.2 Future Work

In Chapter 3 and Chapter 4, the solution existence condition is derived based on the number of unknown parameters and the number of available least squares equations obtained from the calibration sources, but each of the steps in the iterative process may require a smaller number of calibration sources, the question of whether the same or different sources are required

for each of the separate steps will be an interesting topic to be resolved. For the two proposed antenna array calibration algorithms, it will also be interesting to study the importance of the quality of the initialisation values and in which conditions their iterative processes will result in a local optimum.

The MSP GPS signal cancellation algorithm proposed in Chapter 5 does not include Doppler errors into the signal model and thus loses its performance under this condition. It will be beneficial to study efficient implementations under MSP framework to fully cancel GPS signals in the presence of Doppler errors.

The work presented in this thesis was implemented in Matlab as post processing functions. In order to achieve on-line weak interference DOA estimation, the algorithms especially the MSP GPS cancelation algorithm needs to be extended to be implemented for real time applications. The algorithms in this work can be used as initialisation functions for tracking algorithms such as Kalman filters, particle filters and their extensions. The real time application also requires the on-line interference detection to work, which requires a robust interference detector.

The weak interference DOA estimation performance in the real environment needs to be analysed by more data. It is also interesting to evaluate the estimation variance with interferences whose SNR is lower than -25dB as there might be other interfering sources limiting the accuracy.

Appendix A. Lemmas for Matrix Manipulation

The lemmas in this appendix are given in references [57, 114].

Lemma 1: For any M × 1 complex vector *X* and any M × M complex diagonal matrix *D* we have

$$D \cdot X = Q_1(X) \cdot d$$

where the components of the M × 1 vector d and M × M matrix $Q_1(X)$ are given by

$$d_i = D_{ii} \quad i = 1,2,\dots,M$$

$$[Q_1(X)]_{ij} = X_i \cdot \delta_{ij} \quad i,j = 1,2,\dots,M$$

Lemma 2: For any N × 1 complex vector *X* and any M × M complex symmetric circulant matrix *A* we have

$$A \cdot X = Q_2(X) \cdot a$$

where the components of the L × 1 vector *a* are given by

$$a_i = A_{1i}, \quad i = 1,2,\dots,L$$

where L = M/2 + 1 when M is even and L = M/2 + ½ when M is odd.

The M × L matrix $Q_2(X)$ is the sum of the four M × L following matrices:

$$[W_1]_{pq} = \begin{cases} X_{p+q-1}, & p+q \le M+1 \\ 0, & otherwise \end{cases}$$

$$[W_2]_{pq} = \begin{cases} X_{p-q+1}, & p \ge q \ge 2 \\ 0, & otherwise \end{cases}$$

$$[W_3]_{pq} = \begin{cases} X_{M+1+p-q}, & p < q \le l \\ 0, & otherwise \end{cases}$$

$$[W_4]_{pq} = \begin{cases} X_{P+q-M-1}, & 2 \le q \le l, p+q \ge M+2 \\ 0, & otherwise \end{cases}$$

$l = M/2$ for even M and $l = (M + 1)/2$ for odd M.

Lemma 3: For any M × 1 complex vector *X* and any M × M banded complex symmetric Toeplitz matrix *A* we have

$$A \cdot X = Q_3(X) \cdot a$$

where the L × 1 vector a is given by

$$a_i = A_{1i}, \quad i = 1,2, \dots, L$$

And L is the highest superdiagonal that is different from zero. The M × L matrix $Q_3(X)$ is given by the sum of the two M × L following matrices

$$[W_1]_{pq} = \begin{cases} X_{p+q-1}, & p + q \leq M + 1 \\ 0, & otherwise \end{cases}$$
$$[W_2]_{pq} = \begin{cases} X_{p-q+1}, & p \geq q \geq 2 \\ 0, & otherwise \end{cases}$$

Proof: The proof of the lemmas is based on the special properties of diagonal matrices, circulant matrices and Toeplitz matrices. For detailed discussions, please refer to references [57, 114].

Bibliography

[1] M. S. Grewal, L. R. Weill, and A. P. Andrews, *Global Positioning Systems, Inertial Navigation, and Integration*. New York: John Wiley & Sons, 2001.

[2] E. D. Kaplan and C. J. Hegarty, *Understanding GPS Principles and Applications*. Norwood, MA: Artech House, 2006.

[3] K. T. Woo, "Optimum semi-codeless carrier phase tracking of L2," *NAVIGATION,* vol. 47, pp. 82 - 99, 2000.

[4] B. Parkinson and J. J. Spilker, *Global Position System: Theory and Applications Volume I*. Washington D.C.: American Institute of Aeronautics and Astronautics, 1996.

[5] R. Landry and A. Renard, "Analysis of potential interference sources and assessment of present solutions for GPS/GNSS receivers," in *4th Saint Petersburg International Conference on Integrated Navigation Systems*, 1997.

[6] Z. M. Ponos and M. L. Dukic, "Analysis of GPS receiver anti-jamming characteristics," *IEICE TRANSACTIONS on Communications,* vol. E83-B, pp. 2411-2418, 2000.

[7] J. A. Volpe, "Vulnerability assesment of the transportation infrastructure relaying on the global positioning system," National Transportation Systems Center, 2001.

[8] Y. Zheng, "Adaptive antenna array processing for GPS receivers," Master of Engineering Science Thesis, School of Electrical and Electronic Engineering, University of Adelaide, Adelaide, Australia, 2008.

[9] F. Bastide, D. Akos, C. Macabiau, and B. Roturier, "Automatic gain control (AGC) as an interference assessment tool," in *Proceedings of ION GPS 2003*, Portland, OR, 2003, pp. 2042-2053.

[10] J. W. Betz, "Effect of partial-band interference on receiver estimation of C/N0: theory," in *ION GPS 2001*, Long Beach, CA, 2001, pp. 16-27.

[11] A. T. Balaei, A. G. Dempster, and J. Barnes, "A novel approach in the detection and characterization of CW interference on the GPS signal using the receiver C/No estimation," in *2006 IEEE/ION, Position, Location, And Navigation Symposium*, San Diego, CA, 2006, pp. 1120-1126.

[12] A. Ndili and P. Enge, "GPS receiver autonomous interference detection," in *IEEE Position Location and Navigation Symposium*, Palm Springs, CA, 1998, pp. 123-130.

[13] A. T. Balaei, B. Motella, and A. G. Dempster, "GPS Interference detected in Sydney-Australia," in *International Symposium on GPS/GNSS (IGNSS 2007)*, Sydney, Australia, 2007.

[14] W. R. Vincent, R. W. Adler, P. McGill, J. R. Clynch, G. Badger, and A. A. Parker. (2003) The hunt for RFI - unjamming a coast harbor. *GPS World*.

[15] S. Logan. (2010) J911: Fast jammer detection and location using cell-phone crowd-sourcing. *GPS World*.

[16] A. Brown, D. Reynolds, D. Roberts, and M. S. Serie, "Jammer and interference location system - design and initial test results," in *Proceedings of the 12th International Technical Meeting of the Satellite Division of The Institute of Navigation (ION GPS 1999)*, Nashville, TN, 1999, pp. 137-142.

[17] W. Sun and M. G. Amin, "Interference suppression for GPS coarse/acquisition signals using antenna array," *2004 Ieee International Conference on Acoustics, Speech, and Signal Processing, Vol Iv, Proceedings,* pp. 929-932, 2004.

[18] J. W. Ketchum and J. G. Proakis, "Adaptive Algorithms for Estimating and Suppressing Narrow-Band Interference in Pn Spread-Spectrum Systems," *Ieee Transactions on Communications,* vol. 30, pp. 913-924, 1982.

[19] L. B. Milstein, "Interference Rejection Techniques in Spread Spectrum Communications," *Proceedings of the Ieee,* vol. 76, pp. 657-671, Jun 1988.

[20] K. D. Rao and M. N. S. Swamy, "New approach for suppression of FM jamming in GPS receivers," *IEEE Transactions on Aerospace and Electronic Systems,* vol. 42, pp. 1464-1474, Oct 2006.

[21] B. Badke and A. S. Spanias, "Partial band interference excision for GPS using frequency-domain exponents," *2002 Ieee International Conference on Acoustics, Speech, and Signal Processing, Vols I-Iv, Proceedings,* pp. 3936-3939, 2002.

[22] P. T. Capozza, B. J. Holland, T. M. Hopkinson, and R. L. Landrau, "A single-chip narrow-band frequency-domain excisor for a Global Positioning System (GPS) receiver," *Ieee Journal of Solid-State Circuits,* vol. 35, pp. 401-411, Mar 2000.

[23] R. C. DiPietro, "An FFT based technique for suppressing narrow-band interference in PN spread spectrum communications systems," in *Proceedings of IEEE International Conference on Acoustics, Speech, and Signal Processing (ICASSP 89)*, Glasgow, UK, 1989.

[24] Y. M. Zhang, A. R. Lindsey, and M. G. Amin, "Combined synthesis and projection techniques for jammer suppression in DS/SS communications," *2002 Ieee International Conference on Acoustics, Speech, and Signal Processing, Vols I-Iv, Proceedings,* pp. 2757-2760, 2002.

[25] M. G. Amin, L. Zhao, and A. R. Lindsey, "Subspace array processing for the suppression of FM jamming in GPS receivers," *IEEE Transactions on Aerospace and Electronic Systems,* vol. 40, pp. 80-92, Jan 2004.

[26] H. Subbaram and K. Abend, "Interference Suppression Via Orthogonal Projections - a Performance Analysis," *IEEE Transactions on Antennas and Propagation,* vol. 41, pp. 1187-1194, Sep 1993.

[27] M. Trinkle and W. C. Cheuk, "Null-steering GPS dualpolarized antenna arrays," in *Proceedings of the 6th International Symposium*

on Satellite Navigation Technology including Mobile Positioning and Location Services (SatNav 03), Melbourne, Australia, 2003.

[28] R. L. Fante and J. J. Vaccaro, "Evaluation of adaptive spacetime-polarization cancellation of broadband interference," in *Proceedings of IEEE Position Location and Navigation Symposium (PLANS 02)*, Palm Springs, CA, 2002.

[29] G. Lachapelle, M. Petovello, L. Scott, S. Skone, and J. Raquet, "GNSS solutions: adaptive antenna arrays, multi-GNSS tropospheric monitoring, and high-dynamic receivers," *Inside GNSS, Engineering Solutions for the Global Navigation Satellite System,* vol. 1, pp. 20-25, 2006.

[30] G. Seco-Granados, J. A. Fernandez-Rubio, and C. Fernandez-Prades, "ML estimator and hybrid beamformer for multipath and interference mitigation in GNSS receivers," *IEEE Transactions on Signal Processing,* vol. 53, pp. 1194 - 1208, 2005.

[31] M. D. Zoltowski and A. S. Gecan, "Advanced adaptive null steering concepts for GPS," in *Proceedings of IEEE Military Communications Conference (MILCOM 95)*, San Diego, CA, 1995, pp. 1214-1218.

[32] M. Trinkle and D. A. Gray, "GPS interference mitigation: overview and experimental results," in *Proceedings of the 5th International Symposium on Satellite Navigation Technology & Applications (SatNav 01)*, Canberra, Australia, 2001.

[33] Y. Zhang, M. G. Amin, and A. R. Lindsey, "Anti-jamming GPS receivers based on bilinear signal distributions," in *Proceedings of IEEE Military Communications Conference (MILCOM 01)*, McLean, VA, 2001, pp. 1070-1074.

[34] R. L. Fante and J. J. Vaccaro, "Wideband cancellation of interference in a GPS receive array," *IEEE Transactions on Aerospace and Electronic Systems,* vol. 36, pp. 549-564, Apr 2000.

[35] G. F. Hatke, "Adaptive array processing for wideband nulling in GPS systems," *Conference Record of the Thirty-Second Asilomar Conference on Signals, Systems & Computers, Vols 1 and 2,* pp. 1332-1336, 1998.

[36] P. Xiong, M. J. Medley, and S. N. Batalama, "Spatial and temporal processing for global navigation satellite systems: The GPS receiver paradigm," *IEEE Transactions on Aerospace and Electronic Systems,* vol. 39, pp. 1471-1484, Oct 2003.

[37] W. L. Myrick, J. S. Goldstein, and M. D. Zoltowski, "Low complexity anti-jam space-time processing for GPS," *2001 Ieee International Conference on Acoustics, Speech, and Signal Processing, Vols I-Vi, Proceedings,* pp. 2233-2236, 2001.

[38] J. Wang and M. G. Amin, "Multiple Interference Cancellation Performance for GPS Receivers with Dual-Polarized Antenna Arrays," *EURASIP Journal on Advances in Signal Processing,* 2008.

[39] J. Lindstrom, D. M. Akos, O. Isoz, and M. Junered, "GNSS interference detection and localization using a network of low cost front-end modules," in *Proceedings of the 20th International Technical Meeting of the Satellite Division of The Institute of Navigation (ION GNSS 2007)*, Fort Worth, TX, 2007, pp. 1165 - 1172.

[40] O. Isoz, A. T. Balaei, and D. Akos, "Interference detection and localization in GPS L1 band," in *Proceedings of the 2010 International Technical Meeting of The Institute of Navigation*, San Diego, CA, 2010, pp. 925 - 929.

[41] R. J. R. Thompson, E. Cetin, and A. G. Dempster, "Unknown source localization using RSS in open areas in the presence of ground reflections," in *2012 IEEE/ION Position Location and Navigation Symposium (PLANS)*, Sydney, NSW, Australia, 2012, pp. 1018-1027.

[42] R. J. R. Thompson, J. Wu, A. T. Balaei, and A. G. Dempster, "Detection of RF interference to GPS using day-to-day C/No differences," presented at the 2010 International Symposium on GPS/GNSS, Taipei, Taiwan, 2010.

[43] K. Gromov, D. Akos, S. Pullen, P. Enge, and B. Parkinson, "GIDL: Generalized interference detection and localization system," in *Proceedings of the 13th International Technical Meeting of the Satellite Division of The Institute of Navigation (ION GPS 2000)*, Salt Lake City, UT, 2000, pp. 447-457.

[44] E. Cetin, R. J. R. Thompson, and A. G. Dempster, "Interference Localisation within the GNSS Environmental Monitoring System (GEMS)," in *International Symposium on GPS/GNSS (IGNSS 2011)*, Sydney, Australia, 2011.

[45] M. Trinkle, E. Cetin, R. J. R. Thompson, and A. G. Dempster, "Interference localisation within the GNSS environmental monitoring system (GEMS) - initial field test results," in *Proceedings of the 25th International Technical Meeting of The Satellite Division of the Institute of Navigation (ION GNSS 2012)*, Nashville, TN, 2012.

[46] S.-S. Jan and P. Enge, "Finding source of electromagnetic interference (EMI) to GPS using a network sensors," in *Proceedings of the 2001 National Technical Meeting of The Institute of Navigation*, Long Beach, CA, 2001, pp. 533-540.

[47] M. Trinkle and D. A. Gray, "Interference localisation trials using adaptive antenna arrays," in *Proceedings of the 15th International Technical Meeting of the Satellite Division of The Institute of Navigation (ION GPS 2002)*, Portland, OR, 2002, pp. 613 - 619.

[48] Y. T. J. Morton, J. B. Y. Tsui, D. M. Lin, L. L. Liou, M. M. Miller, Q. Zhou, M. P. French, and J. Schamus, "Assessment and handling of CA code self-interference during weak GPS signal acquisition," in *Proceedings of the 16th International Technical Meeting of the Satellite Division of The Institute of Navigation (ION GPS/GNSS 2003)*, Portland, OR, 2003, pp. 646 - 653.

[49] Y. T. Morton, M. Miller, J. Tsui, D. Lin, and Q. Zhou, "GPS civil signal self-interference mitigation during weak signal acquisition," *IEEE Transactions on Signal Processing,* vol. 55, pp. 5859-5863, 2007.

[50] B. D. Van Veen and K. M. Buckley, "Beamforming: a versatile approach to spatial filtering," *IEEE ASSP Magazine,* vol. 5, pp. 4-24, 1988.

[51] J. Li and M. Trinkle, "Miniaturized GPS interference canceller for UAV application," in *Proceedings of International Global Navigation Satellite Systems Symposium on GPS/GNSS*, Sydney, Australia, 2007, pp. 1-10.

[52] Z. B. Lin, "Antenna nulling technique for GPS adaptive antenna," in *National Technical Meeting Proceedings*, Westin Long Beach Hotel, Long Beach, California, 1998.

[53] T.-T. Lin, "A blind anti-jammer pre-processor for GPS receivers," *IEICE TRANSACTIONS on Communications,* vol. E88-B, pp. 2215-2219, 2005.

[54] T. F. Wong, T. M. Lok, J. S. Lehnert, and M. D. Zoltowski, "A linear receiver for DS-SSMA with antenna arrays and blind adaptation," *IEEE Transactions on Information Theory,* vol. 44, pp. 659-676, 1998.

[55] R. T. Derryberry, T. F. Wong, and J. S. Lehnert, "An iterative blind adaptive receiver for DS-SSMA system," in *Military Communications Conference, 1998. MILCOM 98. Proceedings., IEEE*, Boston, MA, 1998, pp. 160-164.

[56] M. Trinkle and D. A. Gray, "Adaptive antenna arrays for GPS interference localisation," in *Proceedings of the 5th International Symposium on Satellite Navigation Technology & Applications (SatNav 2001)*, Canberra, Australia 2001 2001.

[57] B. Friedlander and A. J. Weiss, "Self-calibration for high resolution array processing," in *Advances in Spectrum Analysis and Array Processing*. vol. 2, S. Haykin, Ed., ed Englewood Cliffs, New Jersey: Prentice-Hall, Inc., 1991, pp. 349-414.

[58] D. A. Gray and H. D. Assumpcao, *Beamforming and array processing*. Adelaide, Australia: The University of Adelaide.

[59] G. Bienvenu and L. Kopp, "Adaptivity to background noise spatial coherence for high resolution passive methods," in *International Conference on Acoustics, Speech and Signal Processing*, Denver, Colorado, 1980, pp. 307-310.

[60] R. O. Schmidt, "Multiple emitter location and signal parameter estimation," in *RADC Spectrum Estimation Workshop*, Griffiths AFB, Rome, New York, 1979, pp. 243-258.

[61] R. O. Schmidt, "A signal subspace approach to multiple emitter location and spectral estimation," Ph.D. Thesis, Stanford University, California, 1981.

[62] M. Zoltowski and F. Haber, "A vector space approach to direction finding in a coherent multipath environment," *IEEE Transactions on Antennas and Propagation,* vol. 34, pp. 1069-1079, 1986.

[63] P. Stoica and A. Nehorai, "MUSIC, maximum likelihood, and Cramer-Rao bound," *IEEE Transactions on Acoustics, Speech and Signal Processing,* vol. 5, pp. 720 - 741, 1989.

[64] T. J. Shan, M. Wax, and T. Kailath, "On spatial smoothing for direction-of-arrival estimation of coherent signals," *IEEE Transactions on Acoustics, Speech, and Signal Processing,* vol. ASSP-33, pp. 806-811, 1985.

[65] R. T. Williams, S. Prasad, A. K. Mahalanabis, and L. H. Sibul, "An improved spatial smoothing technique for bearing estimation in a multipath environment," *IEEE Transactions on Acoustics, Speech, and Signal Processing,* vol. 36, pp. 425-432, 1988.

[66] B. Friedlander, "A sensitivity analysis of the MUSIC algorithm," *IEEE Transactions on Acoustics, Speech and Signal Processing,* vol. 38, pp. 1740 - 1751, 1990.

[67] P. Stoica and A. Nehorai, "MUSIC, Maximum Likelihood, and Cramer-Rao bound: further results and comparison," *IEEE Transactions on Acoustics, Speech, and Signal Processing,* vol. 38, pp. 1740-1751, 1990.

[68] H. Krim and M. Viber, "Two decades of array signal processing research," *IEEE Signal Processing Magazine,* pp. 67-94, 1996.

[69] F. Belloni, A. Richter, and V. Koivunen, "Extension of root-MUSIC to non-ULA array configurations," in *Proceedings of the IEEE International Conference on Acoustics, Speech, and Signal Processing (ICASSP)*, Toulouse, France, 2006, p. IV.

[70] D. A. Gray, *Subspace method for array signal processing*. Adelaide, Australia: Lecture notes, School of Electrical & Electronic Engineering, the University of Adelaide.

[71] P. Stoica and A. Nehorai, "Performance comparison of subspace rotation and MUSIC methods for direction estimation," *IEEE Transactions on Signal Processing,* vol. 39, pp. 446-453, 1991.

[72] A. Kangas, P. Stoica, and T. Soderstrom, "Finite sample and modelling error effects on ESPRIT and MUSIC direction estimators," *IEE Proceedings on Radar, Sonar and Navigation,* vol. 141, pp. 249 - 255, 1994.

[73] B. C. Ng and A. Nehorai, "Optimum active array shape calibration," in *25th Asilomar conference on Signals, Systems, and Computers*, California, 1991, pp. 893-897.

[74] B. C. Ng and A. Nehorai, "Active array sensor location calibration," in *1993 IEEE International Conference on Acoustics, Speech, and Signal Processing, 1993. ICASSP-93*, Minneapolis, MN, 1993, pp. 21 - 24.

[75] A. J. Weiss and B. Friedlander, "Array shape calibration using sources in unknown locations-a maximum likelihood approach," *IEEE Transactions on Acoustics, Speech and Signal Processing,* vol. 37, pp. 1958 - 1966, 1989.

[76] A. J. Weiss and B. Friedlander, "Array shape calibration using eigenstructure methods," presented at the 23rd Asilomar Conference on Signals, Systems, and Computers, Pacific Grove, California, 1989.

[77] B. Friedlander and A. J. Weiss, "Eigenstructure methods for direction finding with sensor gain and phase uncertainties," in *IEEE International Conference on Acoustics, Speech, and Signal Processing*, New York, 1988, pp. 2681-2684.

[78] B. Friedlander and A. J. Weiss, "Direction finding in the presence of mutual coupling," *IEEE Transactions on Antennas and Propagation,* vol. 39, pp. 273 - 284, 1991.

[79] M. Zhang and Z. Zhu, "Array shape calibration using sources in known directions," in *IEEE National Aerospace and Electronics Conference (NAECON)*, Dayton, Ohio, 1993, pp. 70-73.

[80] A. Flieller, A. Ferreol, P. Larzabal, and H. Clergeot, "Robust bearing estimation in the presence of direction-dependent modelling errors: identifiability and treatment," in *1995 International Conference on Acoustics, Speech, and Signal Processing, 1995. ICASSP-95*, 1995, pp. 1884 - 1887.

[81] T. Ratnarajah and A. Manikas, "An $H\infty$ approach to mitigate the effects of array uncertainties on the MUSIC algorithm," *IEEE Signal Processing Letters,* vol. 5, pp. 185-188, 1998.

[82] H. S. Mir and C. M. Keller, "A comparison of external array self-calibration algorithms using experimental data," in *IEEE International Conference on Acoustics, Speech, and Signal Processing, 2004. Proceedings. (ICASSP '04)*, 2004, pp. 213-216.

[83] Z. XU and M. Trinkle, "Interference angle of arrival estimation within the GNSS Environmental Monitoring System (GEMS) using antenna arrays," in *International Symposium on GPS/GNSS (IGNSS 2011)*, Sydney, Australia, 2011.

[84] A. L. Swindlehurst and T. Kailath, "A performance analysis of subspace-based methods in the presence of model errors, part I: the MUSIC algorithm," *IEEE Transactions on Signal Processing,* vol. 40, pp. 1758-1774, 1992.

[85] U. S. Kim, D. S. De Lorenzo, D. Akos, J. Gautier, P. Enge, and J. Orr, "Precise phase calibration of a controlled reception pattern GPS antenna for JPALS," in *IEEE/ION Position Location and Navigation Symposium*, Monterey, CA, 2004.

[86] U. S. Kim, D. S. De Lorenzo, J. Gautier, P. Enge, and J. Orr, "Phase effects analysis of patch antenna CRPAs for JPALS," in *Proceedings of the 17th International Technical Meeting of The Satellite Division of the Institute of Navigation (ION GNSS 2004)*, Long Beach, CA, 2004, pp. 1531-1538.

[87] S. Backen, D. M. Akos, and M. L. Nordenvaad, "Post-processing dynamic GNSS antenna array calibration and deterministic beamforming," in *Proceedings of the 21st International Technical Meeting of The Satellite Division of the Institute of Navigation (ION GNSS 2008)*, Savannah, GA, 2008, pp. 2806 - 2814.

[88] C.-L. Chang and J.-C. Juang, "A new pre-processing approach against array uncertainty for GNSS position," in *IEEE/ION Position Location and Navigation Symposium*, Monterey, CA, 2008, pp. 892 - 897.

[89] P. B. Anantharamu, D. Borio, and G. Lachapelle, "Self-Contained antenna array calibration using GNSS signals," *NAVIGATION,* vol. 59, pp. 209-220, 2012.

[90] A. Konovaltsev, M. Cuntz, and M. Meurer, "Novel calibration of adaptive GNSS antenna," in *Proceedings of the 23rd International Technical Meeting of The Satellite Division of the Institute of Navigation (ION GNSS 2010)*, Portland, OR, 2010, pp. 3229 - 3234.

[91] I. S. D. Solomon, "Over-the-Horizon radar array calibration," Doctor of Philosophy Thesis, Department of Electrical and Electronic Engineering, University of Adelaide, Adelaide, Australia, 1998.

[92] I. S. D. Solomon, D. A. Gray, Y. I. Abramovich, and S. J. Anderson, "Over-The-Horizon radar array calibration using echoes from ionised meteor trails," *Radar, Sonar and Navigation, IEE Proceedings -,* vol. 145, pp. 173-180, 1998.

[93] I. S. D. Solomon, D. A. Gray, Y. I. Abramovich, and S. J. Anderson, "Receiver array calibration using disparate sources," *IEEE*

Transactions on Antennas and Propagation, vol. 47, pp. 496 - 505, 1999.

[94] W. Chen, Q. Yin, and A. Feng, "Array calibration for compensating gain/phase mismatch and mutual coupling effects in Smart Antenna Systems," presented at the IEEE International Symposium on Wireless Communication Systems, 2008.

[95] A. Manikas and N. Fistas, "Modelling and estimation of mutual coupling between array elements," in *IEEE International Conference on Acoustics, Speech, and Signal Processing (ICASSP)*, Adelaide, Australia, 1994, pp. 553-556.

[96] T. Svantesson, "The effects of mutual coupling using a linear array of thin dipoles of finite length," in *Ninth IEEE SP Workshop on Statistical Signal and Array Processing*, Portland, OR, 1998, pp. 232 - 235.

[97] E. BouDaher, F. Ahmad, M. G. Amin, and A. Hoorfar, "DOA estimation with co-prime arrays in the presence of mutual coupling," in *Proceeding of the 23rd European Signal Processing Conference*, Nice, France, 2015.

[98] J. F. Bohme, "Separated estimation fo wave parameters and spectral parameters by maximum likelihood," in *International Conference on Acoustics, Speech and Signal Processing (ICASSP)*, Tokyo, Japan, 1986, pp. 2819-2822.

[99] A. G. Jaffer, "Maximum likelihood direction finding of stochastic sources: A separable solution," in *International Conference on Acoustics, Speech and Signal Processing (ICASSP)*, New York, 1988, pp. 2893-2896.

[100] P. Stoica, B. Ottersten, M. Viberg, and R. L. Moses, "Maximum likelihood array processing for stochastic coherent sources," *IEEE Transactions on Signal Processing,* pp. 96-105, 1996.

[101] Y. Bresler, "Maximum likelihood estimation of a linearly structured covariance with application to antenna array processing," in *4th ASSP Workshop on Spectrum Estimation and Modeling*, Mineapolis, Minnesota, 1988, pp. 172-175.

[102] M. Wax, T. J. Shan, and T. Kailath, "Location and spectral density estimation of multiple sources," in *16th Asilomar Conference on Signals, Systems, and Computers*, 1982, pp. 322-326.

[103] P. Stoica and A. B. Gershman, "Maximum-likelihood DOA estimation by data-supported grid search," *IEEE Signal Processing Letters,* vol. 6, pp. 273 - 275, 1999.

[104] I. Ziskind and M. Wax, "Maximum likelihood localization of multiple sources by alternating projection," *IEEE Transactions on Acoustics, Speech and Signal Processing,* vol. 36, pp. 1553 - 1560, 1988.

[105] M. Feder and E. Weinstein, "Parameter estimaton of superimposed signals using the EM algorithm," *IEEE Transactions on Acoustics, Speech and Signal Processing,* pp. 477-489, 1988.

[106] M. I. Miller and D. R. Fuhrmann, "Maximum-likelihood narrow-band direction finding and the EM algorithm," *IEEE Transactions on Acoustics, Speech and Signal Processing,* pp. 1560-1577, 1990.

[107] J. A. Fessler and A. O. Hero, "Space-alternating generalised expectation-maximisation algorithm," *IEEE Transactions on Signal Processing,* vol. 42, pp. 4664-4677, 1994.

[108] J. Capon, "High-resolution frequency-wavenumber spectrum analysis," *Proceedings of the IEEE,* vol. 57, pp. 1408-1418, 1969.
[109] R. Roy, "ESPRIT: Estimation of Signal Parameters via Rotational Invariance Techniques," Ph.D, Dissertation, Stanford University, Stanford, California, 1987.
[110] M. Haardt and M. E. Ali-Hackl, "Unitary ESPRIT: how to exploit additional information inherent in the relational invariance structure," in *IEEE International Conference on Acoustics, Speech, and Signal Processing (ICASSP)*, Adelaide, Australia, 1994, pp. 229 - 232.
[111] M. Haardt and J. A. Nossek, "Unitary ESPRIT: how to obtain increased estimation accuracy with a reduced computational burden," *IEEE Transactions on Signal Processing,* vol. 43, pp. 1232 - 1242, 1995.
[112] H. L. Van Trees, *Optimum array processing: part IV of detection, estimation, and modulation theory*. New York: John Wiley & Sons, Inc., 2002.
[113] S. U. Pillai and B. H. Kwon, "Forward/backward spatial smoothing techniques for coherent signal identification," *IEEE Transactions on Acoustics, Speech and Signal Processing,* vol. 37, pp. 8 - 15, 1989.
[114] B. Friedlander and A. J. Weiss, "Direction finding using spatial smoothing with interpolated arrays," *IEEE Transactions on Aerospace and Electronic Systems,* vol. 28, pp. 574 - 587, 1992.
[115] A. J. Weiss and B. Friedlander, "Performance analysis of spatial smoothing with interpolated arrays," in *IEEE International Conference on Acoustics, Speech, and Signal Processing (ICASSP)*, Toronto, Ont. , Canada, 1991, pp. 1377 - 1380.
[116] M. Wax and J. Sheinvald, "Direction finding of coherent signals via spatial smoothing for uniform circular arrays," *IEEE Transactions on Antennas and Propagation,* vol. 42, pp. 613-620, 1994.
[117] A. J. Van Dierendonck, P. Fenton, and T. Ford, "Theory and performance of narrow correlator spacing in a GPS receiver," *NAVIGATION,* vol. 39, pp. 265-284, 1992.
[118] L. Garin, F. V. Diggelen, and J.-M. Rousseau, "Strobe & edge correlator multipath mitigation for code," in *Proceedings of the 9th International Technical Meeting of the Satellite Division of The Institute of Navigation (ION GPS 1996)*, Kansas City, MO, 1996, pp. 657 - 664.
[119] L. Garin and J. M. Rousseau, "Enhanced strobe correlator multipath mitigation for carrier code," in *Proceedings of ION International Technical Meeting*, 1997, pp. 559-568.
[120] G. McGraw and M. Braash, "GNSS multipath mitigation using gated and high resolution correlator concepts," in *Proceedings of ION International Technical Meeting*, 1999, pp. 333-342.
[121] R. D. J. Van Nee, J. Siereveld, P. Fenton, and B. R. Townsend, "The multipath estimating delay lock loop: approaching theoretical accuracy limits," in *IEEE Position Location and Navigation Symposium*, Las Vegas, Nevada, 1994.
[122] M. Brenneman and Y. Morton, "An efficient algorithm for short delay time multipath estimation and mitigation," in *Proceedings of the 23rd International Technical Meeting of The Satellite Division of the Institute of Navigation (ION GNSS 2010)*, Portland, OR, 2010, pp. 152 - 160.

[123] S. Rougerie, G. Carrie, L. Ries, F. Vincent, R. Pascaud, E. Corbel, and M. Monnerat, "A new approach based on SAGE algorithm for multipath mitigation in GNSS receivers," in *Proceedings of the 23rd International Technical Meeting of The Satellite Division of the Institute of Navigation (ION GNSS 2010)*, Portland, OR, 2010.

[124] S. Rougerie, L. Ries, A. Konovaltsev, M. Cuntz, F. Vincent, R. Pascaud, and G. Carrie, "Comparison of SAGE and classical multi-antenna algorithms for multipath mitigation in real-world environment," in *2010 5th ESA Workshop on Satellite Navigation Technologies and European Workshop on GNSS Signals and Signal Processing (NAVITEC)*, 2010, pp. 1-8.

[125] S. Rougerie, G. Carrie, L. Ries, F. Vincent, R. Pascaud, E. Corbel, and M. Monnerat, "Multipath mitigation methods based on antenna array," in *Proceedings of the 2011 International Technical Meeting of The Institute of Navigation*, San Diego, CA, 2011, pp. 596-605.

[126] P. Closas and C. Fernandez-Prades, "A statistical multipath detector for antenna array based GNSS receivers," *IEEE Transactions on Wireless Communications,* vol. 10, pp. 916 - 929, 2011.

[127] Y. T. Yu and H. T. Hui, "Design of a mutual coupling compensation network for a small receiving monopole array," *IEEE Transactions on Microwave Theory and Techniques,* vol. 59, pp. 2241 - 2245, 2011.

[128] H. M. Aumann, A. J. Fenn, and F. G. Willwerth, "Phased array antenna calibration and pattern prediction using mutual coupling measurements," *IEEE Transactions on Antennas and Propagation,* vol. 37, pp. 844-850, 1989.

[129] H. T. Hui, "Improved compensation for the mutual coupling effect in a dipole array for direction finding," *IEEE Transactions on Antennas and Propagation,* vol. 51, pp. 2498 - 2503, 2003.

[130] H. T. Hui, "A practical approach to compensate for the mutual coupling effect in an adaptive dipole array," *IEEE Transactions on Antennas and Propagation,* vol. 57, pp. 3523-3532, 2004.

[131] F. Sellone and A. Serra, "A novel online mutual coupling compensation algorithm for uniform and linear arrays," *IEEE Transactions on Signal Processing,* vol. 55, pp. 560 - 573, 2007.

[132] T. T. Zhang, Y. L. Lu, and H. T. Hui, "Compensation for the mutual coupling effect in uniform circular arrays for 2D DOA estimations employing the maximum likelihood technique," *IEEE Transactions on Aerospace and Electronic Systems,* vol. 44, pp. 1215 - 1221, 2008.

[133] H.-S. Lui, H. T. Hui, and M. S. Leong, "A note on the mutual-coupling problems in transmitting and receiving antenna arrays," *IEEE Antennas and Propagation Magazine,* vol. 51, pp. 171 - 176, 2009.

[134] Y. T. Yu, H.-S. Lui, C. H. Niow, and H. T. Hui, "Improved DOA estimations using the receiving mutual impedances for mutual coupling compensation: an experimental study," *IEEE Transactions on Wireless Communications,* vol. 10, pp. 2228 - 2233, 2011.

[135] O. Isoz, "Interference Detection and Localization in the GPS L1 Frequency Band," Doctor of Philosophy Thesis, Department of Computer Science, Electrical Engineering and Space Technology, Lulea University of Technology, Lulea, Sweden, 2012.

[136] B. Friedlander, "A signal subspace method for adaptive interference cancellation," *IEEE Transactions on Acoustics, Speech and Signal Processing,* vol. 36, pp. 1835-1845, 1988.
[137] P. H. Madhani, P. Axelrad, K. Krumvieda, and J. Thomas, "Application of successive interference cancellation to the GPS pseudolite near-far problem," *IEEE Transactions on Aerospace and Electronic Systems,* vol. 39, pp. 481-488, 2003.
[138] F. M. G. Sousa and F. D. Nunes, "Near-far effect mitigation for GNSS software receivers using subspace projection," in *2010 5th ESA Workshop on Satellite Navigation Technologies and European Workshop on GNSS Signals and Signal Processing (NAVITEC)*, 2010, pp. 1-6.
[139] F. D. Nunes and F. M. G. Sousa, "GNSS near-far mitigation through subspace projection without phase information," *IEEE Transactions on Aerospace and Electronic Systems,* vol. 48, pp. 2746-2755, 2012.
[140] E. P. Glennon and A. G. Dempster, "A novel GPS cross correlation mitigation technique," in *Proceedings of the 18th International Technical Meeting of the Satellite Division of The Institute of Navigation (ION GNSS 2005)*, Long Beach, CA, 2005, pp. 190 - 199.
[141] E. P. Glennon and A. G. Dempster, "Cross correlation mitigation by adaptive orthogonalization using constraints - new results," in *Proceedings of the 19th International Technical Meeting of the Satellite Division of The Institute of Navigation (ION GNSS 2006)*, Fort Worth, TX, 2006, pp. 1811 - 1820.
[142] E. P. Glennon, R. C. Bryant, A. G. Dempster, and P. J. Mumford, "Post correlation CWI and cross correlation mitigation using delayed PIC," in *Proceedings of the 20th International Technical Meeting of the Satellite Division of The Institute of Navigation (ION GNSS 2007)*, Fort Worth, TX, 2007, pp. 236 - 245.
[143] E. P. Glennon and A. G. Dempster, "Delayed PIC for postcorrelation mitigation of continuous wave and multiple access interference in GPS receivers," *IEEE Transactions on Aerospace and Electronic Systems,* vol. 47, pp. 2544-2557, 2011.
[144] E. P. Glennon and A. G. Dempster, "Cross correlation mitigation techniques for software GPS C/A code receivers," in *International Symposium on GPS/GNSS (IGNSS 2007)*, Sydney, Australia, 2007.
[145] S. M. Kay, *Fundamentals of statistical signal processing: estimation theory*. Englewood Cliffs, New Jersey: PTR Prentice-Hall, Inc., pp. 94 - 95, 1993.
[146] P. Stoica and A. Nehorai, "Performance study of conditional and unconditional direction-of-arrival estimation," *IEEE Transactions on Acoustics, Speech and Signal Processing,* vol. 38, pp. 1783-1795, 1990.
[147] A. Paulraj and T. Kailath, "Eigenstructure methods for direction of arrival estimation in the presence of unknown noise fields," *IEEE Transactions on Acoustics, Speech and Signal Processing,* vol. 34, pp. 13-20, 1986.
[148] S. Prasad, R. T. Williams, A. K. Mahalanabis, and L. H. Sibul, "A transform-based covariance differencing approach for some classes of

parameter estimation problems," *IEEE Transactions on Acoustics, Speech and Signal Processing,* vol. 36, pp. 631-641, 1988.
[149] J. P. Le Cadre, "Parametric methods for spatial signal processing in the presence of unknown colored noise fields," *IEEE Transactions on Acoustics, Speech and Signal Processing,* vol. 37, pp. 965-983, 1989.
[150] M. Wax, "Detection and localization of multiple sources in noise with unknown covariance," *IEEE Transactions on Signal Processing,* vol. 40, pp. 245-249, 1992.
[151] P. Stoica, M. Viberg, and B. Ottersten, "Instrumental variable approach to array processing in spatially correlated noise fields," *IEEE Transactions on Signal Processing,* vol. 42, pp. 121-133, 1994.
[152] B. Friedlander and A. J. Weiss, "Direction Finding Using Noise Covariance Modeling," *IEEE Transactions on Signal Processing,* vol. 43, pp. 1557 - 1567, 1995.
[153] H. Ye and R. D. DeGroat, "Maximum likelihood DOA estimation and asymptotic Cramer-Rao bounds for additive unknown colored noise," *IEEE Transactions on Signal Processing,* vol. 43, pp. 938 - 949, 1995.
[154] V. Nagesha and S. Kay, "Maximum likelihood estimation for array processing in colored noise," *IEEE Transactions on Signal Processing,* vol. 44, pp. 169 - 180, 1996.
[155] M. Wax, J. Sheinvald, and A. J. Weiss, "Detection and localization in colored noise via generalized least squares," *IEEE Transactions on Signal Processing,* vol. 44, pp. 1734-1743, 1996.
[156] B. Goransson and B. Ottersten, "Direction estimation in partially unknown noise fields," *IEEE Transactions on Signal Processing,* vol. 47, pp. 2375 - 2385, 1999.
[157] M. Pesavento and A. B. Gershman, "Maximum-likelihood direction-of-arrival estimation in the presence of unknown nonuniform noise," *IEEE Transactions on Signal Processing,* vol. 49, pp. 1310 - 1324, 2001.
[158] C. Qi, Z. Chen, Y. Wang, and Y. Zhang, "DOA estimation for coherent sources in unknown nonuniform noise fields," *IEEE Transactions on Aerospace and Electronic Systems,* vol. 43, pp. 1195-1204, 2007.
[159] M. Li and Y. Lu, "Maximum likelihood DOA estimation in unknown colored noise fields," *IEEE Transactions on Aerospace and Electronic Systems,* vol. 44, pp. 1079 - 1090, 2008.